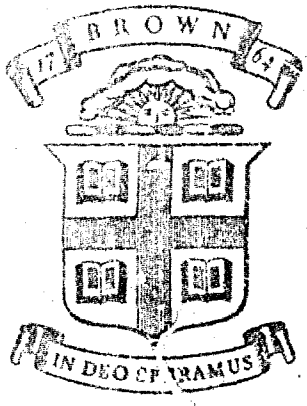

Division of Engineering
BROWN UNIVERSITY
PROVIDENCE, R. I.

AD 643838

RADIATIVE TRANSFER IN A GAS OF UNIFORM PROPERTIES IN LOCAL THERMODYNAMIC EQUILIBRIUM PART I: ABSORPTION COEFFICIENTS IN NONHYDROGENIC GASES

B. L. HUNT and M. SIBULKIN

DDC
RECEIVED
MAR 17 1967
B

Advanced Research Projects Agency
Ballistic Missile Defense Office
and the Fluid Dynamics Branch
Office of Naval Research

Report No.
Nonr-562 (35)/16

ARCHIVE COPY

December 1966

Best Available Copy

RADIATIVE TRANSFER IN A GAS OF UNIFORM PROPERTIES IN LOCAL THERMODYNAMIC EQUILIBRIUM

PART 1: ABSORPTION COEFFICIENTS IN NONHYDROGENIC GASES

by

Brian L. Hunt and Merwin Sibulkin

Division of Engineering
Brown University
Providence, Rhode Island

December 1966

This work was supported by the Advanced Research Projects Agency (Ballistic Missile Defense Office) and by the Fluid Dynamics Branch of the Office of Naval Research under Contract Nonr 562(35), Task NR 061-132.

Reproduction in whole or in part is permitted for any purpose of the United States Government. Distribution of this document is unlimited.

SUMMARY

This report discusses the data needed to perform radiative transfer calculations in nonhydrogenic gases in local thermodynamic equilibrium and presents some approximate methods for computing the radiative energy transferred by spectral lines where the properties of the gas are uniform.

The methods currently available for calculating the cross sections of radiative processes are described and compared. An accurate method for calculating the species composition of nitrogen is described and the results of such a calculation are presented. The important line broadening mechanisms are discussed and the potentially accurate, modern theories of line broadening are outlined. The results of these theories are used to justify approximate line profiles which are simple enough for use in radiative transfer calculations.

Simple approximations to the exact curves of growth of intensity are described for lines with Doppler profiles and for lines with profiles of a class which includes the dispersion and quasi-static forms. The concept of the effective width of a line intensity profile is introduced and techniques are developed for dealing with the overlapping of the intensity profiles of small groups of closely spaced lines (as, for example, in a multiplet).

TABLE OF CONTENTS

ge

LIST OF TABLES

PRINCIPAL SYMBOLS

a	exponent for asymptotic line profile (see Eq. (3.6))
a	ratio of dispersion line width to Doppler line width, $w\sqrt{\ell n\ 2}/w_D$.
a_o	$h^2/4\pi^2 m_e e^2$, radius of first Bohr orbit
A	line width constant
b	asymptotic line profile constant (see Eq. (3.6))
B_ν	Planck function
B_e^i	rotational constant for the ith molecular electronic level
c	velocity of light in a vacuum
C_4	quadratic Stark coefficient
$C_{\ell L}$	angular momentum factor which arises in the calculation of photoionization cross sections
C_ℓ	$\sum_L C_{\ell L}$
D	width of a group of lines
e	charge of electron
E_i	energy of the ith electronic level
$f_{\ell u}$	absorption oscillator strength for a transition from state ℓ to state u
F_o	Holtsmark normal field strength
F_{SL}	fractional parentage coefficient
g_i	statistical weight of state i
$g(\nu;n,\ell)$	bound-free Gaunt factor
g_{ff}	free-free Gaunt factor
h	Planck's constant
I_ν	specific intensity of radiation
I	frequency integrated specific intensity of radiation $\int_o^\infty I_\nu d\nu$

k	Boltzmann's constant
K_ν	linear spectral absorption coefficient
ℓ	orbital angular momentum quantum number
L	total orbital angular momentum quantum number
$L(\nu)$	normalized line profile
m_e	mass of electron
m_S	mass of species S
M^*	effective number or clusters in a group
n	principal quantum number
n^*	effective principal quantum number
N	number of lines in a group
N^*	effective number of lines in a group
N_L	Loschmidt number ($2.6871 \times 10^{19} cm^{-3}$)
N_o	total number of nitrogen nuclei per unit volume
N_S	number of particles of species S per unit volume
$\bar{N}_S$	N_S/N_o
NI, NII, etc.	first, second, etc. spectrum of nitrogen (i.e. spectra associated with N, N^+, etc. respectively)
Q	partition function
Q_{el}	partition function due to electronic energy levels
Q_{int}	partition function due to internal energy levels
Q_{tr}	partition function due to translational energy
Q_r^i	rotational partition function for the ith molecular electronic energy level
Q_v^i	vibrational partition function for the ith molecular electronic energy level
r_m	mean distance between particles (excluding electrons)

R	Rydberg wave number constant
R_D	Debye radius
s	path length
T	temperature
w	line width parameter (see Eq. (3.10))
w_D	line semi-half width due to Doppler broadening
w_{res}	line semi-half-width due to resonance broadening
W	effective width of intensity profile (see Section 3.3)
W_r	$W/2w$
z	number of charges
z_e	effective charge (see Section 5.3)
$\Delta\chi$	reduction in ionization energy
λ	wave length
ν	frequency
ν	continuous variable representing the truncation point for the partition function series (Appendix I only)
ν_o	central frequency of a line
ρ	density
ρ_o	$m_{N_2} N_L$ $(1.25 \times 10^{-3}$ gm cm$^{-3})$
$\mathcal{R}_{\ell L}$	radial matrix element for photoionization
σ	radial matrix element for a bound-bound transition
σ_ν	spectral absorption cross section
$f(\ell)$	relative strength of a line within a multiplet
$f(u)$	relative strength of a multiplet within a transition array
τ	optical depth of a line defined by Eq. (3.11)
τ_m	optical depth of a multiplet defined by Eq. (3.17)

χ	ionization potential
χ_{eff}	$\chi - \Delta\chi$
ω_e^i	vibrational constant for the ith electronic level

subscripts

C	continuum
D	Doppler broadened
ℓ	lower state
L	line
res	resonance broadened
u	upper state

GENERAL INTRODUCTION AND OUTLINE OF REPORTS

The transfer of energy by radiative processes in gases has been a subject of study for many years by astrophysicists and spectroscopists. The aim of these workers has for the most part been to examine the spectral distribution of radiation and to use it to predict the internal structure and state of the gas from which the radiation emerged. More recently, the high temperatures associated with nuclear explosions and with the gases surrounding a space vehicle as it enters a planetary atmosphere have lead to interest in the subject of radiative gas dynamics which combines radiative transfer and fluid mechanics.

In gas dynamic problems, radiation appears as a frequency integrated flux in the energy equation. Therefore, the spectral distribution of the radiated energy is, in principle, not required. In practice, however, no exact method of avoiding the computation of the spectral distribution has been devised except in the limiting cases of optically thin and optically thick media. A widely used approximation which avoids spectral difficulties is the "gray gas" approximation which treats the radiative properties of the gas (specifically the absorption coefficient) as independent of frequency. The gray gas has been the model for much of the work in radiative gas dynamics but recently some progress has been made in the use of nongray absorption coefficients.

A principal difficulty in any attempt to approximate real absorption coefficients is that not much is known of the relative roles played by the various radiating mechanisms even in simple transfer problems and, in particular, the importance of spectral lines is uncertain. The work presented here examines the radiative processes which occur in gases for the

simplest possible case, namely a gas of uniform properties in local thermodynamic equilibrium. Since it happens that the relative importance of the various radiative processes depends strongly on the state of the gas and the path length, this investigation was carried out for a specific range of conditions chosen to include those achieved by a space vehicle reentering the earth's atmosphere.

This work is in three parts. Part 1 describes the various radiative processes, discusses how the corresponding absorption cross sections and occupation numbers may be calculated, presents approximate methods for computing the radiative energy transferred by spectral lines and gives an account of the relevant theories of line broadening.

Part 2 examines some characteristics of line radiation in a hydrogenically distributed spectrum. Some fairly simple calculations help to reveal the factors which determine the distribution of relative importance among the stronger lines. Also presented are new methods of accounting for the many weak lines and an indication of their importance relative to the strong lines.

Part 3 is an account of the calculation of specific intensities in uniform nitrogen allowing for all important radiative processes and with particular emphasis on the lines. The data is tabulated and discussed, the method of calculation is described and, finally, the results are presented graphically and interpreted in detail.

1. INTRODUCTION

The basic equation governing the transfer of radiant energy in a non-scattering gas in local thermodynamic equilibrium may be written

$$dI_\nu/ds = K_\nu(B_\nu - I_\nu) \tag{1.1}$$

where I_ν is the specific intensity of radiation in the direction s per unit frequency ν per unit time per unit area, B_ν is the Planck distribution function and K_ν is the linear absorption coefficient. The quantity K_ν is here defined to include stimulated emission and completely specifies the radiative properties of the gas; this Part is concerned with the methods of calculating K_ν which are currently available for light non-hydrogenic atoms and ions, in particular nitrogen.

1.1. The Absorption Coefficient

Absorption and emission of radiation in a gas correspond to changes in internal energy undergone by atoms and molecules and changes in the translational energy of free electrons. Since the discussion of this Part is restricted to atoms and ions, the energy changes we have to consider are exclusively electronic. Fortunately, this aspect can be separated from the problem of finding the number of particles in a given state so that the absorption coefficient due to a species S can be written

$$K_{\nu,S} = \sum_i N_{Si}\,\sigma_{\nu i}[1 - \exp(-h\nu/kT)] \tag{1.2}$$

where N_{Si} is the number density of particles of species S in state i (known as the occupation number of state i), $\sigma_{\nu i}$ is the cross section for absorption from state i, and the factor $[1 - \exp(-h\nu/kT)]$ accounts for

stimulated emission. The main problem in finding the occupation numbers is to determine the total number of particles present for each species, this is considered in detail in Chap. 2 where plotted values of the species composition of nitrogen are presented.

1.2. Absorption Cross Sections

The cross section $\sigma_{\nu i}$ of Eq. (1.2) is the sum of a number of cross sections each corresponding to an independent electronic process with initial state i and it is usually most convenient to consider each one separately. A sketch of a simple arrangement of electronic energy levels is shown in Fig. 1. As can be seen from the figure, three distinct types of absorptive transition can occur: bound-bound, bound-free (or photoionization) and free-free. Free-free transitions give rise to cross sections which are continuous for all values of frequency, bound-free cross sections are zero for frequencies below a threshold value but finite and continuous for higher values, in contrast the cross section of a bound-bound transition is significant only over a very small frequency interval and can in some senses be treated as a singularity occurring at a single frequency.

Bound-bound transitions are discussed in Chaps. 3 and 4: Chap. 3 is concerned with the calculation of the frequency integrated line absorption coefficient while Chap. 4 discusses line profiles as predicted by the relevant theories of line-broadening. Finally, Chap. 5 describes methods for calculating the cross sections due to bound-free and free-free transitions.

2. SPECIES COMPOSITION AND OCCUPATION NUMBERS

2.1 Introduction

In a gas in local thermodynamic equilibrium the occupation number density N_{Si}, of the ith energy level in a given species, S, may be found from the Boltzmann formula

$$N_{Si} = g_i N_S \exp(-E_i/kT)/(Q)_S \qquad (2.1)$$

where N_S is the total number of particles of species S per unit volume, E_i is the energy of the ith level above the species ground state, g_i is the statistical weight of the ith state, and $(Q)_S$ is the partition function of species S. The species composition is determined by a set of mass action equations together with species conservation and charge neutrality conditions. In the case of a single diatomic gas, like nitrogen, the mass action equations are ionization and dissociation equations which have the general form

$$\frac{N_S N_{S'}}{N_{SS'}} = \frac{(Q)_S (Q)_{S'}}{(Q)_{SS'}} e^{-D/kT} \qquad (2.2)$$

For an ionization reaction, for example, S' is the electron gas and D is χ, the ionization energy of species SS'. Since the partition functions $(Q)_S$, $(Q)_{S'}$ and $(Q)_{SS'}$ depend on the number densities of the various species (except at low temperatures), their evaluation is coupled to the solution of the mass action equations (which themselves must be solved by an iterative procedure). It is clear therefore that an accurate determination of the species composition is a complex problem. Section 2.2 discusses the problem of predicting the truncation point of a partition function.

Section 2.3 describes the calculation of species composition in the particular case of nitrogen; the results presented here will be of use in Part 3.

2.2. Partition Functions

The partition function of species S may be written to a close approximation as the product of a translational partition function, $(Q_{tr})_S = V(2\pi m_S kT/h^2)^{3/2}$ (where V is the volume and m_S the mass of a particle of species S), with an internal partition function $(Q_{int})_S$ which involves the energy levels associated with the internal structure. In the case of a diatomic molecule the internal energy levels are those of rotational, vibrational and electronic excitation whereas only the electronic levels exist for a monatomic particle. Unfortunately, the higher temperatures at which the monatomic particles occur lead to a complication of the electronic partition function which is discussed in the next few paragraphs.

The definition of the electronic partition function of species S is

$$(Q_{el})_S \equiv \sum_{i=1}^{\infty} g_i e^{-E_i/kT} \qquad (2.3)$$

where g_i is the statistical weight of the ith energy level, E_i is its value relative to the ground state of species S and the index i is chosen such that $E_{i+1} > E_i$. It is well known that the series in Eq. (2.3) is divergent since it represents the partition function of an atom in an unbounded volume of non-interacting particles. When the interactions between particles are allowed for, the series terminates at some level, i_{max}, Eq. (2.3) thus becomes

$$(Q_{el})_S = \sum_{i=1}^{i_{max}} g_i \, e^{-E_i/kT} \qquad (2.4)$$

At low temperatures ($\lesssim$ 7000°K) the exponential factors in Eq. (2.4) become so small that the summation may be truncated after a few terms and the value of i_{max} is not important. At higher temperatures, on the other hand, later members of the series become important and because the energy levels tend to a limit, χ the ionization energy, the last terms in the series are frequently the dominant ones since the g_i increase with i. The value of i_{max} is then of great importance in the calculation of the partition function and since the value of i_{max} depends on the interaction force and the density of interacting particles, it follows that the partition function must be density dependent. One consequence of this density dependence is that the perfect gas equation of state does not strictly hold (since the derivative of Q with respect to volume is not zero) but it is shown in Appendix I that the departure over the range of conditions considered here is negligible in the case of hydrogen (which is the only gas which can be treated analytically).

The termination of the partition function series is interpreted as a reduction in the number of bound states to a finite number which implies a reduction in the ionization potential. There will therefore be a corresponding change in the value of χ to be used in the mass action equation: the vacuum ionization potential χ has to be replaced by an effective ionization potential $\chi_{eff} = \chi - \Delta\chi$. This effect is additional to the influence of the partition function on the species composition. The effective ionization energy is related to the termination of the partition function by the obvious relation $E_{i_{max}} \leq \chi_{eff}$ while for hydrogen-like states, the highest bound quantum number n_{max} is given by the largest value of n_{max} satisfying the relation

$$\frac{hRc}{(n_{max})^2} \leq \Delta\chi \qquad (2.5)$$

where R is the Rydberg wave number constant.

The depression of the ionization potential clearly depends on the mechanism of interaction between the particles; at sufficiently low temperatures the interaction will be through a Van der Waals force but at such temperatures (except at extremely low densities) the partition function will be dominated by its leading terms and the details of the cut-off point are not important. At higher temperatures, the dominant interaction is by the electrostatic forces of charged particles and it is with this effect that we are concerned. The problem of the determination of $\Delta\chi$ as produced by the interaction of charged particles has received considerable attention but as yet there does not appear to be complete agreement on the model to be used. According to most authors, an adaption of the theory due to Debye and HÜckel for electrolytes[1] is valid in some form and over some range of relatively low densities and high temperatures while at high densities Unsöld's[2] nearest neighbor effect is dominant; a recent paper by Stewart and Pyatt[3] presents a more elaborate theory in which the Debye-HÜckel and nearest neighbor expressions appear as limiting cases. Bond, Watson and Welch,[4] however, suggest that at low densities and a low degree of ionization the Bohr radius should not exceed the mean distance between particles. These theories are discussed in the next paragraph but it should be remarked that even the best of them are not highly accurate since they all postulate a sharp cut-off between bound and free states and neglect the displacement of the higher bound levels which occurs due to external force fields.

The Debye-HÜckel theory examines the screening effect of charged particles surrounding an atom. According to this theory the characteristic

distance for the reduction in the Coulomb potential is the Debye radius, R_D, defined by

$$R_D \equiv \left[\frac{kT}{4\pi e^2(N_e + \sum_z z^2 N_z)}\right]^{1/2} \tag{2.6}$$

where N_e is the number of electrons per unit volume and N_z the number of z times charged particles per unit volume. One can now either[5] calculate the polarization energies of an ion and an electron and from them the reduction in ionization energy or[6] treat all states whose semi-major axis exceeds the Debye radius as free. These two procedures are qualitatively equivalent but lead to results which differ by a factor of two. These are respectively

$$\Delta\chi_z = (z+1)e^2/R_D \tag{2.7}$$

and

$$\Delta\chi_z = (z+1)e^2/2R_D \,. \tag{2.8}$$

The Debye-Hückel theory involves an averaging over charges which is only valid if the Debye sphere contains a minimum number of charged particles, according to Duclos and Cambel[7] the condition is

$$N_e + \sum_z N_z \geq \frac{1}{8\pi}\frac{1}{R_D^3} \tag{2.9}$$

which implies that there must be at least one sixth of a charged particle in the Debye sphere. Combining Eqs. (2.6) and (2.9) gives

$$\frac{N_e + \sum_z z^2 N_z}{N_e + \sum_z N_z}\left\{N_e + \sum_z z^2 N_z\right\}^{1/2} \leq \left[\frac{1}{\pi}\left(\frac{kT}{e^2}\right)^3\right]^{1/2} \tag{2.10}$$

and since the ratio $(N_e + \sum_z z^2 N_z)/(N_e + \sum_z N_z) \lesssim 2.6$ for $kT < 3eV$ and $\rho/\rho_o > 10^{-6}$, then Eq. (2.10) must become

$$N_e + \sum_z z^2 N_z \leq \frac{1}{7\pi} \left(\frac{kT}{e^2}\right)^3 . \tag{2.11}$$

It can thus be seen that the equality of Eq. (2.9) represents an upper bound on charged particle density since the Debye volume increases more rapidly than the charged particle density and hence the number of particles in the Debye volume must decrease as the number in unit volume in space increases. Ecker and Kroll[8] agree with the Duclos and Cambel result except for a factor of 3/4 in the limiting density. Bond, Watson and Welch[4] on the other hand suggest that the Debye criterion should be used provided $R_D > r_m$, the mean distance between particles (not electrons), otherwise the ionization limit should be depressed to the first state whose Bohr radius, a_n, is less than r_m. Since we have that

$$r_m \equiv \left[\frac{3}{4\pi} \frac{1}{N_a + \sum_z N_z}\right]^{1/3} , \tag{2.12}$$

where N_a is the number density of atoms, the condition for validity of the Debye theory becomes, inserting Eq. (2.12) into the relation $R_D \geq r_m$,

$$N_a + \sum_z N_z \leq \frac{3}{4\pi} \frac{1}{R_D^3} . \tag{2.13}$$

In contrast to Eq. (2.9) this constitutes an upper bound on the number of particles in the Debye sphere. As an example suppose that the first ion dominates, then since $N_e \simeq N_+$ and all other species are negligible, the combination of Eqs. (2.13) and (2.6) with (2.10) gives

$$\frac{1}{288\pi} \leq N_e \leq \frac{1}{\pi}\left(\frac{kT}{e^2}\right)^3 \qquad (2.14)$$

which is a very small range of conditions. Most recent workers,[3,5-9] however, use the Debye criterion at much lower densities than the lower limit of Eq. (2.14). we have to choose between the methods and, in the absence of any direct evidence, we follow the majority and do not use the mean particle distance criterion. The question remains as to whether the upper bound of Eq. (2.10) is ever reached in our range of conditions. Some numerical checks confirm that for temperatures above 1/2 eV, Eq. (2.10) is satisfied up to densities of at least 10 times atmospheric.

A calculation of species composition can therefore be set up as follows. Starting with arbitrary truncation points for the partition functions, the system of mass actior plus conservation equations are repeatedly solved and the results from each solution are used to calculate the depression of ionization potential according to Debye-Hückel theory and hence to correct the truncation points of the partition functions. The solution of the mass action and conservation equations for given partition functions is itself an iterative procedure. A rapidly convergent scheme is presented in Appendix IV. The composition calculation for nitrogen (some details of which are discussed in the next section) has been programmed for the IBM 360 computer and proves to be a rapidly convergent computation (50 points take less than 3 minutes).

2.3. The Composition of a Nitrogen Plasma

The application to nitrogen of some of the ideas of the previous section will now be discussed. The results of this section will be used in the radiative transfer calculations of Part 3.

The lowering of the ionization potentials of any of the components can be significant but the higher ions have such high excited energy levels that the truncation point of the partition functions is not relevant under our conditions. We therefore account for the effect in N and N^+ (details of the energy levels used are given in Appendix II) and include terms in the higher ions which contribute more than 1% (see Table 2.1 for details); the calculated partition functions of N and N^+ are plotted in Figs. 2 and 3. Debye-Hückel theory in the form Eq. (2.7) was used since the criterion is somewhat less arbitrary than that of Eq. (2.8).

It should be mentioned that use of an approximate partition function was investigated and the details are given in Appendix III. It seems worthwhile to give a summary here, however. If one truncates the partition functions after the first few terms, the errors in number densities of N and N^+ can be considerable, but it turns out that the electron density and the occupation numbers of the various energy levels are much more nearly correct. The electron density is little affected because at low ionization, where it is most sensitive to errors in $(Q_{el})_N$, either the temperature is low and therefore the cut-off point is unimportant, or the density is high and the "exact", density-dependent truncation point is at low energy levels, i.e., close to the arbitrary cut-off chosen for the approximate partition function. The occupation numbers are insensitive to partition function because where the truncated approximation is very badly in error, ionization is high and the partition function cancels out between the Saha equation and the Boltzmann formula (Eq. (2.1)), whereas at low ionization, the approximated partition function is more nearly correct. A detailed investigation of this approximation (Appendix III) shows that errors in occupation number of about 50% can occur at the higher temperatures and densities of the range

$1eV < kT < 3eV$, 10^{-6}atmos $< \rho/\rho_o < 1$ atmos. The investigation also revealed that the occupation numbers at high temperatures and low ionization are sensitive to the cut-off point of the partition function and hence even our density-dependent truncation point will not yield very accurate results under these conditions.

Finally, we consider the partition function of molecular species. Molecular species only exist at relatively low temperatures and hence there is no problem of truncation in the case of their partition functions. However, vibrational and rotational states also exist and are coupled to each other and to the electronic energy levels. As demonstrated in Appendix III, we will achieve the greatest accuracy if the partition functions used in the equations of chemical equilibrium are the same as those used in the Boltzmann formula. Because of this we are restricted in our treatment of the molecular partition functions of nitrogen to one which is consistent with the absorption cross section material of Allen[10] which we use for the radiative properties of the band-systems (see Part 3). Allen's data is, as far as we are concerned, a cross section per particle in the lower electronic state (superscript i) of the transition. We therefore have to find $(N^i)_S$, the number of molecules in the lower electronic state, with reasonable accuracy. This may be done by first solving the equations of chemical equilibrium for the total number of molecules, N_S, using the truncated partition functions in the form

$$(Q_{int})_S = \sum_{i=1}^{q_S} (Q_r^i)_S (Q_v^i)_S (g^i)_S \exp\left[-(E^i)_S/kT\right]$$

and then using the Boltzmann relation in the form

$$(N^i)_S = (g^i)_S (Q_r^i)_S (Q_v^i)_S N_S \exp\left[-(E^i)_S/kT\right]/(Q_{int})_S \quad .$$

The rotational and vibrational partition functions used are those given by Allen,

$$Q_v^i = [1 - \exp(-hc\omega_e^i/kT)]^{-1} \tag{2.15}$$

and

$$(Q_r^i) = kT/hcB_e^i \tag{2.16}$$

where ω_e^i and B_e^i are spectroscopic constants taken from Allen's report. These expressions treat the molecule as a harmonic oscillator and rigid rotor respectively. For N_2 the first excited level has an energy of 6.2eV and the summation for $(Q_{int})_{N_2}$ may be truncated after the first term, for N_2^+ on the other hand 3 excited levels must be included. Details are to be found in Table 2.1.

The partition functions of Table 2.1 were incorporated in a computer program to find the particle densities in nitrogen. The mass action equations for given partition functions were solved by the iterative technique discussed in Appendix IV. The results as functions of density and temperature are presented in Figs. 4 to 7. After these calculations were started, a paper by Drellishak, Aeschliman and Cambel[11] became available; they also use density dependent partition functions according to Debye-Hückel theory but choose the cut-off according to the alternative criterion (i.e., bound states have a semi-major axis less than the Debye radius) this gives rise to a somewhat higher value of partition function. Bearing in mind this difference and different molecular partition functions, the results of Ref. 11 are in reasonable agreement with ours.

TABLE 2.1

Expressions used for the partition functions of nitrogen

$$(Q_{int})_{N_2^+} = kT \times 10^3 \left\{ 8.34[1-\exp(-0.274/kT)]^{-1} + 18.56 \frac{\exp(-1.12/kT)}{[1-\exp(-0.236/kT)]} + 7.74 \frac{\exp(-3.18/kT)}{1-\exp(-0.300/kT)} \right\}$$

$$(Q_{int})_{N_2} = 4.03 \times 10^3 \times \frac{kT}{1-\exp(-0.292/kT)}$$

$(Q_{el})_N$ density dependent, see Appendix II for energy levels.

$(Q_{el})_{N^+}$ density dependent, see Appendix II for energy levels.

$$(Q_{el})_{N^{++}} = 6 + 12 \exp(-7.102/kT)$$

$$(Q_{el})_{N^{+++}} = 1 + 9 \exp(-8.340/kT)$$

$$(Q_{el})_{N^{++++}} = 2 + 6 \exp(-10.003/kT)$$

3. BOUND-BOUND TRANSITIONS

3.1. Introduction

Bound-bound transitions occur between discrete energy levels of the atom. They would therefore occur at a precise value of frequency if it were not for certain perturbations of the energy levels due primarily, in our case, to neighboring particles. These perturbations are discussed in the next chapter under the title "Line-Broadening" and it is sufficient to observe here that for all cases of interest to us the resulting line width is very small in the sense that the spectral structure of a line is on a quite different scale of frequency variation than those of either the Planck function or the continuous absorption coefficient arising from other processes.

This difference in scale leads to two important simplifications of the transfer problem. In the first place, the Planck function can be taken as constant across a line and for some line profiles analytic expressions for line intensity can be obtained (Section 3.3 discusses some relevant cases). In the second place, although the transfer problem is highly non-linear in absorption coefficient, an effective separation of the frequency integrated intensity into line and continuum contributions occurs if the state of the gas is uniform.

This second simplification can be easily demonstrated as follows. The formal solution of the equation of radiative transfer (Eq. 1.1) in a uniform medium with cool, transparent walls is

$$I = \int_0^\infty d\nu B_\nu [1-\exp(-K_\nu s)] \qquad (3.1)$$

Now, let $K_{\nu L}$ and $K_{\nu C}$ be the absorption coefficients due to lines and continuum respectively. Then, $K_\nu = K_{\nu L} + K_{\nu C}$ and, adding $B_\nu[\exp(-K_{\nu C}s)-\exp(-K_{\nu C}s)]$ to the integrand of Eq. (3.1), we get

$$I = \int_0^\infty d\nu B_\nu[1-\exp(-K_{\nu L}s)]\exp(-K_{\nu C}s) + \int_0^\infty d\nu B_\nu[1-\exp(-K_{\nu C}s)]$$

Finally, if we recognize that the term $1-\exp(-K_{\nu L}s)$ is negligible compared to the second term everywhere except in the neighborhood of the unperturbed line frequencies ν_i, we can write

$$I = \sum I_{Li} \exp(-K_{\nu iC}s) + I_C \qquad (3.2)$$

where we define

$$I_{Li} \equiv B_{\nu i}\int_0^\infty d\nu[1-\exp(-K_{\nu L}s)]$$

and

$$I_C \equiv \int_0^\infty d\nu B_\nu[1-\exp(-K_{\nu C}s)] \quad .$$

This result is apparently well known.[12,13] The interpretation is that near a line the line and continuum coefficients each reduce the intensity associated with the other but the overall effect on the continuous radiation is negligible because the frequency intervals affected are very small while the reduction in each line gives rise to a factor $\exp(-K_{\nu iC}s)$.

A further simplification of line transfer problems arises from the fact that the value of the frequency integrated line cross section is independent of the line profile. Because of this the cross section for a transition from

a lower state J to an upper state J' can be written in the form

$$\sigma_{\nu JJ'} = \frac{\pi e^2}{mc} f_{JJ'} L(\nu) \tag{3.3}$$

where $L(\nu)$ represents the line profile defined so that $\int_0^\infty L(\nu)d\nu = 1$ and $f_{JJ'}$, the f-number, is defined in terms of the dipole matrix element of quantum mechanics and thus depends on the wave functions of the two states involved. It may also be interpreted as a correction to the classical solution for the energy radiated by a harmonic oscillator and for this reason it is frequently called an oscillator strength. The determination of f and of $L(\nu)$ are largely separate problems; the former is discussed in Section 3.2, but a complete chapter (Chap. 4) is devoted to a discussion of line profiles. The final three sections of this chapter consider solutions to the transfer equation for lines with some common types of profiles and a treatment of the problem of the merging of closely spaced lines as, for example, in multiplets.

3.2. Oscillator Strengths

The oscillator strength of a line is equal to a constant times the frequency integrated cross section as can be seen from Eq. (3.3). In Russell-Saunders coupling (which holds for the stronger lines of most light or medium elements), the radial and angular contributions to the matrix element may be separated and the oscillator strength written in the form[14]

$$f_{JJ'} = \frac{8\pi^2 m_e}{3h} \frac{\nu_{JJ'}}{g_J} S(L) S(L') \sigma^2 \tag{3.4}$$

where g_J is the statistical weight of the lower state and the remaining factors are as follows. $S(L)$ is the relative strength of a line within

a multiplet, it depends on inner quantum numbers J and J' and on total angular momentum quantum numbers L and L'. Values of $f(\ )$ have been compiled by Allen.[15] $f(\ )$ is the relative strength of a multiplet within a transition array. An early paper by Goldberg[16] gives tables of a related quantity from which $f(\ )$ can be obtained with the aid of a normalizing factor,[17] fortunately most of Goldberg's values have been normalized and tabulated in the books by Allen[15] and Aller.[18] In order to take account of the possible parentages of a number of equivalent electrons, a further paper by Menzel and Goldberg[19] is sometimes required (where Ref. 19 does not apply see Kelly and Armstrong[20]). These tabulations are convenient to use but unfortunately they do not cover all the cases of interest and for the exceptions it is necessary to turn to the more general expressions obtained by Rohrlich[21] (which are also presented by Griem[5]) and by Shore and Menzel.[22] These expressions take account of the parentage of equivalent electrons and they give both $f(\ )$ and $f(\ )$ in terms of the Racah coefficients which are tabulated in a number of places,[5,23-25] the most extensive of which appears to be that of Nikiforov.[24] The final quantity appearing in Eq. (3.4), σ, is the radial matrix element for the jumping electron. It is the determination of this quantity which is the main problem in f-number calculations; some of the methods currently available are discussed in the following paragraphs.

The most popular general method is that due to Bates and Damgaard[26] (which is also given in detail in Griem's book[5]). They observed that the most significant contribution to the radial matrix element σ frequently comes from a region in which the potential has almost reached its asymptotic Coulomb orm. They therefore use hydrogenic wave functions but replace each principal quantum number n by an effective quantum number n^* determined

from the experimentally measured value of tne energy level. Comparison of this method with experimental results and the predictions of more accurate theoretical methods shows good agreement when the jumping electron is outside closed shells or in an excited level, but may be orders of magnitude in error when the jumping electron is one of a number of equivalent electrons. Griem[5] has evaluated f-numbers using the Bates-Damgaard method for many of the lines listed in Refs. 27 and 28. A check of his values for some lines of NI against the results due to Kelly (see below) of more accurate self-consistent field methods shows good agreement in the visible and infrared, but an underestimate of approximately an order of magnitude for the ultraviolet lines. This discrepancy is due to the fact that ultraviolet lines originate from particles in a low state of excitation where the Bates and Damgaard method is least accurate. Another defect is that this method cannot predict values for transitions between states within the same shell (which often give rise to very strong lines). Finally, a modification to the Bates and Damgaard method which takes some account of the nonhydrogenic form of the wave functions may be found in the paper by Burgess and Seaton[29] whose primary purpose is to develop a similar method for bound-free transitions. This modification removes the worst inaccuracies of the Bates and Damgaard method (naturally at the expense of greater complication) but depends on experimental knowledge of energy levels which is unfortunately not always available.

Nonhydrogenic wave-functions are used in the class of methods known as self-consistent field approximations. Of these, the most widely used for accurate calculations is based on the wave-functions of Hartree and Fock. It is, however, very lengthy and has only been applied to a few lines of a few elements. Kelly[30] has used it to calculate f-numbers for several

important lines in the ultraviolet spectra of nitrogen and oxygen; these calculations can be expected to be accurate to about 20%. Also due to Kelly is an extensive list[62] of values of σ^2 for nitrogen and oxygen which he calculated using a simplification due to Slater of the Hartree-Fock method. Thanks to these values one can calculate the oscillator strengths for any of the important lines of nitrogen and oxygen to within a factor of about 2 and can reasonably expect the average accuracy of all the strong lines to be rather better than that.

3.3. The Curve of Growth for a Single Line with Wing Profile $b/(\nu-\nu_o)^a$

It was pointed out in Section 3.1 that the equation of radiative transfer for a line is simplified by the narrowness of the line. For a single line Eq. (3.1) therefore becomes

$$I = B_{\nu_o} \int_0^\infty [1-\exp(-K_\nu s)]d\nu \quad . \tag{3.5}$$

Performing the quadrature in Eq. (3.5) clearly requires the specification of the function $K_\nu(\nu)$. However, when $K_\nu s \ll 1$ for all ν the expression reduces to

$$I = B_{\nu_o} s \int_0^\infty K_\nu d\nu \tag{3.6}$$

which is a particular form of the well-known optically thin limit; it should be observed that this expression does not depend on the profile (compare Eq. (3.3)). There are a number of profiles for which the integration in Eq. (3.5) can be performed in closed form. However, we will be concerned here with the asymptotic limit of large path-length for a particular class of profiles.

The normalized profile $L(\nu)$ of Eq. (3.3) which we will consider has the form

$$L(\nu) \sim \frac{b}{|\nu-\nu_o|^a}, \qquad a > 1$$

for $\nu-\nu_o >> b$. The results to be derived are not new, at least expressions for the important cases of $a = 2.0$ and $a = 2.5$ can be found, but no derivation appears to be available and the general form does not appear to have been obtained before. For sufficiently large path-length, the line will become heavily self-absorbed near the line center and the intensity in this core region will be B_{ν_o}, independent of the core profile, the only effective part of the absorption coefficient will then have the form

$$K_\nu = \int_0^\infty K_\nu d\nu \times b/|\nu-\nu_o|^a$$

Defining the transformation $z \equiv K_\nu s$ and taking appropriate care of the limits we get from Eq. (3.5)

$$I = B_{\nu_o} 2\frac{1}{a}(bs\int_0^\infty K_\nu d\nu)^{1/a}\int_0^\infty z^{-(1+1/a)}(1-e^{-z})dz \qquad (3.7)$$

The integral over z of Eq. (3.7) may be performed by parts to yield

$$I = 2\frac{1}{a}(bs\int_0^\infty K_\nu d\nu)^{1/a} B_{\nu_o}[a(1-e^{-z})z^{-1/a}\Big|_0^\infty + a\int_0^\infty z^{-1/a}e^{-z}dz] \qquad (3.8)$$

where the first term in the square bracket is zero for $a > 0$ and the second term is a form of the complete gamma function for $a > 1$. Equation (3.8) therefore becomes

$$I = 2B_{\nu_o} (bs\int_0^\infty K_\nu d\nu)^{1/a} \Gamma\left(1 - \frac{1}{a}\right) \quad . \tag{3.9}$$

It now becomes convenient to define quantities w and τ as follows

$$w \equiv b^{1/(a-1)}\left[\Gamma\left(1 - \frac{1}{a}\right)\right]^{a/(a-1)} \tag{3.10}$$

and

$$\tau \equiv s\int_0^\infty \kappa_\nu d\nu/w \quad . \tag{3.11}$$

Then Eq. (3.9) can be written

$$I/2wB_{\nu_o} = \tau^{1/a} \tag{3.12}$$

and the corresponding form of the optically thin result (Eq. (3.6)) is

$$I/2wB_{\nu_o} = \tau/2 \quad . \tag{3.13}$$

The intersection of these two curves occurs at

$$\tau = 2^{a/(a-1)} \tag{3.14}$$

For $\tau > 2^{a/(a-1)}$ we call the line self-absorbed (or, sometimes, optically thick), for $\tau < 2^{a/(a-1)}$ we describe the line as not self-absorbed or optically thin.

The quantity w has the dimensions of frequency and can be interpreted as representing the width of the absorption coefficient profile (as we will show, it is precisely the semi-half-width of a dispersion profile). The dimensionless parameter τ is an optical depth based on an absorption coefficient $\int_0^\infty K_\nu d\nu/w$. The relationship between this absorption coefficient and that of a line with a dispersion profile ($a = 2$) is sketched on Fig. 8a; it

can be seen that in this case, the value of $\int_0^\infty K_\nu d\nu/w$ is π times the peak absorption coefficient of the line. The quantity I/B_{ν_0} has the dimensions of frequency and will be called the "effective" or "equivalent" width of the line. From this definition it follows that the energy transferred by a line is equal to the effective width of the line times the value of the Planck intensity at the line center. When the line is self-absorbed, so that the central part of the line is blackened out, the effective width has a fixed relationship to the intensity profile (specifically, half the effective width is the distance from the line center at which the spectral intensity has a value of $1 - \exp\{-[\Gamma(1 - \frac{1}{a})]^{-a}\}$ times the black-body value). Figure 8b shows the equivalent width and the spectral distribution of intensity for a typical self-absorbed line. When the line is not self-absorbed, the equivalent width is still defined as before but it is no longer meaningful as a representative width of the intensity profile (see Fig. 8c). Finally, the ratio of effective width to line width (i.e., absorption coefficient half-width) is $I/2wB_{\nu_0}$. This quantity has the value $2^{1/(a-1)}$ at the intersection point of the asymptotic relationships Eqs. (3.12) and (3.13).

The two cases of most interest are those of a dispersion profile, where $a = 2$, and a quasi-statically broadened line, where $a = 2.5$. The corresponding forms of Eqs. (3.12), (3.13) and (3.14) are to be found in Refs. 31 and 32. Reference 31 also obtains the complete curve of growth of a pure dispersion profile and it is of interest to compare the asymptotic forms to the exact curve. A dispersion profile has the form

$$L(\nu) = \frac{1}{\pi} \frac{w_{dis}}{(\nu-\nu_o)^2+w_{dis}^2} \tag{3.15}$$

where w_{dis} is the semi-half-width (i.e., it is half the width of the line

where the absorption coefficient has half its maximum value). This profile becomes $w_{dis}/\pi(\nu-\nu_o)^2$ in the wings and, using $\Gamma(1/2) = \sqrt{\pi}$ in Eq. (3.10), we obtain $w = w_{dis}$.

The exact curve plotted from values given by Penner[31] is shown on Fig. 9 and compared with the asymptotic results Eq. (3.12) and (3.13). It can be seen that the line is well approximated by its asymptotic forms, the maximum error being about 10%. It will be seen later that in practice lines sometimes depart from the true dispersion profile in the core. In such cases the asymptotes discussed here are a slightly better approximation to the correct curve of growth than the true dispersion curve of growth is.

3.4. The Curve of Growth for a Group of Lines with Wing Profiles $b/(\nu-\nu_o)^a$

As one passes along a ray, the intensity and hence the effective width of a line increases and, in many cases, eventually interferes with neighboring lines. This section discusses the effect of this interference as it occurs in a group of lines in a uniform gas. The method of presentation is as follows. First, we consider a multiplet of lines with dispersion profiles and give a simplified model of the curve of growth, we then extend this result to a more general group of lines and finally apply the same ideas to a group of quasi-statically broadened lines.

A multiplet is the group of all transitions between two terms. The individual lines therefore arise from the splitting of energy levels by the inner quantum number, J. This splitting is so small that the Planck function can be taken constant across the multiplet; the multiplet, however, cannot in general be treated as a single degenerate line since for an important range of conditions the individual lines are isolated from each other. An exact treatment of the behavior of a multiplet must take into account the

spacing and strengths of the lines and is therefore both complicated and different for each multiplet.

We first discuss three parts of the curve of growth of a typical multiplet. Consider a multiplet containing N lines with dispersion profiles, and assume that the lines each have the same half-width w but different strengths. We define an equivalent width for the multiplet, $W \equiv I/B_{\nu_o}$ where I is the total integrated intensity and B_{ν_o} is the Planck intensity at the center frequency of the multiplet. The equivalent width ratio, W_r, is defined by $W_r \equiv W/2w = I/2wB_{\nu_o}$. Now, at low densities and small path-lengths all the lines are optically thin and we may write

$$W_{r,1} = \tau_m/2 \tag{3.16}$$

where, for a path-length s, τ_m is given by

$$\tau_m \equiv \frac{s}{w} \sum_{i=1}^{N} \int_o^\infty K_{\nu i} d\nu. \tag{3.17}$$

Usually, there will be some optically thicker condition at which all the lines are self-absorbed but no significant overlapping occurs; in this case one gets

$$W_{r,2} = \sqrt{N^*}\ \sqrt{\tau_m}, \tag{3.18}$$

where

$$\sqrt{N^*} \equiv \sum_{i=1}^{N} \left(\int_o^\infty K_{\nu i} d\nu\right)^{1/2} / \left(\sum_{i=1}^{N} \int_o^\infty K_{\nu i} d\nu\right)^{1/2} = \sum_{i=1}^{N} [f_i(\ell)]^{1/2} \tag{3.19}$$

and is a property of the multiplet. One can show without much difficulty that $N^* \leq N$. Finally, for very large optical depths the multiplet width will be much less than the effective line widths and the whole group will

behave like a single line:

$$W_{r,3} = \sqrt{\tau_m} \tag{3.20}$$

Clearly from Eqs. (3.18) and (3.20), the error in treating a multiplet as a single line under conditions where the lines are isolated but self-absorbed is an underestimate by a factor $\sqrt{N^*}$. If the lines are very closely spaced the group can behave like a single line as soon as it becomes self-absorbed but multiplets of low-lying states invariably exhibit a considerable range of the intermediate growth rate at conditions of interest to us. We will therefore consider Eqs. (3.16), (3.18) and (3.20) as holding for three major regions of growth and discuss the transitions between them. A typical curve of growth is sketched on Fig. 10.

The intersection between the curves defined by Eqs. (3.16) and (3.18) occurs at

$$\tau_m = 4N^* \tag{3.21}$$

This intersection point corresponds to the point of change from optically thin to optically thick behavior of an isolated line whose absorption coefficient is

$$\int_0^\infty K_\nu d\nu = \sum_{i=1}^{N} K_\nu d\nu / N^*$$

Curves (3.18) and (3.20) do not intersect but curve (3.20) will start to describe the growth somewhere in the neighborhood of the optical path length for which the effective line width of the multiplet treated as a single line (W_3) equals the frequency spread of the multiplet, similarly, it will depart from the behavior of Eq. (3.18) approximately when the effective line width of a single line equals the average inter-line spacing of the multiplet.

The behavior between these two points may vary considerably, however, as may be seen from the following two examples.

Firstly, suppose that the lines are of uniform strength and evenly spaced. Then the overlapping of adjacent lines will occur simultaneously, the entire center-portion of the multiplet will be blackened out, and growth will occur only by virtue of the wings of the two outermost lines. There will therefore be a region of relatively slow growth until the effective width of the inner lines exceeds the spread of the multiplet and the behavior of Eq. (3.20) commences, this type of transition is shown on Fig. 10.

As a second example, suppose that the N lines occur in M well separated clusters of closely spaced lines of approximately equal strength. After the growth as isolated lines, the line centers of the M clusters will blacken out first and the M clusters will each, as in the previous example, have a relatively slow rate of growth until a point is reached where the effective line widths exceed the inter-line spacing within each cluster and the multiplet then starts to behave like M isolated lines. Finally, after another transition region of slow growth, the multiplet will behave like a single line. The case where $M = 2$ is shown on Fig. 10.

A number of multiplets of NI were examined and found to be more closely approximated by the case of evenly spaced lines than by the case of isolated clusters. However, the concept of isolated clusters is useful since we will see in Part 3 that it is sometimes possible to group together weak, adjacent multiplets. In most cases these do not ever merge to a super-line in our range of conditions and the model we treat is that of N lines distributed in M non-merging clusters.

The intersection of the optically thin region with the self-absorbed but isolated region does not depend on M, so for $\tau_m \leq 4N^*$ we use Eq. (3.16).

For $\tau_m > 4N^*$ we treat the lines as isolated (Eq. (3.18)) until $W_2 = D$ where D is the sum of the widths of all the clusters. Then for $D\sqrt{N^*/M^*} > W_2 > D$ the transition region of slow growth commences and the equivalent width is approximately constant and given by

$$W_{23} = D \tag{3.22}$$

From here on ($W_3 = W_2\sqrt{M^*/N^*} \geq D$) we treat the system as M isolated clusters by means of the equation

$$W_{r,3} = \sqrt{M^*}\ \sqrt{\tau_m} \tag{3.23}$$

where

$$\sqrt{M^*} = \sum_{i=1}^{M}\left(\int_0^\infty K_{\nu i}d\nu\right)^{1/2}/\left(\sum_{i=1}^{M}\int_0^\infty K_{\nu i}d\nu\right)^{1/2} \tag{3.24}$$

Lines with moderately highly excited upper states are subject to quasi-static broadening, as discussed in the chapter on line broadening (Chap. 4). They are also relatively weak and at least partially degenerate. The ideas of this section can be applied with certain modifications. No permanently isolated clusters exist so that the equivalent of $\sqrt{M^*}$ is unity. The growth rate is slower (a single self-absorbed line grows as $\tau^{2/5}$ compared to the dispersion rate of $\tau^{1/2}$) and the equations to be used are as follows. We start by recalling from Section 3.3 the definition of equivalent line width

$$w \equiv b^{2/3}[\Gamma(3/5)]^{5/3} \tag{3.25}$$

where b is a constant obtained from the asymptotic form of the normalized Holtsmark profile, $L(\nu) \sim b/(\nu-\nu_o)^{5/2}$. The corresponding optical depth for

a group of lines is

$$\tau_m \equiv s \sum_{i=1}^{N} \int_0^\infty K_{\nu i} d\nu / w \tag{3.26}$$

and the effective number of lines is

$$N^* \equiv \left[\sum_{i=1}^{N} \left(\int_0^\infty K_{\nu i} d\nu \right)^{2/5} / \left(\sum_{i=1}^{N} \cdot \int_0^\infty K_{\nu i} d\nu \right)^{2/5} \right]^{5/3} \tag{3.27}$$

Then, if

$$\tau_m \leq 2^{5/3} N^* \tag{3.28}$$

we use

$$I = B_{\nu_o} \tau_m w \quad . \tag{3.29}$$

However, if $\tau_m > 2^{5/3} N^*$, the expression to be used depends upon the effective width

$$W = 2(N^*)^{3/5} \tau_m^{2/5} w \quad .$$

If $W \leq D$ we have

$$I = B_{\nu_o} W \tag{3.30}$$

but if $W > D$ and $W(N^*)^{-3/5} \leq D$ the intensity is given by

$$I = B_{\nu_o} D \tag{3.31}$$

and, finally, for $W(N^*)^{-3/5} > D$ we have

$$I = B_{\nu_o} W(N^*)^{-3/5} \tag{3.32}$$

These growth expressions have been programmed as a FORTRAN subroutine for a general wing decay law $b/(\nu-\nu_o)^a$ and will be applied in the calculations presented in Part 3.

3.5 The Curve of Growth for Doppler Broadened Lines

This section is concerned with the radiation from Doppler broadened lines. The approach is analogous to that of Sections 3.3 and 3.4. However, the form of the Doppler profile causes an additional difficulty which requires special treatment. First we discuss approximations to the single-line curve of growth and then consider the treatment of groups of lines.

The broadening of a line due to the thermal motion of the radiating particles is known as Doppler broadening and is discussed in Section 4.2. The resulting absorption coefficient can be written in the form

$$K_\nu = K_{\nu_o} \exp\{- [\frac{(\nu-\nu_o)\sqrt{\ell n\ 2}}{w_D}]^2 \} \tag{3.33}$$

where w_D is the semi-half-width of a Doppler broadened line given by (see Eq. (4.2))

$$w_D = \frac{\nu_o}{c} (\frac{2kT}{m_R} \ell n\ 2)^{1/2} \tag{3.34}$$

and K_{ν_o} is the peak absorption coefficient. This peak value is related to the frequency-integrated absorption coefficient by the expression

$$K_{\nu_o} = \int_o^\infty K_\nu d\nu \times \sqrt{\frac{\ell n\ 2}{\pi}}\ \frac{1}{w_D} . \tag{3.35}$$

The intensity is given by substituting the expression for K_ν into Eq. (3.5) and changing the variable of integration to $x \equiv (\nu-\nu_o)\sqrt{\ell n\ 2}/w_D$, to

obtain

$$\frac{I\sqrt{\ln 2}}{B_{\nu_o} w_D} = \int_0^\infty \{1 - \exp[-K_{\nu_o} s \exp(-x^2)]\}dx. \tag{3.36}$$

The above integration cannot be performed in closed form. Penner[31] presents a series representation of Eq. (3.36); the series is uniformly valid but only converges reasonable rapidly at comparatively low values of optical depth. Penner also gives a simple expression which is approximately correct for small optical depth and an asymptotic expansion for large optical depth. For our purposes, the approximate expression and the leading term of the asymptotic expansion are all that are required. These are respectively,

$$\frac{I\sqrt{\ln 2}}{B_{\nu_o} w_D} = \sqrt{\pi}\,\tau_D \exp(-\sqrt{\tau_D}/2) \tag{3.37}$$

and

$$\frac{I\sqrt{\ln 2}}{B_{\nu_o} w_D} = 2\sqrt{\ln \tau_D} \tag{3.38}$$

where

$$\tau_D \equiv K_{\nu_o} s.$$

τ_D is analogous to the τ of Section 3.3 except for a constant, $(\ln 2/\pi)^{1/2}$ (compare Eq. (3.35)).

The curves defined by Eqs. (3.37) and (3.38) intersect at the point $\tau_D \tilde{=} 26$. If one uses Eq. (3.38) for $\tau_D > 26$ and Eq. (3.37) for $\tau_D < 26$ than the error compared to the exact curve is always within about 15%. The exact and approximate curves are compared on Fig. 11.

Using Eqs. (3.37) and (3.38), the specific intensity from a multiplet of N lines can be written in the form

$$\frac{I\sqrt{\ln 2}}{B_{\nu_o} w_D} = R_1 \sqrt{\pi}\, \tau_{D,m} \exp[-(\tau_{D,m}/N)^{1/2}/2] \tag{3.39}$$

or

$$\frac{I\sqrt{\ln 2}}{B_{\nu_o} w_D} = R_2\, 2\sqrt{\ln \tau_{D,m}} \tag{3.40}$$

where

$$\tau_{D,m} \equiv \Big(\sum_{i=1}^{N} K_{\nu_o,i}\, d\nu\Big) s = \sum_{i=1}^{N} \tau_{D,i}$$

and R_1 and R_2 are given by the expressions

$$R_1 = \sum_{i=1}^{N} \frac{\tau_{D,i}}{\tau_{D,m}} \exp\Big(-\frac{1}{2}\big[\sqrt{\tau_{D,i}} - \sqrt{\tau_{D,m}/N}\big]\Big) \tag{3.41}$$

and

$$R_2 = \sum_{i=1}^{N} \Big(\frac{\ln \tau_{D,i}}{\ln \tau_{D,m}}\Big)^{1/2} . \tag{3.42}$$

By reference to Section 3.4 it can be seen that, for a dispersion profile, the quantities corresponding to R_1 and R_2 are unity and $\sqrt{N^*}$ respectively. N^* is a property of the multiplet. It is unfortunate that in the Doppler broadened case, both R_1 and R_2 depend on the distance s and on the line width w_D.

Any expressions for R_1 and R_2 would be useful which involved only a universal property of the multiplet and the optical depth for the multiplet $\tau_{D,m}$. Such expressions mean that it is unnecessary to treat each line individually.

Unfortunately, it has not proved possible to express R_1 and R_2 in this way except where the lines are of equal strength. In this case, one gets

$$R_1 = 1 \quad \text{and} \quad R_2 = N \ln(\tau_{D,m}/N)/\ln \tau_{D,m}. \tag{3.43}$$

One may also observe that in the general expression (3.41) as $\tau_{D,m} \to 0$, $R_1 \to 1$, the equal strength value of Eq. (3.43).

In order to avoid considering the individual strength of each line of a Doppler broadened multiplet, Eq. (3.43) may be used as an approximation for lines of unequal strengths. Some checks of the accuracy of Eq. (3.43) against actual multiplets revealed errors of 20%-30%.

The effect of overlapping intensity profiles can be treated in exactly the same way as when the lines are dispersion or quasi-statically broadened (see Section 3.4).

We remark in closing this section that the far wings of a real line never have a Doppler form. However, the treatment of a line with a profile formed by different broadening mechanisms depends on the relative sizes of the associated line widths and a discussion is delayed until Section 4.7.

4. LINE BROADENING*

4.1 Introduction

It has been pointed out in Chap. 3 that the radiation associated with bound-bound transitions is confined to a small interval of frequency but that when self-absorption occurs, the profile $L(\nu)$ plays an important role in determining the amount of energy transferred. This chapter considers the problem of calculating the function $L(\nu)$. It particularly deals with forms which are simple enough to be of use in the prediction of radiative transfer from the many lines of a non-hydrogenic gas. As in other sections, some of the discussion is about nitrogen and will be applied in Part 3.

There are three mechanisms which can cause line broadening. (a) Since atomic states have finite lifetimes, the uncertainty principle implies that there must be a range of possible energies associated with each state and hence a range of frequencies for every line. This phenomenon is called natural broadening (or radiation damping). (b) Because of the Doppler effect, the frequency of emission (or absorption) of radiation by a particle in motion is shifted according to the velocity along the line of emission (or absorption). The macroscopic result in a gas where the particles are in thermal motion is therefore a broadening of the line. (c) The third mechanism is a perturbation of the energy levels of the radiating atom resulting from interactions with other particles; this is called pressure broadening. The interactions of importance are due to the van der Waals force, the electric fields of charged particles (called Stark broadening) and the coupling of two similar particles (called resonance or self-broadening). Of

*We are indebted to Professor Hans R. Griem of the University of Maryland who very kindly discussed with us a number of points in connection with the treatment of line profiles and who supplied us with references 37, 39 and 43.

these mechanisms, those of importance in a non-hydrogenic gas in the range of conditions 10^{-5} to 1 atmosphere density and 5000 to 35000°K are Doppler, resonance and Stark broadening, they are each discussed in greater detail in the following sections, Stark broadening is given the greatest attention because of its dominance and complexity.

4.2. Doppler Broadening

The theory of Doppler broadening is well established and may be found in a number of texts (e.g., Refs. 31, 33). In the absence of any other broadening mechanism it involves a statistical average over the Doppler shifts of the individual particles. It is therefore a purely temperature dependent effect which produces a characteristic, symmetrical, narrow line with very low wings. Analytically, the line shape is

$$L(\nu) = \frac{1}{\sqrt{\pi}} \frac{\sqrt{\ell n\ 2}}{w_D} \exp\left[- \frac{(\nu-\nu_o)^2 \ell n\ 2}{w_D^2}\right] \qquad (4.1)$$

where ν_o is the line center frequency and w_D is half the width at half the peak intensity (i.e. $L(\nu_o \pm w_D) = \frac{1}{2} L(\nu_o)$) it is given by

$$w_D = \frac{\nu_o}{c} \sqrt{\frac{2kT}{m_R} \ell n\ 2} \qquad (4.2)$$

where m_R is the mass of the radiating particle.

4.3 Resonance Broadening

Resonance broadening occurs where the radiating and perturbing particles are of the same type and are uncharged (since otherwise Stark broadening would far exceed the resonance interaction). From the point of view of classical mechanics one can consider the gas as consisting of a collection

of oscillators which are coupled by some force (e.g. an electrostatic force), the interaction of the oscillators through this force results in each oscillator having a spread of frequencies around its natural value. When the oscillators have the same natural frequency, a resonance effect greatly strengthens the coupling force and produces a greater spreading of frequencies; it is this phenomenon which is called resonance broadening. Now, imagine the perturber in an initial state 1. If the upper state 2 of the radiating transition can be reached from state 1 by a dipole transition, then the perturbing atom will broaden state 2 by a resonance interaction. Clearly this is only of importance where there are a significant number of particles in state 1. This implies that state 1 must have a low-lying energy level because there will only be a significant number of atoms if the temperature is low while at low temperatures the number of excited states is small.

Resonance broadening results in unshifted dispersion profiles,

$$L(\nu) = \frac{1}{\pi} \frac{w_{res}}{(\nu-\nu_o)^2 + w_{res}^2} \tag{4.3}$$

where w_{res} (the semi-half-width) may be calculated in an impact approximation (see next section) and has the form[5]

$$w_{res} \tilde{=} 3\pi \left(\frac{g_\ell}{g_u}\right)^{1/2} \left(\frac{e^2 f_{res}}{m_e 2\pi \nu_{res}}\right) N_a. \tag{4.4}$$

Here f_{res}, ν_{res}, g_ℓ and g_u all belong to the resonance line and are, respectively, the absorption oscillator strength, the frequency, the lower state statistical weight and the upper state statistical weight, N_a is the number of perturbing atoms per unit volume. Evaluating the constant,

Eq. (4.4) becomes

$$w_{res}(ev) \tilde{=} 0.175 \times \left(\frac{g_\ell}{g_u}\right)^{1/2} f_{res} \frac{1}{h\nu_{res}(ev)} \frac{N_a}{N_L} \qquad (4.5)$$

where N_L is the Loschmidt number.

It can easily be checked that for transitions from low-lying states under conditions of low ionization this line width can be greater than that due to Stark broadening (see next section).

4.4 A Brief Review of the Theory of Stark Broadening

The problem of Stark broadening (i.e. the broadening of spectral lines by charged particles) has received considerable attention, but until recently the treatments were unsatisfactory in a number of important respects. Now, however, the work of Griem, Baranger, Kolb and their co-workers has provided a general, accurate theory (see Refs. 5, 34 and papers referred to therein). This section gives a brief description of some of the main features of the broadening mechanism and its theoretical treatment with particular emphasis on non-hydrogenic gases.

A detailed discussion of the Stark effect is given, for example, by Bethe and Salpeter[35] and so only a very brief description need be given here. When an atom is subjected to an electric field, the energy levels are each split into a number of components. If this is viewed as a perturbation problem where the expansion parameter is the field strength, then it turns out that the first-order effect is identically zero and the magnitude of the splitting is proportional to the square of the field strength ("quadratic Stark effect") except for very strong fields (where higher order effects become important) and for energy levels which are degenerate with respect to the orbital angular quantum number, ℓ, where the first-order (linear)

effect occurs and is dominant. Since hydrogen and its isoelectronic sequence (He II, Li III, etc.) and the highly excited states of more complex atoms are degenerate with respect to ℓ, the linear Stark effect governs the splitting of the associated energy levels; under these circumstances it turns out that (in contrast to levels split by the quadratic Stark effect) broadening by the slowly moving ions is important and the full apparatus of modern line-broadening theory is required to account properly for the complex line shapes which result (see Refs. 5 and 34).

We turn now to the theoretical treatment of line broadening through the Stark effect. An exact analysis would proceed as follows: the field at the radiating atom is calculated for a general sequence of perturbers with different velocities and trajectories, this field is then substituted into a quantum mechanical expression describing the transition and a statistical average over the perturbers performed to yield the line shape. Fortunately, in practice this procedure can be considerably simplified by the existence of two good approximations which are asymptotically correct in the opposing limits of interaction times which are, in one case, very much less than $(|\nu-\nu_o|)^{-1}$ (the impact approximation) and, in the other case, very much greater than $(|\nu-\nu_o|)^{-1}$ (the quasi-static approximation). In the impact approximation, corresponding to rapidly moving particles, the process is treated as a series of discrete encounters with single particles. In the quasi-static approximation, for slowly-moving particles, the perturbations on any given emitter are treated as coming from a cloud of stationary particles. In both cases, statistical averaging is necessary to achieve a macroscopic result. Electrons, being rapidly moving, can nearly always be treated by the impact approximation; in principle, for $\nu-\nu_o$ sufficiently large, electrons should be treated by the quasi-static approximation. Although this effect is significant for some hydrogenic lines, it is of no importance

for non-hydrogenic lines whose wings decay to a negligible level more rapidly than the wings of hydrogenic lines (see Ref. 5, pages 92 and 93).

Ions sometimes broaden according to the impact approximation, sometimes according to the quasi-static approximation and sometimes according to neither limit. Fortunately, the quasi-static approximation always holds for ion perturbers in the wings of a line and where it may break down, i.e. near the line center, electron broadening usually dominates. Indeed, the influence of ion perturbers in a non-hydrogenic gas may often be neglected entirely without losing reasonable accuracy; this is particularly true where the radiating particle is itself an ion, since the local density of positively charged particles will be reduced. The linear Stark effect greatly increases the broadening effect of ions so that the study of hydrogenic lines requires proper accounting for both electronic and ionic broadening.

The simultaneous action of ions and electrons is treated by a simplified form of the exact treatment described earlier: first, the Stark splitting due to a typical field of stationary ions is calculated, then the electron broadening of these lines is determined from the impact approximation and, finally, statistical averaging over the various possible field strengths is carried out. It frequently happens that in the upper state of a transition the electron is so much more weakly bound than in the lower state that perturbations of the lower energy level may be neglected. In general, one can say that this is the case for all transitions except those where the jumping electron is one of several equivalent electrons in both states or the levels are both broadened by the linear Stark effect.

Finally, a few words relating the older treatments of line broadening to modern theory will prove useful in the next section. The old impact (or collision) theory due to Lorentz, Weisskopf, Lindholm, Foley and others (see,

for example, Aller[18] for a description and references) is contained as a special case in the modern impact approximation. The older treatment is based on the "adiabatic" theory which treats all collisions as elastic in the sense that only the two levels between which the system is radiating are perturbed, this is correct only for low perturber velocities (i.e., for electrons, at low temperatures). In addition, the older theory does not account for the influence of overlapping lines, which may result from the near degeneracy of the field-free spectrum or from Stark splitting produced by the quasi-static ion field or even from the excitation by the ion field of nearby forbidden transitions. The current form of the quasi-static approximation is similar to the old statistical (or Holtsmark) theory except that it improves the distribution function for the positions of the perturbing particles by accounting for their mutual interactions.

4.5 Stark Broadening of Strong, Non-hydrogenic Lines

In this section we discuss the results of Stark broadening theory as applied to strong non-hydrogenic lines at space vehicle re-entry conditions and with particular reference to nitrogen.

According to both the adiabatic and the general impact theories, an isolated line has a dispersion profile, however, the shift (d) and the half-width (w) are different in the two theories. We recall from Section 3.3 a dispersion profile has the form

$$L(\nu) = \frac{1}{\pi} \frac{w}{(\nu-\nu_o+d)^2 + w^2} . \qquad (4.6)$$

Before discussing expressions for w, which will be our main concern in this section (shift is of no importance in radiative transfer problems), we first show that ion broadening may be neglected. The influence of ion

broadening in non-hydrogenic gases appears, in part, in an asymmetric line shape such that[5] one wing decays as $(\nu-\nu_o)^{-2}$ (as in the absence of quasi-static broadening) while the other wing is asymptotic to $(\nu-\nu_o)^{-7/4}$. Before this latter term is of the same order as the electron contributed impact broadening, the absorption coefficient of a typical nitrogen line has dropped to 10^{-5} times its peak value, as may be checked from the formulae and tables of Griem (ref. 5, Chapter 4). The influence of ion broadening on the core profile can also be estimated from Griem's work. Equation (4.90) of ref. 5 is an empirical expression for line half-widths due to both electrons and ions in terms of the half-width due to electrons alone as obtained from the inspection of calculated helium profiles. This equation is

$$w_{total} \tilde{=} [1 + 1.75\alpha\ (1 - 0.75r)]\, w_{e\ell} \qquad (4.7)$$

where α is a measure of ion broadening (absent if $\alpha = 0$) and r is a measure of the mutual interactions between the perturbing ions. Taking values of α from Tables 4-5 and 4-6 of Griem's book and estimating values of r, one finds that the ion broadening effect on w is at worst (high densities) about 10% which is less than the estimated accuracy of the best theory.

The general impact approximation results in an analytic expression for line width, w, (ref. 5, Eqs. 4.68, 4.79 and 4.80) which is accurate to about 20%* but which unfortunately requires considerable computation to

*This claim requires a little qualification. It does not hold for some high orbital angular quantum number states due, as discussed in the next section, to Debye-shielding of the electrons and partial degeneracy with respect to ℓ although the experimental results of Day and Griem[39] for two 4f states of NII show that, even using the worst estimate of experimental errors, the theoretical results of ref. 5 are correct to within 35%. Another source of uncertainty is that a number of experimenters (see Jalufka, Oertel and Ofelt[43] and references therein) have found the theory to be in error by a factor of 2.5 to 3.0 for AII. However, the results of Day and Griem[39] confirm an accuracy of 20% for NII.

evaluate. In view of the other inaccuracies in radiative transfer problems (in oscillator strengths, energy levels, etc.) such computation is not justified for our use here. However, Griem[5] has evaluated w for 17 lines from the first spectrum of nitrogen and 75 lines from the second spectrum of nitrogen at several temperatures covering our range of interest; these results, normalized by their values at 20,000°K, have been used to plot Figs. 12 and 13. The temperature dependence of the line widths can be seen to vary considerably, the lines with negative slopes belong to high orbital angular momentum upper states and are beginning to exhibit the dominance of inelastic collisions. As discussed earlier, Debye shielding of the electrons (not accounted for in Griem's calculation) may be significant for these states and therefore the line widths may be less accurate than those of the lower states. Note that because the broadening is assumed to be caused entirely by perturbation of the upper states, Griem's results provide the widths of more (unfortunately not many more) lines than those actually tabulated.* Besides choosing an average temperature dependence, we also have to obtain an expression with which to predict the line-widths not covered by Griem's calculations; a number of approximate expressions are available in the literature and we now discuss them.

The adiabatic theory of line broadening due to upper level perturbation gives the following result for the line half-width[18]

$$4\pi w = 38.8 |C_4|^{2/3} \left(\frac{8kT}{\pi m_e}\right)^{1/6} N_e \qquad (4.8)$$

where C_4 is the quadratic Stark coefficient of the upper state. In its most general form, C_4 is given by

---

*Since the influence of the lower state is neglected, lines with the same upper state should have the same frequency width, however, the value for NII tabulated in[5] do not all satisfy this requirement -- apparently due to computational errors.

$$C_4 = \frac{e^4}{m_e 8\pi^2 hc^2} \sum_i \lambda_{ui}^2 f_{ui} \qquad (4.9)$$

or

$$C_4 \text{ cm}^4\text{sec}^{-1} = 1.24 \times 10^{-7} \sum_i (\lambda_{ui} \text{ cm})^2 f_{ui} \qquad (4.10)$$

where the summation is over all states i to which a dipole transition (both emissive and absorptive) is allowed from the upper state u whose energy level is being perturbed. In practice, the summation is usually dominated by a few strong transitions. Substituting Eq. (4.10) into Eq. (4.8) and evaluating the constant gives

$$w \text{ eV} = 1.3 \times 10^{-16} \left[\left| \sum_i (\lambda_{ui} \text{ cm})^2 f_{ui} \right| \right]^{2/3} (N_e \text{ cm}^{-3})(kT \text{ eV})^{1/6}. \qquad (4.11)$$

Griem et al[38] have compared Eq. (4.11) with the general theory for several low-lying lines of HeI and, over our temperature range, the discrepancy is within a factor of 3. It will also be recalled that the adiabatic theory is asymptotically correct at low temperatures. A simplified form of Eq. (4.11) is available for a hydrogenic gas since then[42]

$$2\pi C_4 \simeq 1.02 \left(\frac{n_u^*}{z}\right)^6 \times 10^{-17} \text{ cm}^4\text{sec}^{-1} \qquad (4.12)$$

where we have included a small numerical correction pointed out by Sibulkin[44]; n_u^* is the effective quantum number of the upper state. Substituting this result in Eq. (4.8) one gets

$$w \simeq 8.98 \times 10^{-23} \left(\frac{n_u^*}{z}\right)^4 (N_e \text{ cm}^{-3})(kT \text{ eV})^{1/6}. \qquad (4.13)$$

No derivation of Eq. (4.12) is given in Ref. 42 but presumably it is obtained by an approximate evaluation of Eq. (4.10) for a hydrogenic spectrum and

oscillator strengths. Since this treatment cannot account for same-shell transitions it is likely to be inaccurate for non-hydrogenic gases.

An analytic expression is also available in the opposite limit of high temperatures where weak, inelastic collisions dominate. Baranger[34] together with Stewart obtained the following expression for the width of non-hydrogenic ion lines due to weak, inelastic collisions with electrons,

$$w = \frac{h^2}{3\sqrt{3}\, m_e^2} N_e \int_0^\infty dv \, \frac{f(v)}{v} \sum_i \frac{\ell_>}{(2\ell_u+1)} (4\ell_>^2-1)\sigma_{ui}^2 g_{ff} \qquad (4.14)$$

where the summation is over all states i which can be reached from the perturbed state u by dipole transitions, $\ell_> \equiv \max(\ell_u, \ell_i)$ and g_{ff} is the free-free Gaunt factor for the electron transition. If we now put $g_{ff} = 1$, we can perform the velocity integration and, assuming a Coulomb force law, apply a sum rule to obtain, following Armstrong[45],

$$w = \frac{h^2}{6\sqrt{3}\, m_e^2} N_e \left(\frac{2m_e}{\pi kT}\right)^{1/2} \left(\frac{n_u^*}{z}\right)^2 [5n_u^{*2} + 1 - 3\ell_u(\ell_u+1)] \qquad (4.15)$$

or, numerically,

$$w \text{ eV} = 0.637 \times 10^{-22} N_e (kT \text{ eV})^{-1/2} \left(\frac{n_u^*}{z}\right)^2 [5n_u^{*2} + 1 - 3\ell_u(\ell_u+1)]. \qquad (4.16)$$

Using an approximation due to Unsold[46] it is possible to reduce Eq. (4.16) still further to the result obtained by Stewart and Pyatt[47],

$$w = \frac{h^3}{(2\pi m_e)^2} \left(\frac{2\pi m_e}{kT}\right)^{1/2} N_e \frac{(n_u^*)^4}{z^2} \qquad (4.17)$$

or

$$w \text{ eV} = 3.3 \times 10^{-22} (kT \text{ eV})^{-1/2} (N_e \text{ cm}^{-3}) \frac{(n_u^*)^4}{z^2}. \qquad (4.18)$$

Note that Eq. (4.18) contains the same dependence on n_u^* as does Eq. (4.13), the z and temperature dependences are quite different, however.

From the work of Griem et al. on HeI[38], we expect Eq. (4.11) to agree with the more accurate results of Griem[5] to within a factor of 2 or 3; a number of direct checks on both NI and NII confirm this expectation and we can also see from Figs. 12 and 13 that a temperature dependence of $T^{1/6}$ is an approximate average of the correct behavior (accurate to within 25% for our temperature range). Equation (4.13) agrees with Griem's results to within a factor of 5 for NI but is low by a factor of approximately 40 for NII. In contrast, Eqs. (4.16) and (4.18) overestimate the widths of NI lines by a factor of about 10 and the widths of NII lines by a factor of 4, in both cases, the temperature dependence of Eqs. (4.16) and (4.18) is incorrect at these temperatures.

For low-lying lines not covered by Griem's calculations, the best that we can do appears to be to use the result of adiabatic theory, Eq. (4.11) (the higher lines are treated quasi-statically as discussed in the next section). Thus, we use the following expression for the electron impact line width

$$w \text{ eV} = A \, N_e/N_L \, (kT \text{ eV})^{1/6} \tag{4.19}$$

where N_L is the Loschmidt number and A is either evaluated by matching Griem's results to Eq. (4.19) at 20,000°K or obtained from the adiabatic expression (see Eq. (4.11))

$$A = 3.5 \times 10^3 \left[\left| \sum_i (\lambda_{ui} \text{ cm})^2 \, f_{ui} \right| \right]^{2/3}. \tag{4.20}$$

There is one exceptional class of strong lines for which the perturbation of the lower state is not negligible and so cannot be treated by Eq. (4.20), namely same-shell transitions where the jumping electron is one of

several equivalent electrons in both states (which normally give lines in the ultraviolet). For these lines, the adiabatic theory gives (see Aller[18])

$$A = 3.5 \times 10^3 \left[\left| \sum_i (\lambda_{ui}\ \mathrm{cm})^2 f_{ui} - \sum_{\ell i} (\lambda_{\ell i}\ \mathrm{cm})^2 f_{ui} \right| \right]^{2/3} \qquad (4.21)$$

where subscript ℓ denotes the lower state.

4.6 Stark Broadening of Lines with Highly Excited Upper States

Lines with highly excited upper states (not covered by Griem's results) will be subject to linear Stark broadening. In many cases, however, they will also be either optically thin or merged into a pseudo-continuum, so that the energy transferred is independent of the profile. However, calculations carried out on hydrogen (see Part II) suggest that under some important conditions (low densities, moderate temperatures and high path lengths) lines can be isolated but self-absorbed up to upper quantum numbers of 10 or so. It is debatable whether the accuracy of the overall calculation would be significantly impaired if one were to use impact line profiles for these high lines but, taking a cautious approach, this section discusses an attempt to account for the peculiarities of these lines.

Perturbation of states with moderate to high principal quantum numbers ($n \geq 4$ or 5) and high orbital angular quantum numbers is complicated by certain characteristics of these states. In the first place, L-S coupling starts to break down[36] so that different selection rules operate. According to Day[37], however, this should have little effect on the width. Secondly, the energy levels become relatively closely spaced. This close spacing has two effects: it increases the importance of inelastic collisions and it implies at least a partial degeneracy in orbital angular quantum number. Inelastic collisions are due to electrons whose trajectories are relatively

distant from the radiating atom. Such electrons are subject to a Debye shielding effect[38]. This shielding is not taken into account in non-hydrogenic electron impact theory with the result that the line broadening is overestimated. However, the electron impact line width cannot be greater than the electron impact line width of a corresponding line in a hydrogenic gas[38,39] and we thus have an upper bound which is approached as the degeneracy of the levels increases. A further consequence of the degeneracy of the states under discussion is that ion broadening becomes important in the line wings. Very accurate calculations of profiles have been performed[40] for the strongest hydrogen lines and approximations valid for higher hydrogen lines are also available[41]. Even the approximations (obtained by folding a dispersion profile due to electron impacts into a quasi-static profile due to ion fields) are too complex for us to use here. Instead we take account only of the behavior in the line wings (this is (see next section) what we do for the dispersion profiles but in this case the approximation is much worse). Even the wing shape is not simple[5] since there is a gradual breakdown in the validity of the impact approximation for electrons as $\nu-\nu_o$ increases until eventually they too are described by the quasi-static theory. When the impact approximation holds, the line wings are made up of an electron contribution which decays as $(\nu-\nu_o)^{-2}$ plus an ionic contribution which decays as $(\nu-\nu_o)^{-5/2}$ whereas when the electrons broaden quasi-statically, both contributions decay as $(\nu-\nu_o)^{-5/2}$. The latter is the simplest to deal with and is valid at the lower temperatures. At the upper temperatures of our range the intensity profiles of the lines will almost always merge before the effective widths reach the pure quasi-static region but nonetheless the most generally applicable, simple treatment appears to be to treat both electron and ion broadening as quasi-static. The analytic expressions for the widths of degenerate lines are obtained as described in the next paragraph.

In principle, in the theory of quasi-static broadening the interaction between the perturbing particles should be taken into account. This effect is small, however, for neutral radiators except at high densities and is in any case least in the wings of the line which are caused by close, two-particle encounters. For our purposes the Holtsmark theory of statistically independent perturbers will be sufficiently accurate even for charged radiators. The simplest form of this theory is given for a single class of perturbers by Aller[18] and by Margenau and Lewis[42]. The resulting asymptotic form may be written to conform with Griem[32] as

$$L(\nu) \sim C(2\pi c\, F_o)^{3/2} \frac{1}{\lambda^3} \frac{1}{(2\pi\Delta\nu)^{5/2}} \quad \text{for large} \quad \Delta\nu(=\nu-\nu_o) \tag{4.22}$$

where C is a constant for a given line, λ is the line wavelength and F_o is the Holtsmark normal field strength given by

$$F_o = 2.60\, zeN^{2/3} \tag{4.23}$$

where N is the number of perturbers (whose charge must be z) per cubic centimeter. If one now allows for more than one class of perturber, Eq. (4.23) holds but F_o becomes

$$F_o = 2.60e\, (N_e + \sum_{z_p} z_p N_{z_p})^{2/3} \tag{4.24}$$

where N_{z_p} is the number-density of z_p-times ionized particles. Thus substituting Eq. (4.24) into Eq. (4.22) we get

$$L(\nu) \sim C(5.20e\pi c)^{3/2} (N_e + \sum_{z_p} z_p N_{z_p}) \frac{1}{\lambda^3} \frac{1}{(2\pi\Delta\nu)^{5/2}} \tag{4.25}$$

which is consistent with Griem's asymptotic result for quasi-static broadening by electrons and singly ionized particles[5]. The constant C can be found from the approximate analysis due to Griem[41] for Holtsmark broadening of hydrogen-like lines. If one follows Griem's analysis but does not replace the wavelength by a hydrogenic value one gets

$$C \simeq \frac{9}{16} \left(\frac{h}{z_r m_e e 4\pi^2 c}\right)^{3/2} \lambda^3 \, (n_u^2 - n_\ell^2)^{3/2} \tag{4.26}$$

where z_r is the charge on the radiating particle, n_u is the upper state quantum number and n_ℓ is the lower state quantum number. This result assumes that both levels are degenerate in orbital angular quantum number ℓ and takes account of the perturbation of both levels. It is clear from Griem's analysis that where the lower state is non-hydrogenic (and therefore may be ignored) we may simply set $n_\ell = 0$ in Eq. (4.26). Combining Eqs. (4.26) and (4.25) we get

$$L(\nu) = \frac{9}{16} \left(\frac{1.30\ h}{m_e \pi}\right)^{3/2} z_r^{-3/2} \left(N_e + \sum_{z_p} z_p N_{z_p}\right) \frac{(n_u^2 - n_\ell^2)^{3/2}}{(2\pi\Delta\nu)^{5/2}} \tag{4.27}$$

or, numerically,

$$L(\nu)\ eV^{-1} = 2.12 \times 10^{-4}\ z_r^{-3/2} \left(N_e + \sum_{z_p} z_p N_{z_p}\right) \frac{1}{N_L} \frac{(n_u^2 - n_\ell^2)^{3/2}}{(\Delta h\nu\ eV)^{5/2}} \tag{4.28}$$

where N_L is the Loschmidt number. The corresponding expression for the line intensity is given in Section 3.3 where a width parameter is introduced, namely

$$w \equiv b^{2/3} \left[\Gamma(3/5)\right]^{5/3} \tag{4.29}$$

where b is related to $L(\nu)$ by $L(\nu) \sim b/(\nu-\nu_o)^{5/2}$. Identifying b in Eq. (4.28) and inserting it into Eq. (4.29) yields

$$w = A(N_e/N_L + \sum_{z_p} z_p N_{z_p}/N_L)^{2/3} \tag{4.30}$$

where

$$A \equiv 0.691 \times 10^{-2} z_r^{-1} (n_u^2 - n_\ell^2). \tag{4.31}$$

4.7 The Relative Importance of Doppler and Stark Broadening

In this section, we first examine the curve of growth of intensity of a line broadened simultaneously by Doppler and any dispersion profile producing effect. The important parameter is the ratio of dispersion to Doppler half-widths which is next calculated for some typical cases in nitrogen. Finally from these results it is demonstrated that Doppler broadening may be neglected over a wide range of conditions.

A widely used, approximate expression for a line broadened simultaneously by the Doppler effect and a dispersion profile producing mechanism is

$$K_\nu = K_o \frac{a}{\pi} \int_{-\infty}^{\infty} \frac{\exp(-t^2)}{a^2 + (\xi - t)^2}\, dt \tag{4.32}$$

where

$$a \equiv \frac{w}{w_D}\sqrt{\ell n\, 2}\,, \qquad \xi \equiv \frac{(\nu-\nu_o)\sqrt{\ell n\, 2}}{w_D}\,,$$

$$K_o \equiv \frac{\sqrt{\pi \ell n\, 2}}{m_e c} e^2 \frac{f_{mn} N_m}{w_D}\,,$$

w is the dispersion semi-half-width and w_D is the Doppler semi-half-width. It can easily be shown that

$$\lim_{a\to\infty} K_\nu = \lim_{\xi/a\to\infty} K_\nu = \frac{\pi f_{mn} N_m e^2}{m_e c} \frac{1}{\pi} \frac{w}{w^2 + (\nu-\nu_o)^2} \tag{4.33}$$

which is the pure dispersion profile. The first limit, $a \to \infty$, is the case of dispersion broadening much greater than Doppler broadening which, of course, must be asymptotic to the pure dispersion case. The second limit, $\xi/a \to \infty$, shows that far out in the wings of the line $[(\nu-\nu_o) >> w]$ the absorption coefficient behaves as though there were no Doppler broadening present; this result is to be expected since the Doppler profile falls off much more rapidly than the dispersion profile.

Since the line center is blackened out at large optical depths, the detailed shape of the core is then irrelevant and the asymptotic growth is that of a pure dispersion profile with semi-half-width w, and (see Section 3.3) the combined intensity is given by

$$I \sim 2B_{\nu_o} \sqrt{w \int_0^\infty K_\nu d_\nu s} \quad \text{for large } s. \tag{4.34}$$

On the other hand for small optical depth, the intensity is independent of the line shape and thus, if the influence of Doppler broadening is confined to a sufficiently narrow core region, the curve of growth will be independent of the Doppler broadening. The curve of growth of a combined Doppler-dispersion profile has been plotted by Penner[31] as a function of a and optical depth based on the Doppler part of the profile. Figure 14 shows this curve of growth transformed to an optical depth based on the dispersion part of the profile. It can be seen that for $a > 0.5$, the pure dispersion growth is followed almost exactly. For $a > 0.05$, the pure dispersion curve underestimates the combined curve by at most a factor of 2 and that only for a small range of optical depths. Values of a which we may expect in our problem are discussed next.

Using the hydrogenic approximation to the adiabatic result, Eq. (4.13), and the Doppler half-width Eq. (4.2) we get for a,

$$a = 26 \times (n_u^*)^4 \, N_e/N_L \, (h\nu_o \text{ eV})^{-1}(kT \text{ eV})^{-1/3}. \qquad (4.35)$$

Except for the ultraviolet lines, the important lines of NI lie in the frequency range 1 to 6eV with values of $(n_u^*)^4 > 25$, hence, for kT < 3eV

$$a > 75 \, N_e/N_L.$$

At a density of 10^{-4} atmospheres, $N_e/N_L \tilde{=} 2 \times 10^{-4}$ and the corresponding value of a is 0.015. Thus we can say that for densities greater than 10^{-4} atmospheres the maximum error on any line is a factor of 4 (with the exception of some ultraviolet lines where the factor can reach 8), and this will only apply to those lines (if any) whose optical depths lie in the range where the Doppler profile influences the radiated intensity. Except in the case of very long path-lengths, most lines will be optically thin at low densities and so independent of the profile shape. Even the errors in the ultraviolet lines are not as severe as the factor of 8 obtained above since these lines are subject to resonance broadening which increases the dispersion half-width above the value used in Eq. (4.35). The overall errors in neglecting Doppler broadening in NI are therefore likely to be small compared to those arising from other sources.

The ionic lines will suffer more on account of their higher frequencies, indeed the resonance lines of NIII are likely to be Doppler broadened until well into the wings. It was at first thought that the lines of NIII would not carry much energy on account of their high frequencies. However, early results from detailed calculations (reported in Part 3) demonstrated that a number of these lines are the dominant transfer mechanisms at high

temperatures. It therefore became necessary to take account of the Doppler broadening of some of the ionic lines. We do this as follows.

For $a > 0.05$ we ignore the Doppler effect and treat the line as a pure dispersion line. For $a < 0.05$ we compute the intensity due to a pure Doppler shape by the approximate methods discussed in Section 3.5. Next, we calculate the intensity accounting only for the dispersion contour. Finally, we compare the two values of intensity and take the larger.

The treatment just described is equivalent to approximating the line by a pure Doppler core region followed by pure dispersion wings and neglecting the transition region between these two profiles.

The effect on intensity of such an approach is shown by a dashed line on Fig. 14 for the case of $a = 5 \times 10^{-5}$. It can be seen that the error in the transition region is small.

5. CONTINUUM CROSS SECTIONS

5.1 Introduction

This chapter discusses some of the methods available for calculating the cross sections for bound-free and free-free transitions; in the calculations reported in Part 3 molecular bands are included in the continuum but since the method of treatment is peculiar to the band systems of nitrogen, the discussion is deferred until Part 3. Continuous cross sections are more readily available, in general, than those for lines, and the associated radiation has been more extensively studied. This means that the task of preparing data for radiative transfer calculations is much easier for the continuum contributions than it is for the lines.

5.2 Bound-Free Cross Sections

The bound-free absorption cross section for a particle in initial state i may be written[29]

$$(\sigma_\nu)_i = \frac{8}{3}\frac{\pi^2}{hc} a_o^2 e^2 h\nu \frac{S}{g_i} \tag{5.1}$$

where $a_o \equiv h^2/4\pi^2 mc^2$ is the first Bohr radius, g_i is the statistical weight of the initial state and S depends on the transition probabilities of all transitions from i to ionized states such that $h\nu \geq I_i$, where I_i is the ionization energy of state i. In Eq. (5.1), $h\nu$ is measured in Rydberg units.

In Russell-Saunders coupling, the radial and angular contributions may be separated and the expression

$$\frac{S}{g_i} = \sum_{\ell'L'} C_{\ell'L'} R_{\ell'L'} \tag{5.2}$$

is obtained where the primes denote the final states of the electron and ion plus electron and $\bar{R}_{\ell'L'}$ is the integral over the radial component of the wave function (analogous to the σ^2 of Eq. (3.4)). Fortunately, $\bar{R}_{\ell'L'}$ is generally independent of L' (Ref. 5, page 109) because the integral is dominated by the wave functions in the outer regions where the term splitting is small. Multiplet splitting of the ground state may also be ignored since even the hydrogenic decay from the photoelectric edge (which is as $1/\nu^3$ and which is more rapid than the non-hydrogenic decay) is responsible for a change in absorption coefficient of only about 1% across a typical multiplet width. We can therefore simplify Eq. (5.2) to

$$\frac{S}{(2S+1)(2L+1)} = C_{\ell-1}\bar{R}_{\ell-1} + C_{\ell+1}\bar{R}_{\ell+1} \tag{5.3}$$

where $C_{\ell'} \equiv \sum_{L'} C_{\ell'L'}$. When the jumping electron is equivalent in the initial state to $q-1$ others, a number of photoionization edges will normally result, each corresponding to a different ion term and thus to a different parentage of the initial state. It is then necessary to treat each parentage separately and apply the fractional parentage coefficients mentioned in Section 3.2, i.e. one gets[48]

$$C_{\ell-1} = \{F_{SL}(qS'L')\}^2 \frac{\ell}{2\ell+1} \; ; \quad C_{\ell-1} = \{F_{SL}(qS'L')\}^2 \frac{\ell+1}{2\ell+1} \tag{5.4}$$

where $\{F_{SL}(qS'L')\}^2$ is the fractional parentage coefficient to be found in Refs. 19 and 20. It remains therefore to calculate

$$\bar{R}_{\ell'} = \bar{R}_{\ell'}(\ell', n, \nu, \ell) \tag{5.5}$$

and the remainder of the section is devoted to this problem.

As in the case of line cross sections, the most accurate method of calculation is by means of self-consistent field functions but, as mentioned

before, such calculations are very lengthy. Fortunately they are not so necessary in the case of bound-free transitions owing to the widely used and fairly accurate method of Burgess and Seaton. This method is similar in approach to the Bates and Damgaard[26] analysis of bound-bound transitions. That is, it is a semi-empirical method based on hydrogenic wave functions. It is, however, more complicated to apply than the Bates-Damgaard method because it includes an empirical correction for the non-hydrogenic wave functions. A description of the method can be found in the original paper[29] and in Griem's book[5]; a paper by Peach[49] is useful as an example of its application. Several comparisons of the predictions of this method with those obtained from more exact calculations using self-consistent field functions (see Section 3.2) and with experimental results have been performed by Burgess and Seaton[29] and by Armstrong and his co-workers[45,50]. These comparisons show that the method is accurate for the photoionization of an electron which is alone in its shell and in general gives good agreement for light, more complex systems. The method of Burgess and Seaton implies a general restriction on photon energy, namely $h\nu - I_i \ll z^2$ Rydbergs, this restriction is not serious at the temperatures of interest in re entry problems (< 3 eV) since it occurs at photon energies far from the maximum of the Planck function. It is nevertheless worth recording that there exists an approximation which is valid for high photon energies (Ref. 45, page 76).

Seaton[51] gives a formula from which $\sigma_{i,i'}$ may be calculated for an initial configuration $2p^q$ (which corresponds to the most important transitions in nitrogen). It is not clear from the paper whether Seaton's expression is obtained analytically or whether (as seems more likely) it is an empirical fit to other calculations. Seaton suggests that, at least for positive ions, the accuracy of the formula should be within 20% and a

comparison due to Johnston et al.[50] with more exact predictions for a transition in NII confirms this for low photon energies.

The final method to be discussed is the hydrogenic approximation. The formula for the bound-free absorption coefficient of a hydrogenic gas is (see e.g. Ref. 33, Chap. 5)

$$\sigma_n = \frac{128}{3\sqrt{3}} \frac{\pi^2}{hc} e^2 a_o^2 \left(\frac{1}{h\nu}\right)^3 \frac{z^4}{n^5} g(\nu;n,\ell) \qquad (5.6)$$

where $h\nu$ is measured in Rydberg units and $g(\nu;n,\ell)$ is the Gaunt factor. The Gaunt factor may be regarded as a quantum-mechanical correction factor to the classical result. Extensive tables of Gaunt factors are available[52] while Ref. 53 contains a review of approximate analytic representations; except at high photon energies the Gaunt factor is close to unity. The validity of the hydrogenic approximation is greatest at large values of n and, for given n, for high values of orbital angular momentum. In states of low excitation, the core of passive electrons does not fully shield the nucleus, and the expression (5.6) can be improved somewhat by the use of z_e, an effective charge, in place of z. z_e is defined by $z_e^2 \equiv n^2/I_n$ where the ionization energy I_n is measured in Rydbergs. When the jumping electron is initially one of a number of equivalent electrons, the hydrogenic approximation breaks down completely. However, Armstrong[54] shows that the parentage splitting can be accounted for by the fractional parentage coefficient $\{F_{SL}(qS'L')\}^2$ introduced earlier.

In the nitrogen calculations presented in Part 3, bound-free transitions from the lower-lying states are represented by values of cross section calculated by Sherman and Kulander[60] using the Burgess-Seaton method. The cross sections of higher states are assumed to be hydrogenic.

5.3 Free-Free Cross Sections

Free-free transitions involve the change of energy of a free electron in the field of a positive ion. When the ion is hydrogenic the following expression holds

$$\sigma_{\nu,ff} = \frac{16\pi^2 e^6}{3\sqrt{3}\ ch\ (2\pi m_e)^{3/2}(kT)^{1/2}\nu^3}\ z^2 N_e\ g_{ff}(\nu,kT) \qquad (5.7)$$

where $g_{ff}(\nu,kT)$ is the free-free Gaunt factor which for temperatures of interest to us, is close to unity over the important photon energy range 0.1 eV to 10 eV; accurate values of g_{ff} are tabulated by Karzas and Latter[52].

Until recently, the only theoretical treatment of free-free transitions was for hydrogenic atoms. Now, however, a paper by Peach[55] is available which is an extension of the Burgess-Seaton method (see Section 5.2) to free-free transitions. Peach's original paper applied her method to He and compared the results to Eq. (5.7), differences up to a factor of 2 in both directions occur with a tendency for the hydrogenic expression to underestimate the cross sections. Unfortunately from our point of view, the results were not averaged over electron velocity and it appears at least possible that this process would decrease the discrepancies. In the past, it has been common practice to use an effective value of z^2 to account in a crude way for non-hydrogenic effects, this has the merit of preserving the analytical simplicity of Eq. (5.7).

In Part 3, the free-free cross section is calculated according to the hydrogenic formula, Eq. (5.7). For transitions in the field of the first ion, an effective value of z^2 based on experimental evidence[61] is used.

APPENDIX I. The Influence of a Density-Dependent Partition Function on the Thermal Equation of State of Hydrogen

The equation of state of a gas is given by the equation[56]

$$p = NkTV \frac{\partial(\ell n\, Q)}{\partial V} \tag{I.1}$$

Then, using the standard expressions for partition functions in a gas consisting of hydrogen atoms, ions and electrons we get

$$p = (N_H + N_{H^+} + N_e)kT + N_H VkT \left[\frac{\partial}{\partial V} (\ell n(Q_{e\ell})_H)\right]_T \tag{I.2}$$

which may be written as the sum of translational and electronic contributions to the pressure,

$$p = p_{tr} + p_{e\ell}. \tag{I.3}$$

We see from Eq. (I.2) that the electronic partition function can affect the value of the pressure in two ways. In the first place it determines, through the Saha equation, the number of particles present. The particle densities can be accurately calculated in our range of conditions if the truncation point of the partition function is found from Debye-Hückel theory (see Chap. 2). This, however, leads to the second way in which the partition function influences the pressure. The use of Debye-Hückel theory leads to a density-dependent partition function and, according to Eq. (I.2), this gives rise to a change in the thermal equation of state in the form of an additional term which we call $p_{e\ell}$ in Eq. (I.3). It is this additional term which we discuss now.

The terms of the hydrogenic partition function are conveniently ordered by the principal quantum number n and we may write

$$Q_{el} = \sum_{n=1}^{n_{max}} g_n e^{-E_n/kT} \qquad (I.4)$$

where $g_n = 2n^2$ and $E_n = \chi_H(1-1/n^2)$. Following the procedure of Appendix II we may separate Q_{el} into two parts,

$$Q_{el} = (Q_{el})_{low} + (Q_{el})_{high} \qquad (I.5)$$

where

$$(Q_{el})_{low} \equiv \sum_{n=1}^{n^*-1} 2n^2 e^{-E_n/kT} \qquad (I.6)$$

and

$$(Q_{el})_{high} \equiv \sum_{n=n^*}^{n_{max}} 2n^2 e^{-E_n/kT}$$

$$\tilde{=} \int_{n^*}^{n_{max}} 2n^2 e^{-E_n/kT} dn. \qquad (I.7)$$

We now choose n^* such that the error in replacing E_n by χ_H is small and we get

$$(Q_{el})_{high} \tilde{=} 2/3\, e^{-\chi_H/kT} [(n_{max})^3 - (n^*)^3]. \qquad (I.8)$$

Now since $(Q_{el})_{low}$ is independent of V, we get from Eqs. (I.2), (I.5) and (I.8).

$$p_{el} = N_H VkT \frac{2\nu^2}{Q_{el}} e^{-\chi_H/kT} \left(\frac{\partial \nu}{\partial V}\right)_T. \qquad (I.9)$$

Where we have replaced n_{max} by ν to emphasize that we are treating it as a continuous variable, ν is found from the Debye-Hückel theory discussed in

Section 2.2, Eqs. (2.6) and (2.7), together with the hydrogenic expression for for energy, Eq. (2.5), those combine to give

$$\nu = \left\{\frac{\chi_H^2}{e^4}\frac{kT}{8\pi e^2 N_e}\right\}^{1/4}. \tag{I.10}$$

Writing α for the degree of ionization so that $\alpha = N_e/(N_H+N_{H^+}) = \frac{N_e}{N_L}\frac{1}{2}\frac{V}{V_o}$ we get

$$\nu = \left\{\frac{\chi_H^2}{e^4}\frac{kT}{8\pi e^2 2\alpha N_L}\frac{V}{V_o}\right\}^{1/4} \tag{I.11}$$

so that

$$\left(\frac{\partial \nu}{\partial V}\right)_T = \frac{1}{4}\,\nu\,\frac{1}{V}\,. \tag{I.12}$$

Substituting Eq. (I.12) into Eq. (I.9) we find

$$p_{e\ell} = \frac{1}{2} N_H kT\, \nu^3\, e^{-\chi_H/kT}\, 1/Q_{e\ell}. \tag{I.13}$$

Since the translational pressure due to the hydrogen atoms is given by $(p_H)_{tr} = N_H kT$, this may be written as

$$p_{e\ell} = \frac{1}{2}\,(p_H)_{tr}\,\nu^3\, e^{-\chi_H/kT}\, 1/Q_{e\ell}. \tag{I.14}$$

Now, identifying n_{max} with ν and comparing Eq. (I.8) we see that the quantity $\frac{1}{2}\nu^3\, e^{-\chi_H/kT}$ is related to the high state contribution to the partition function and we make the definition

$$\bar{Q} \equiv \frac{1}{2}\nu^3\, e^{-\chi_H/kT} = \frac{3}{4}\left[(Q_{e\ell})_{high} + Q^*\right] \tag{I.15}$$

where

$$Q^* \equiv 2/3(n^*)^3 e^{-\chi_H/kT} \tag{I.16}$$

In addition we have

$$\frac{(p_H)_{tr}}{p_{tr}} = \frac{N_H}{N_e + N_{H^+} + N_H} = \frac{1 - \alpha}{1 + \alpha} \tag{I.17}$$

so that Eq. (I.14) finally becomes

$$\frac{p_{el}}{p_{tr}} = \frac{\bar{Q}}{Q_{el}} \frac{1 - \alpha}{1 + \alpha} \quad . \tag{I.18}$$

For ν to be approximately continuous as required by the derivation of Eq. (I.18), its value has to be relatively large which implies low densities which in turn implies a high degree of ionization. Equation (I.18) shows that under these circumstances p_{el}/p_{tr} will be small. Numerical checks confirm that for $\alpha > 0.85$, $p_{el}/p_{tr} < 0.05$. The physical interpretation is that there are so few atoms present that the change in their partition function is irrelevant to the total pressure.

Where the ionization is low, ν tends to be low (because the density is usually high) and the integral approximation to $(Q_{el})_{high}$ is less appropriate. However, the error is probably no worse than that caused by treating the energy levels as unperturbed (which is the only treatment available at present). We therefore retain the integral approximation for small values of ν. Thus, Eq. (I.18) is assumed to hold but now we need to evaluate $\bar{Q}/Q_{el}$ more carefully, replacing $\bar{Q}$ by its definition in Eq. (I.15) we obtain

$$\frac{p_{el}}{p_{tr}} = \frac{1}{2} \frac{\nu^3 e^{-\chi_H/kT}}{Q_{el}} \frac{1 - \alpha}{1 + \alpha} \quad . \tag{I.19}$$

Numerical evaluation of Eq. (I.19) shows that p_{el}/p_{tr} is less than 5% for densities up to 1) and temperatures up to 3eV.

APPENDIX II. The Partition Functions of Nitrogen and its First Ion

This appendix is primarily concerned with giving details of the energy levels and statistical weights from which the partition functions shown on Figs. 2 and 3 were calculated. Most of the low and moderate energy levels were obtained from the compilation of Gilmore.[57] This compilation conveniently combines closely spaced energy levels of each electronic configuration. The basic data for Gilmore's tabulation consisted of experimental results listed by Moore[58] supplemented with Gilmore's own estimated values. Gilmore's work covers states with principal quantum numbers up to 8. Above this level, Moore's values[58] were taken and combined where available (the method of combination is given in a later paragraph). Otherwise, hydrogenic estimates asymptotic to the true ionization thresholds were made. For very high, closely spaced energy levels integral approximations to the summed terms were used.

The electronic partition functions were calculated from expressions of the type

$$Q_{el} = S_1 + S_2 + S_3 + I_2 + I_3.$$

The meaning of the terms is as follows

$$S_1 \equiv \sum_{i=1}^{i_{max}^{(1)}} g_i^{(1)} \exp(-E_i^{(1)}/kT)$$

and is a sum over all energy levels with $n \leq 3$. These levels are below the lowest value to which the ionization energy is depressed in our range of conditions. This means that the associated electronic energy configuration of each level need not be distinguished and occasional further combination of Gilmore's values has been possible.

S_2 and S_3 are defined in a similar manner,

$$S_2 \equiv \sum_{i=1}^{i_{max}^{(2)}} g_i^{(2)} \exp(- E_i^{(2)}/kT)$$

and

$$S_3 \equiv \sum_{i=1}^{i_{max}^{(3)}} g_i^{(3)} \exp(- E_i^{(3)}/kT).$$

These sums cover quantum numbers $4 \leq n \leq 10$. Each corresponds to a different electronic core configuration. This distinction is necessary because for a given depression in ionization potential, $\Delta\chi$, the cut-off energy ($\chi_{eff} = \chi - \Delta\chi$) depends upon the ionization energy and this takes different values according to the core configuration. A word about the values listed in Tables II.1 and II.2 is necessary. Some of the energy levels of S_2 and S_3 could have been combined without significant loss of accuracy but were individually specified for aesthetic reasons. The levels in question tend to have large values of statistical weight and, when the series cut-off is in this region, the partition function suffers large discontinuities as a function of density (because we neglect perturbation of the energy levels). These discontinuities lead to nonsmooth functions for the particle densities. This lack of smoothness can be avoided by including a sufficient number of terms in the sums S_2 and S_3.

The quantities I_2 and I_3 are integrals defined as follows

$$I_2 \equiv g_{core}^{(2)} \exp(\quad /kT) \int_{11}^{n_{max}} 2n^2 dn$$

$$= 2/3\, g_{core}^{(2)} \exp(- E_\infty^{(2)}/kT)(n_{max}^3 - 1331)$$

and

$$I_3 \equiv g_{core}^{(3)} \exp(-E_\infty^{(3)}/kT) \int_{11}^{n_{max}} 2n^2 dn$$

$$= 2/3\, g_{core}^{(3)} \exp(-E_\infty^{(3)}/kT)(n_{max}^3 - 1331).$$

where $g_{core}^{(2)}$ and $g_{core}^{(3)}$ are the statistical weights of the corresponding core configurations. I_2 and I_3 are therefore integrals over high states whose energy levels are approximated by the threshold values.

Values of the energies and statistical weights are given for the atom in Table II.1 and for the first ion in Table II.2. It remains to demonstrate the method of combining closely spaced energy levels.

For q closely spaced energy levels we require a mean energy level $\bar{E}$ such that

$$\sum_{i=1}^{q} g_i e^{-E_i/kT} = e^{-\bar{E}/kT} \sum_{i=1}^{q} g_i \qquad \text{(II.1)}$$

If we now write $E_i = \bar{E}+\Delta E_i$ and substitute in Eq. (II.1) we obtain

$$\sum_{i=1}^{q} g_i e^{-\Delta E_i/kT} = \sum_{i=1}^{q} g_i \qquad \text{(II.2)}$$

But if $\Delta E_i/kT \ll 1$, Eq. (II.2) becomes

$$\sum_{i=1}^{q} g_i \Delta E_i = 0 \qquad \text{(II.3)}$$

which yields

$$\bar{E} = \frac{\sum_{i=1}^{q} g_i E_i}{\sum_{i=1}^{q} g_i} \qquad \text{(II.4)}$$

Equation (II.4) can therefore be used to combine any number of energy levels provided only that in each case $|E_i-\bar{E}| \ll kT$.

TABLE II.1

Energy Levels and Statistical Weights of N

Energy Values in Electron Volts

	Core:		$2s^2 2p^2(^3P)$		$2s^2 2p^2(^1D)$	
i	$g_i^{(1)}$	$E_i^{(1)}$	$g_i^{(2)}$	$E_i^{(2)}$	$g_i^{(3)}$	$E_i^{(3)}$
1	4	0	54	13.318	160	15.448
2	10	2.384	216	13.686	250	15.903
3	6	3.575	450	13.957	360	16.069
4	18	10.450	648	14.158	490	16.169
5	12	10.926	882	14.270	640	16.234
6	54	11.875	1152	14.335	810	16.279
7	10	12.356	1458	14.380	1000	16.311
8	108	12.980	1800	14.412		
9	30	13.758				
10	66	15.093				

Core statistical weights	$g_{core}^{(2)} = 9$	$g_{core}^{(3)} = 5$
Ionization energies	$E_\infty^{(2)} = 14.5481$	$E_\infty^{(3)} = 16.447$

TABLE II.2

Energy Levels and Statistical Weights of N^{7}

Energy values in electron volts

	Core:		$2s^2 2p(^2P)$		$2s2p^2(^4P)$	
i	$g_i^{(1)}$	$E_i^{(1)}$	$g_i^{(2)}$	$E_i^{(2)}$	$g_i^{(3)}$	$E_i^{(3)}$
1	9	0	192	25.860	384	32.990
2	5	1.899	300	27.337	600	34.537
3	1	4.053	432	28.081	864	35.201
4	5	5.800	880	28.500	1176	35.601
5	15	11.436	768	28.760	1536	35.861
6	9	13.541	972	28.940	1944	36.041
7	5	17.876	1200	29.068	2400	36.169
8	12	18.480				
9	3	19.232				
10	39	20.933				
11	60	23.270				
12	221	29.045				

Core statistical weights	$g_{core}^{(2)} = 6$	$g_{core}^{(3)} = 12$
Ionization energies	$E_{\infty}^{(2)} = 29.612$	$E_{\infty}^{(3)} = 36.713$

APPENDIX III. The Approximations Involved in the Use of a Density-Independent Partition Function

In radiative transfer calculations we require the species composition in order to find the occupation numbers of the initial levels of the various radiative transitions and we also require the electron and positive charge densities to find the widths of the stark broadened lines. It turns out that these quantities are not very sensitive to the cut-off of the partition functions and can be calculated reasonably accurately without allowing for the high terms of the partition functions. This appendix discusses the effect on occupation numbers and charged particle densities of truncating the partition function after a small, fixed number of terms.

The possibility of such an approximation springs from the following observations. In the first place, at low temperatures the factor $1/kT$ in the exponents of the terms of the partition functions means that the high terms do not contribute significantly and the cut-off is unimportant (except for its existence). (From this fact it follows that the problem is restricted to relatively high temperatures where the gas is completely dissociated and we ignore the molecular species in the remainder of the discussion.) Secondly, excited states of multiply ionized species have large energies with respect to the ground state and the corresponding contributions to the partition functions are small, the multiple ions thus tend to be dominated by a few low-lying states and their partition functions are consequently density independent. Checks performed a posteriori show that we do not need to consider the problem of the exact truncation point for any multiply ionized species in our range of conditions. Furthermore, although $(Q_{el})_{N^+}$ is treated as density dependent in the accurate calculations, it does not vary more than a factor of 3.5 from a sum over its first

four terms (see also Fig. 3). Thus it can be seen that only $(0_{e\ell})_N$ is strongly dependent on density.

It follows that when few atoms are present, the electron and positively charged particle densities may be calculated reasonably accurately no matter what form of the atomic partition function is used. On the other hand, a significant number of atoms (i.e. low ionization) will only be present if the temperature is low or the density is high. If the temperature is low, the terms omitted from the approximate partition function are negligible, as explained previously If the density is high, there will be a large depression in the ionization limit and thus the density-dependent cut-off point will be relatively close to the low-lying, density-independent value which will now be a better approximation. In summary, if we approximate the atomic partition function by its first few terms, then under conditions of low ionization, where the value of the atomic partition function is important, the approximation is reasonably good while for conditions of high ionization, where the approximation is very poor, the charged particle density is independent of its value.

At conditions where the ionization is low, the approximate partition function is relatively accurate, as discussed above, we can therefore use it to find the occupation numbers of the atomic states with reasonable accuracy. There remains, however, the problem of their calculation for higher ionization (where the atomic radiative contribution is not necessarily negligible). Under these conditions, a further observation is of help. Although the region of high ionization is the region of largest error in the density-independent partition function (see Fig. 2), it is also a region in which the occupation numbers become independent of the partition function. This may be seen by noting that $\tilde{N}_e$ and $\tilde{N}_{N^+}$ will be independent of $\tilde{N}_N$ and using Eq. (2.1) to eliminate $\tilde{N}_N$ from the appropriate form of

Eq. (2.2), to obtain

$$\tilde{N}_{N,i} = \frac{\tilde{N}_{N^+}\tilde{N}_e}{(Q_{e\ell})_{N^+}} \frac{1}{112.4} (kT)^{-3/2} \rho/\rho_o \, g_i \exp[-(14.548-\Delta\chi_1-E_i)/kT] \quad \text{(III.1)}$$

A similar result has been independently obtained by Hochstim.[59] The value of $\tilde{N}_N$ is exactly linear in $(Q_{e\ell})_N$ under these conditions and the influence of inaccuracies in $(Q_{e\ell})_N$ can be interpreted by saying that although we may not know accurately the total number of atoms present -- because we do not know whether to count highly excited states as bound or free -- once having decided to treat a particular state as bound we can calculate the associated occupation numbers with reasonable accuracy.

The solution of the system of equations consisting of the first four ionization equations, Eq. (IV.12) to (IV.15) plus the two conservation equations, Eqs. (IV.16) and (IV.17) was obtained by iterative calculations on an IBM 360 computor using both exact and approximate expressions for $(Q_{e\ell})_N$ and $(Q_{e\ell})_{N^+}$. The approximate expressions consist of a fixed number of the terms listed in Appendix II while the "exact" calculations are described in Section 2.2.

The composition predicted by the "exact" theory is shown on Figs. 4-7. Figures 15, 16 and 17 display some of the errors incurred by using vacuum ionization energies and the following truncated partition functions for N and N^+

$$(Q_{e\ell})_N = 4 + 10 \exp(-2.384/kT) + 6 \exp(-3.575) \quad \text{(III.2)}$$

$$(Q_{e\ell})_{N^+} = 9 + 5 \exp(-1.899/kT) + \exp(-4.053/kT) + 5 \exp(-5.800/kT). \quad \text{(III.3)}$$

Figure 15 shows the errors in electron number density which for mass densities less than 1 atmosphere are within 15%. Because the overall charge must be

zero, the total density of positive charges must equal the electron density and does not need to be considered further. The density of atoms suffers the worst errors, as is to be expected, and Fig. 16 shows that these can be two or three orders of magnitude; N^+ is only seriously in error when multiple ionization dominates (Fig. 17).

The error in the occupation numbers for various approximations is shown in Figs. 18-20. Figure 18 is based on the 3-term partition function of Eq. (III.2) and vacuum ionization potentials. The maximum error occurs when the atoms are 60%-70% ionized which means that it moves towards higher densities as the temperature rises, and it grows from 2% at 1.0 eV to over 60% at 3 eV. For densities less than 1 atmosphere, the error is less than 40%. Figure 19 shows the errors caused entirely by the partition function (the calculations plotted on Fig. 19 used correctly depressed ionization energies but the simple 3-term partition function of Eq. (III.2)).

The fact that the errors are worst at high densities and that the partition function and ionization errors are both in the same direction suggests that one may be able to reduce the errors and perhaps compensate for the heavily reduced ionization energy at high densities by truncating the partition function slightly above the exact high-density cut-off. Figure 20 shows the results of such a procedure where the cut-off point of the atomic partition function was chosen to be the true cut-off for densities slightly less than atmospheric. This gives rise to a 13-term partition function of the form

$$Q_{el} = \sum_{i=1}^{10} g_i^{(1)} \exp(-E_i^{(1)}/kT) + \sum_{i=1}^{2} g_i^{(2)} \exp(-E_i^{(2)}/kT) + g_i^{(3)} \exp(-E_i^{(3)}/kT). \qquad \text{(III.4)}$$

The partition function of N^+ was left in its approximate, 4-term form. The maximum error can be seen from Fig. 20 to have been reduced to 20%. However, the choice of cut-off turns out to be critical since use of the true cut-off corresponding to 10^{-1} atmospheres increases the high density error to -50%. It also turns out that severe errors can occur in the occupation numbers of N^+ when the atomic partition function is overestimated.

In conclusion, an approximate partition function based on a small number of low-lying energy levels gives occupation numbers and charged particle densities to an accuracy of about 50% provided the densities are less than atmospheric. In many cases, this will be an acceptable approximation. However, attempting to reduce the inaccuracies by raising the cut-off point of the partition function introduces uncontrolled errors and does not seem to be a fruitful approach.

APPENDIX IV. An Iterative Procedure for the Solution of the Mass Action and Conservation equations

At high temperatures, a diatomic gas A_2 will undergo dissociation,

$$A_2 \rightleftarrows 2A, \tag{IV.1}$$

ionization of the molecules,

$$A_2^{z-1} \rightleftarrows A_2^z + e^-, \tag{IV.2}$$

(where z denotes the number of positive charges on the molecular ion) and ionization of the atoms,

$$A^{z-1} \rightleftarrows A^z + e^- \tag{IV.3}$$

The corresponding equations of mass action can be obtained from Eq. (2.2) by identifying the symbols, inserting the standard approximation $(Q)_S = (Q_{tr})_S(Q_{int})_S$ and evaluating $(Q_{tr})_S$. The resulting equations are, for dissociation:

$$\frac{(N_A)^2}{N_{A_2}} = \left(\frac{\pi m_A kT}{h^2}\right)^{3/2} \frac{[(Q_{el})_A]^2}{(Q_{int})_{A_2}} e^{-D/kT} \tag{IV.4}$$

where D is the dissociation energy, m_A is the mass of an atom of A and $(Q_{el})_A$ is the electronic partition function of A; for molecular ionization:

$$\frac{N_{A_2^z} N_e}{N_{A_2^{z-1}}} = \frac{(Q_{int})_{A_2^z}}{(Q_{int})_{A_2^{z-1}}} \times 2 \times \left(\frac{2\pi m_e kT}{h^2}\right)^{3/2} \exp\left(-\frac{\chi_{A_2^{z-1}}}{kT}\right) \tag{IV.5}$$

where subscript e denotes electrons and the value of $\left(\frac{2\pi m_e}{h^2}\right)^{3/2}$ is 3.03×10^{21} $eV^{-3/2}$ cm^{-3}; and for atomic ionization:

$$\frac{N_{A^z} N_e}{N_{A^{z-1}}} = \frac{(Q_{el})_{A^z}}{(Q_{el})_{A^{z-1}}} \times 2 \times \left(\frac{2\pi m_e kT}{h^2}\right)^{3/2} \exp(-\chi_{A^{z-1}}/kT). \qquad (IV.6)$$

Note that it is possible to reorganize the sets of equations (IV.4), (IV.5) and (IV.6) so that molecular ions are not regarded as being produced by ionization but instead treated as dissociating according to an equation similar to Eq. (IV.4); this is exactly equivalent to the present treatment and the further inclusion of dissociation relations for molecular ions would introduce redundant equations.

The conservation equations for mass and charge are

$$2 \sum_{z=0}^{2z_a} N_{A_2^z} + \sum_{z=0}^{z_a} N_{A^z} = N_o \qquad (IV.7)$$

and

$$\sum_{z=1}^{z_a} zN_{A^z} + \sum_{z=1}^{2z_a} zN_{A_2^z} = N_e \qquad (IV.8)$$

where N_o is constant and is the number of atomic nuclei per unit volume and z_a is the atomic number of A. If a method of evaluating the partition functions is adopted, the set of equations (IV.4) to (IV.8) can be solved by iteration.

In the case of nitrogen, the only molecular ionization process of importance is the reaction

$$N_2 \rightleftarrows N_2^+ + e^- \qquad (IV.9)$$

and further it can easily be checked that for $kT < 3$ eV and $\rho/\rho_o > 10^{-6}$,

the fifth and higher ions never contribute more than 1% of the total particle density and can be ignored. We therefore may truncate the summations in Eqs. (IV.7) and (IV.8) after $z = 1$ for molecules and $z = 4$ for atoms; in addition we have to consider one equation of type (IV.5) and four of type (IV.6).

Taking account of the simplifications discussed above, the explicit form of equations (IV.4) to (IV.8) for nitrogen may be written as

$$\frac{\tilde{N}_{N_2^+}\,\tilde{N}_e}{\tilde{N}_{N_2}} = K_1 = 112.4\,\frac{(Q_{int})_{N_2^+}}{(Q_{int})_{N_2}}\,(kT)^{3/2}\,(\rho/\rho_o)^{-1}\exp(-15.6/kT) \qquad \text{(IV.10)}$$

$$\frac{(\tilde{N}_N)^2}{\tilde{N}_{N_2}} = K_2 = 0.81\times 10^8\,\frac{[(Q_{el})_N]^2}{(Q_{int})_{N_2}}\,(kT)^{3/2}\,(\rho/\rho_o)^{-1}\exp(-9.56/kT) \qquad \text{(IV.11)}$$

$$\frac{\tilde{N}_{N^+}\,\tilde{N}_e}{\tilde{N}_N} = K_3 = 112.4\,\frac{(Q_{el})_{N^+}}{(Q_{el})_N}\,(kT)^{3/2}\,(\rho/\rho_o)^{-1}\exp[-(14.548-\Delta\chi_1)/kT] \qquad \text{(IV.12)}$$

$$\frac{\tilde{N}_{N^{++}}\,\tilde{N}_e}{\tilde{N}_{N^+}} = K_4 = 112.4\,\frac{(Q_{el})_{N^{++}}}{(Q_{el})_{N^+}}\,(kT)^{3/2}\,(\rho/\rho_o)^{-1}\exp[-(29.605-\Delta\chi_2)/kT] \qquad \text{(IV.13)}$$

$$\frac{\tilde{N}_{N^{+++}}\,\tilde{N}_e}{\tilde{N}_{N^{++}}} = K_5 = 112.4\,\frac{(Q_{el})_{N^{+++}}}{(Q_{el})_{N^{++}}}\,(kT)^{3/2}\,(\rho/\rho_o)^{-1}\exp[-(47.463-\Delta\chi_3)/kT] \qquad \text{(IV.14)}$$

$$\frac{\tilde{N}_{N^{++++}}\,\tilde{N}_e}{\tilde{N}_{N^{+++}}} = K_6 = 112.4\,\frac{(Q_{el})_{N^{++++}}}{(Q_{el})_{N^{+++}}}\,(kT)^{3/2}\,(\rho/\rho_o)^{-1}\exp[-(77.45-\Delta\chi_4)/kT] \qquad \text{(IV.15)}$$

$$2\tilde{N}_{N_2^+} + 2\tilde{N}_{N_2} + \tilde{N}_{N} + \tilde{N}_{N^+} + \tilde{N}_{N^{++}} + \tilde{N}_{N^{+++}} + \tilde{N}_{N^{++++}} = 1 \qquad \text{(IV.16)}$$

$$\tilde{N}_{N_2^+} + \tilde{N}_{N^+} + 2\tilde{N}_{N^{++}} + 3\tilde{N}_{N^{+++}} + 4\tilde{N}_{N^{++++}} = \tilde{N}_e \qquad \text{(IV.17)}$$

where the tilde denotes a particle density non-dimensionalized by N_o, the total number of nuclei present and $\Delta\chi_z$ is the ionization depression of Eq. (2.7). The reductions in ionization energies, $(Q_{el})_N$ and $(Q_{el})_{N^+}$ are all density dependent and depend for their evaluation on a previous solution of the mass action equations, as has been described earlier; in this appendix, however we regard them as given and describe the iterative solution of Eqs. (IV.10) to (IV.17).

The solution of this set of equations is made considerably easier by the fact that at most two, and frequently only one, of the species are much more abundant than the others, this can be seen as follows. For $i \geq 2$ we have $K_{i+1} << K_i$, consider first the case where few uncharged particles are present so that $1 \gtrsim \tilde{N}_e \gtrsim 4$ then, if N^z is a z-times ionized particle

$$\tilde{N}_{N^{z+1}} \gtrsim \tilde{N}_{N^z} K_{z+2}$$

and the species N^{z_o} and N^{z_o+1} for which K_{z_o+2} is nearest to unity will dominate since

$$\tilde{N}_{N^z} << \tilde{N}_{N^{z_o+1}} \quad \text{for} \quad z \geq z_o + 2$$

and

$$\tilde{N}_{N^z} << \tilde{N}_{N^{z_o}} \quad \text{for} \quad z \leq z_o - 1$$

by virtue of the values of K_z. In the case where there are a significant number of uncharged particles present, $\tilde{N}_e \tilde{\simeq} \tilde{N}_{N^+}$ and it again turns out that the species for which K_{z+2} is near unity will dominate. $\tilde{N}_{N_2^+}$ can never be important however, since although K_1 can be unity, implying $\tilde{N}_{N_2^+} \tilde{\simeq} \tilde{N}_{N_2}$ at the same time $K_2 >> 1$ so that $\tilde{N}_{N_2} << (\tilde{N}_N)^2$. The criteria for picking the dominant equation are not critical since although it can happen that $K_{z+1} << 1$ and $K_z >> 1$ such that $K_{z+1}K_z \tilde{\simeq} 1$ (i.e. $\tilde{N}_{N^{z-1}} \tilde{\simeq} \tilde{N}_{N^{z-3}}$) at the same time $\tilde{N}_{N^{z-2}} >> \tilde{N}_{N^{z-1}} \tilde{\simeq} \tilde{N}_{N^{z-3}}$ and either equation will give the dominant species $\tilde{N}^{z-2}$. A detailed consideration of the equations leads to the following criteria for the dominant equation

$$K_2\sqrt{K_3} \leq 1, \qquad \text{Eq. (IV.11) is dominant}$$

$$K_2\sqrt{K_3} > 1 \quad \text{and} \quad K_3K_4 \leq 1, \qquad \text{Eq. (IV.12) is dominant;}$$

$$K_4K_3 > 1 \quad \text{and} \quad K_4K_5 \leq 4, \qquad \text{Eq. (IV.13) is dominant;}$$

$$K_4K_5 > 4 \quad \text{and} \quad K_5K_6 \leq 9, \qquad \text{Eq. (IV.14) is dominant}$$

and

$$K_5K_6 > 9, \qquad \text{Eq. (IV.15) is dominant.}$$

Since we have one dominant equation which for given conditions we can identify, we can solve the set of equations by an iterative process organized as follows. Suppose, first, that the dominant equation is one of Eqs. (IV.12) to (IV.15). It therefore has the form

$$\frac{\tilde{N}_{N^{z+1}}\,\tilde{N}_e}{\tilde{N}_{N^z}} = K \qquad \text{(IV.18)}$$

and Eqs. (IV.16) and (IV.17) may be written

$$\tilde{N}_z + \tilde{N}_{z+1} = 1 - \tilde{N}_{c1} \qquad \text{(IV.19)}$$

and

$$z\tilde{N}_z + (z+1)\tilde{N}_{z+1} = \tilde{N}_e - \tilde{N}_{c2} \qquad \text{(IV.20)}$$

respectively where $z \geq 0$ and $\tilde{N}_{c1}$, $\tilde{N}_{c2}$ are the terms in Eqs. (IV.16) and (IV.17) not individually exhibited in Eqs. (IV.19) and (IV.20) and are regarded as small corrections. Eliminating $\tilde{N}_{z+1}$ from Eq. (IV.20) the equations can be written in the form

$$\tilde{N}_{z+1} = A - \tilde{N}_z \qquad \text{(IV.21)}$$

$$\tilde{N}_e = B - \tilde{N}_z = B - A + \tilde{N}_{z+1} \qquad \text{(IV.22)}$$

where

$$A \equiv 1 - \tilde{N}_{c1} \qquad \text{(IV.23)}$$

$$B \equiv (z+1)A + \tilde{N}_{c2} \qquad \text{(IV.24)}$$

If we regard A and B as known, Eqs. (IV.18), (IV.21) and (IV.22) may be easily solved. From the resulting values of $\tilde{N}_z$, $\tilde{N}_{z+1}$ and $\tilde{N}_e$, the particle densities of the remaining species may be calculated by Eq. (IV.10) and the four subsidiary equations out of (IV.11) to (IV.15), corrected values of N_{c1} and N_{c2} can then be calculated and a higher approximation to the

to the dominant species obtained. Checks show that if the iteration is continued until N_{cl} is within 0.5% then all species are within 0.05%. If, now, the dominant equation is Eq. (IV.11), a similar procedure can be used although the equations are slightly different in detail. We have

$$\frac{(\tilde{N}_N)^2}{\tilde{N}_{N_2}} = K_2, \tag{IV.25}$$

and

$$\tilde{N}_N = A - 2\tilde{N}_{N_2} \tag{IV.26}$$

where

$$A = 1 - \tilde{N}_{cl} = 1 - (2\tilde{N}_{N_2^+} + \tilde{N}_{N^+} + \tilde{N}_{N^{++}} + \tilde{N}_{N^{+++}} + \tilde{N}_{N^{++++}}) \tag{IV.27}$$

This iterative procedure is rapidly convergent and has been programmed as a FORTRAN subroutine.

References for Part 1

1. P. Debye and E. Hückel, "On the Theory of Electrolytes, I. Freezing Point Depression and Related Phenomena," Z. Physik 24, 185-206 (1923).
2. A. Unsöld, "Zur Berechnung der Zustandsummen für Atome und Ionen in einem teilweise ionisiertern Gas," Z. Astrophys. 24, 355-362 (1948).
3. J. C. Stewart and K. Pyatt, "Lowering of Ionization Potentials in Plasmas," Astrophys. J. 144, 1203-1211 (1966).
4. J. W. Bond, K. M. Watson and J. A. Welch, Atomic Theory of Gas Dynamics, Addison-Wesley, 1965.
5. H. R. Griem, Plasma Spectroscopy, McGraw-Hill, 1964.
6. K. S. Drellishak, C. F. Knopp and A. B. Cambel, "Partition Functions and Thermodynamic Properties of Argon Plasmas," Phys. Fluids 6, 1280-1288 (1963).
7. D. P. Duclos and A. B. Cambel, "On the Effective Ionization Potential of Atoms in the Interior of a Plasma," Z. Naturf. 16A, 711 (1961).
8. G. Ecker and W. Kroll, "Lowering of the Ionization Energy for a Plasma in Thermodynamic Equilibrium," Phys. Fluids 6, 62-69 (1963).
9. S. G. Brush, "The Effect of the Interaction of Ions on their Equilibrium Concentration," Plasma Physics (Jl. Nuc. En. Part C) 4, 287-289 (1962).
10. R. A. Allen, "Air Radiation Tables: Spectral Distribution Functions for Molecular Band Systems," AVCO Everett Research Laboratory Research Report 236 (1966).
11. K. S. Drellishak, D. P. Aeschliman and A. B. Cambel, "Partition Functions and Thermodynamic Properties of Nitrogen and Oxygen Plasmas," Phys. Fluids 8, 1590-1600 (1965).

12. D. B. Olfe, "Equilibrium Emissivity Calculations for a Hydrogen Plasma at Temperatures up to 10,000°K," Jl. Quant. Spectrosc. Radiat. Transfer 1, 104-134 (1961).

13. V. S. Vorobyov and G. E. Norman, "Energy Radiated in Spectral Lines by an Equilibrium Plasma II," Opt. Spectrosc. 17, 96-101 (1964).

14. E. U. Condon and G. H. Shortley, The Theory of Atomic Spectra, Cambridge University Press, 1935.

15. C. W. Allen, Astrophysical Quantities, London University Press, 1963.

16. L. Goldberg, "Relative Multiplet Strengths in LS Coupling," Astrophys. J. 82, 1-25 (1935).

17. L. Goldberg, "Note on Absolute Multiplet Strengths," Astrophys. J. 84, 11-13 (1936).

18. L. H. Aller, Astrophysics, The Atmospheres of the Sun and Stars, Ronald Press, 1963.

19. D. H. Menzel and L. Goldberg, "Multiplet Strengths for Transitions Involving Equivalent Electrons," Astrophys. J. 84, 1-10 (1936).

20. P. Kelly and B. H. Armstrong, "Fractional Parentage Coefficients for Mixed Configurations in LS Coupling," Astrophys. J. 129, 786-793 (1959).

21. F. Rohrlich, "Theoretical Multiplet Strengths," Astrophys. J. 129, 441-448 (1959).

22. B. W. Shore and D. H. Menzel, "Generalized Tables for the Calculation of Dipole Transition Probabilities," Astrophys. J. Suppl. series 12, No. 106, 187-214 (1965).

23. A. Simon, J. H. Vandersluis and L. C. Biedenharn, "Tables of Racah Coefficients," Oak Ridge National Laboratory ORNL 1679 (1954).

24. A. F. Nikoforov, V. B. Uvarov and Yu. L. Levitan, Tables of Racah Coefficients, Pergamon, 1965.

25. T. Ishidzu (Ed.), Tables of Racah Coefficients, Pan-Pacific Press (Tokyo), 1960.

26. D. R. Bates and A. Dampaard, "The Calculation of the Absolute Strengths of Spectral Lines," Phil. Trans, A 242, 101-122 (1949).

27. C. E. Moore, "A Multiplet Table of Astrophysical Interest," Contributions from the Princeton University Observatory No. 20 (1945).

28. C. E. Moore, "Ultra-Violet Multiplet Table," N.B.S. Circular No. 488 (1950, 1952).

29. A. Burgess and M. J. Seaton, "A General Formula for the Calculation of Atomic Photo-Ionization Cross Sections," Mon. Notes Roy. Astron. Soc. 120, 121-151 (1960).

30. P. S. Kelly, "Some Analytical Self-Consistent Field Functions and Dipole Transition Matrix Elements for Nitrogen and Oxygen and Their Ions," Astrophys. J. 140, 1247-1268 (1964).

31. S. S. Penner, Quantitative Spectroscopy and Gas Emissivities, Addison-Wesley (1959).

32. H. R. Griem, "Wing Formulae for Stark-Broadened Hydrogen and Hydrogenic Lines," Astrophys. Jl. 136, 422-430 (1962).

33. V. A. Ambartsumyan, Theoretical Astrophysics, Pergamon (1958).

34. M. Baranger, "Spectral Line Broadening in Plasmas," Chap. 13 of D. R. Bates (Ed.), Atomic and Molecular Processes, Academic Press, 1962.

35. H. A. Bethe and E. E. Salpeter, Quantum Mechanics of One- and Two-Electron Atoms, Academic Press, 1957.

36. K.B.S. Eriksson, "Coupling of Electrons with High Orbital Angular Momentum Illustrated by 2pnf and 2png in NII," Phys. Rev. 102, 102-104 (1956).

37. R. A. Day, "Measurement of the Stark Widths and Shifts of Nitrogen Ion Lines," University of Maryland Department of Physics and Astronomy, AF 19(628)-269 Report No. 4.

38. H. R. Griem, M. Baranger, A. C. Kolb and G. Oertel, "Stark Broadening of Neutral Helium Lines in a Plasma," Phys. Rev. 125, 177-195 (1962).

39. R. A. Day and H. R. Griem, "Measurements of Stark Profiles of Singly Ionized Nitrogen Lines from a T-Tube Plasma," Phys. Rev. 140, A1129-A1132 (1965).

40. H. R. Griem, A. C. Kolb and K. Y. Shen, "Stark Broadening of Hydrogen Lines in a Plasma," Phys. Rev. 116, 4-16 (1959).

41. H. R. Griem, "Stark Broadening of Higher Hydrogen and Hydrogen-Like Lines by Electrons and Ions," Astrophys. J. 132, 883-893 (1960).

42. H. Margenau and M. Lewis, "Structure of Spectral Lines from Plasmas," Rev. Mod. Phys. 31, 569-615 (1959).

43. N. W. Jalufka, G. K. Oertel and G. S. Ofelt, "Measurements of Stark Broadening of Some Singly Ionized Argon Lines," Phys. Rev. Let. 16, 1073 (1966).

44. M. Sibulkin, "Absorption and Emission Characteristics of an Ideal Radiating Gas," Brown University Division of Engineering report Nonr(562)35/7 (1965).

45. B. H. Armstrong, R. R. Johnston and P. S. Kelly, "Opacity of High-Temperature Air," Air Force Weapons Laboratory Report AFWL-TR-65-17 (1965).

46. A. Unsöld, Physik der Sternatmosphären, Springer-Verlag, 1955.

47. J. C. Stewart and K. D. Pyatt, "Theoretical Study of Optical Properties," Air Force Weapons Center, AFSWC-TR-61-71 (1961).

48. B. H. Armstrong, "Use of Fractional Parentage Coefficients in the Calculation of Photoelectric Cross Sections," Proc. Phys. Soc. 74, 136-137 (1959).

49. G. Peach, "Continuous Absorption Coefficients for Non-Hydrogenic Atoms," Mon. Not. Roy. Astron. Soc. 124, 371-381 (1962).

50. R. R. Johnston, B. H. Armstrong and O. R. Platas, "The Photoionization Contribution to the Radiation Absorption Coefficient of Air," Jl. Quant. Spectrosc. Radiat. Transfer 5, 49-53 (1965).

51. M. J. Seaton, "Thermal Elastic Collision Processes," Rev. Mod. Phys. 30, 979-989 (1958).

52. W. J. Karzas and R. Latter, "Electron Radiative Transitions in a Coulomb Field," Astrophys. J. Suppl. Series 6, 167-212 (1961).

53. P. J. Brussaard and H. C. van der Hulst, "Approximation Formulas for Nonrelativistic Bremsstrahlung and Average Gaunt Factors for a Maxwellian Electron Gas," Rev. Mod. Phys. 34, 507-520 (1962).

54. B. H. Armstrong, J. Sokoloff, P. W. Nicholls, D. H. Holland and R. E. Meyerott, "Radiative Properties of High Temperature Air," J. Quant. Spectrosc. Radiat. Transfer 1, 143-162 (1961).

55. G. Peach, "A General Formula for the Calculation of Absorption Cross Sections for Free-Free Transitions in the Field of Positive Ions," Mon. Not. Roy. Astron. Soc. 130, 361-377 (1965).

56. W. G. Vincenti and C. Kruger, Introduction to Physical Gas Dynamics, Wiley 1965.

57. F. R. Gilmore, "Energy Levels, Partition Functions and Fractional Electronic Populations for Nitrogen and Oxygen Atoms and Ions to 25,000°K," RAND Corporation, Memorandum RM-3748-PR.

58. C. E. Moore, "Atomic Energy Levels 1949," NBS Circular 467 (1949).

59. A. R. Hochstim, "Theoretical Calculations of Thermodynamic Properties of Air," Combustion and Propulsion, 5th AGARD Colloquium, 1962, Pergamon, 1963.

60. M. P. Sherman and J. L. Kulander, "Free-Bound Radiation from Nitrogen, Oxygen, and Air," Space Sciences Laboratory, General Electric Co., R65SD15 (1965).

61. R. A. Allen, A. Textoris and J. Wilson, "Measurements of the Free-Bound and Free-Free Continua of Nitrogen, Oxygen and Air," AVCO-Everett Research Laboratory Research Report 195 (1964).

62. P. S. Kelly, "Transition Probabilities in Nitrogen and Oxygen from Hartree-Fock-Slater Wave Functions," Jl. Quant. Spectrosc. Radiat. Transfer 4, 117-148 (1964).

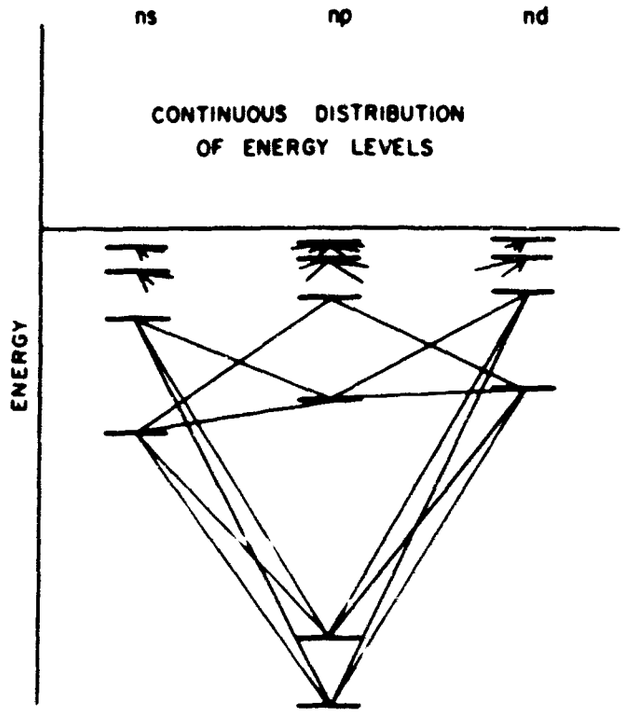

FIG 1a SKETCH SHOWING A SIMPLE ARRANGEMENT OF ENERGY LEVELS AND ILLUSTRATING SOME TYPICAL BOUND - BOUND TRANSITIONS

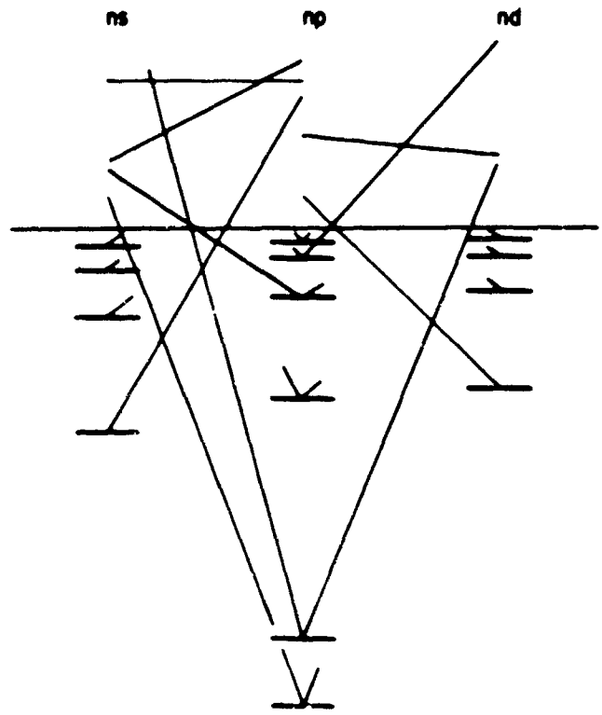

FIG 1b SKETCH SHOWING A SIMPLE ARRANGEMENT OF ENERGY LEVELS AND ILLUSTRATING SOME TYPICAL BOUND - FREE AND FREE - FREE TRANSITIONS

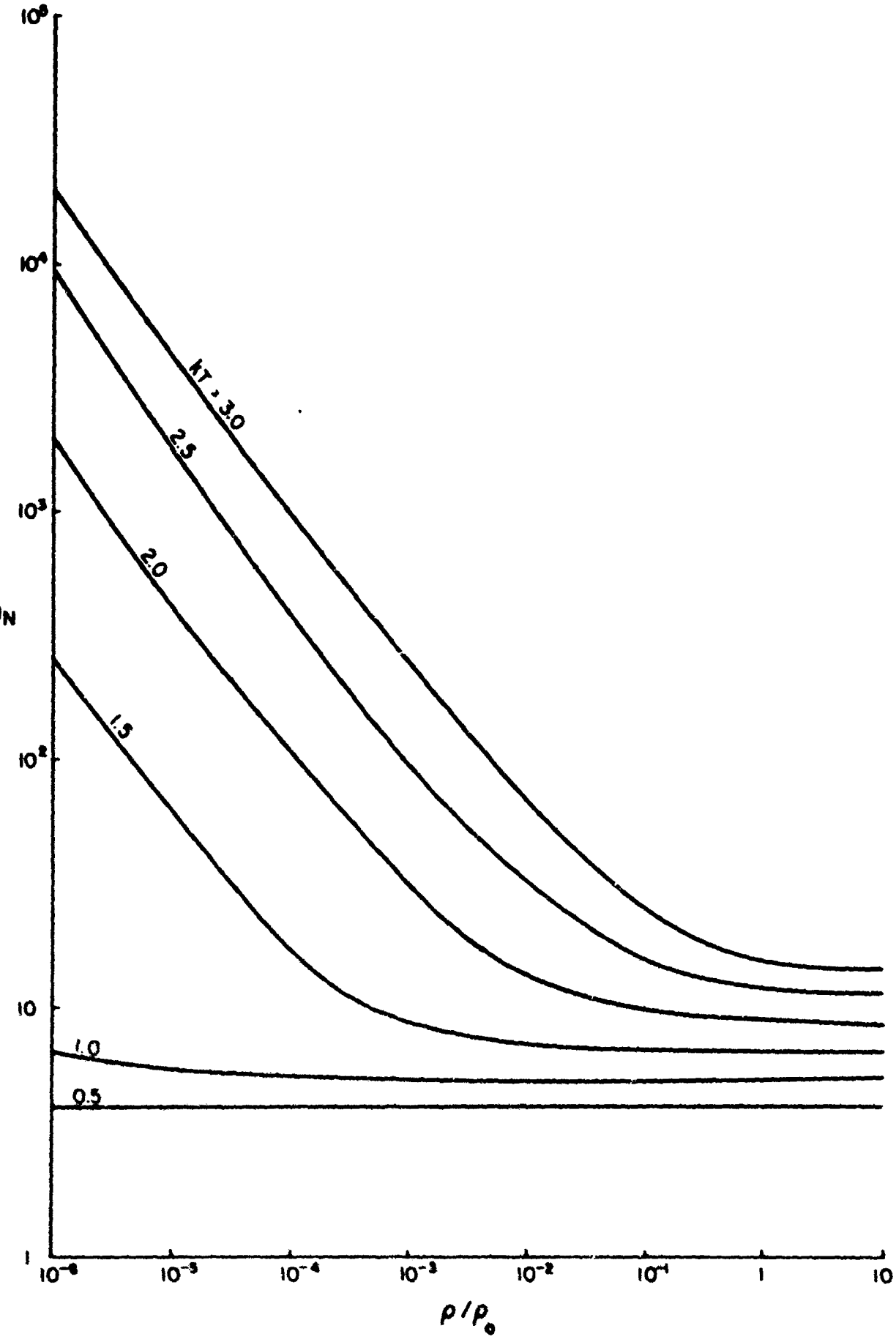

FIG. 2 THE ELECTRONIC PARTITION FUNCTION OF ATOMIC NITROGEN AS A FUNCTION OF DENSITY AND TEMPERATURE

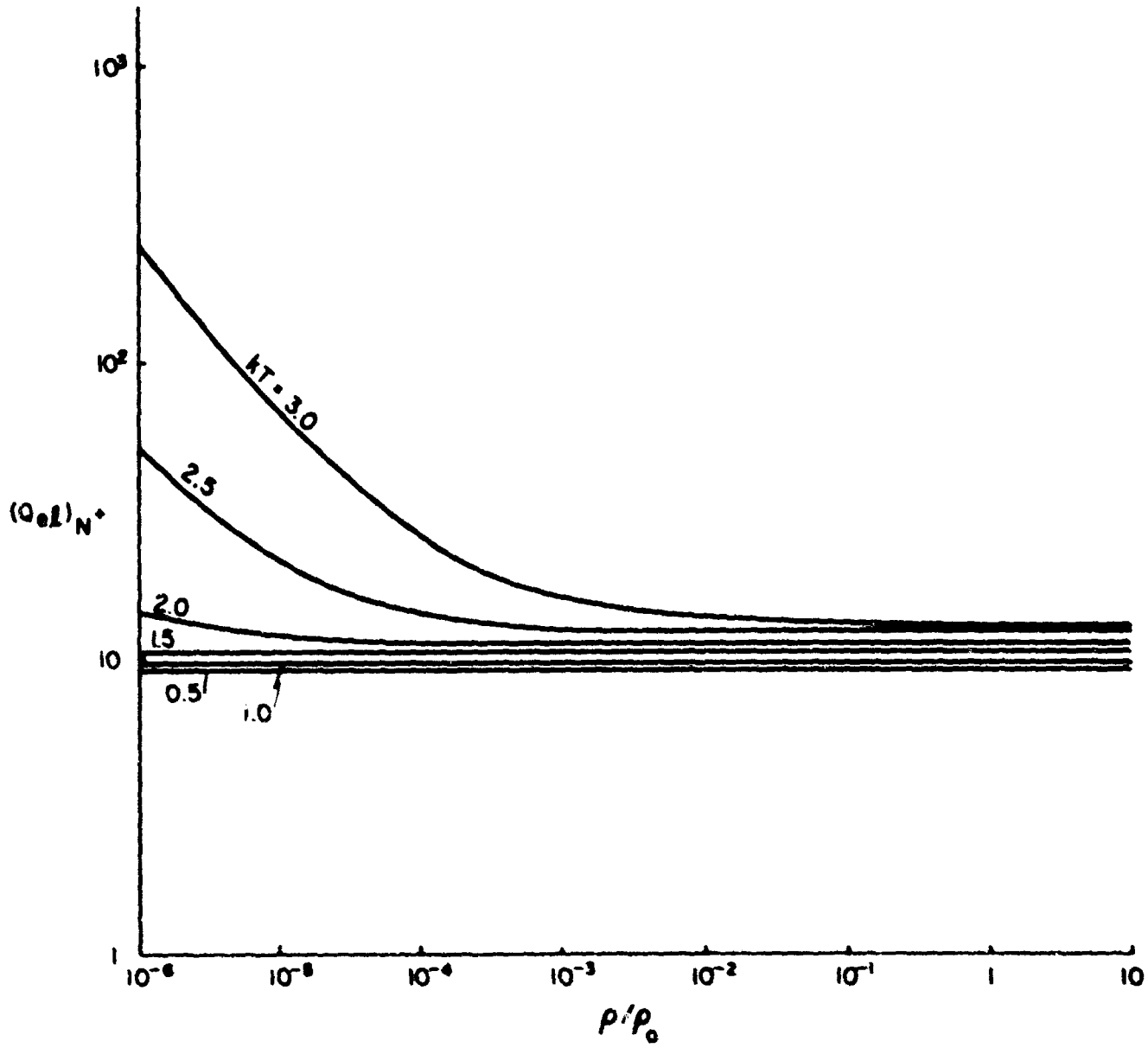

FIG. 3 THE ELECTRONIC PARTITION FUNCTION OF THE FIRST ION AS A FUNCTION OF DENSITY AND TEMPERATURE

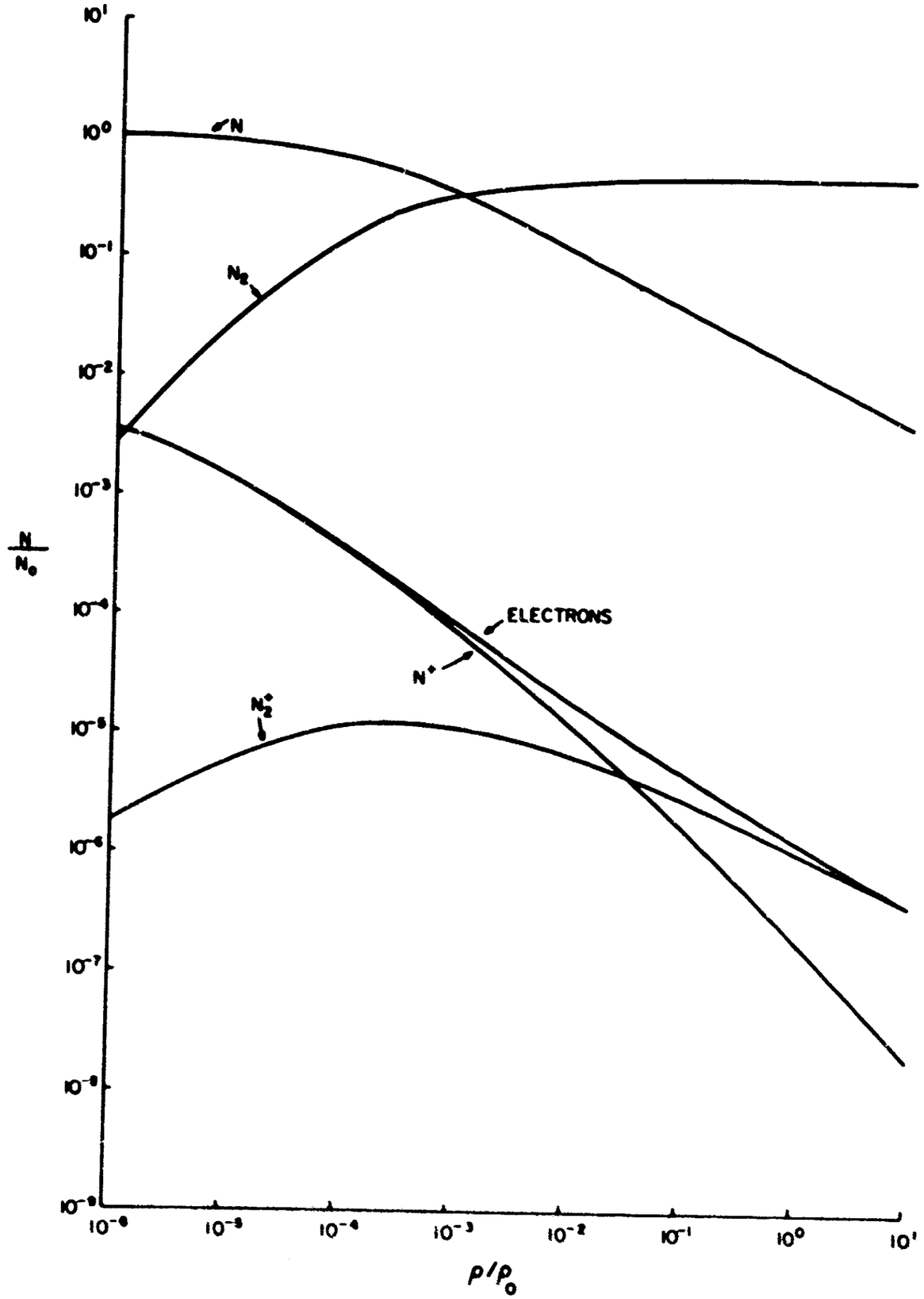

FIG. 4 PARTICLE DENSITIES IN A NITROGEN PLASMA AS A FUNCTION OF DENSITY FOR

$kT = 0.5\,eV \quad (T \cong 5{,}803\,^{\circ}K)$

$N_0 = 5.374 \times 10^{19} \times \rho/\rho_0\,cm^{-3}, \rho_0 = 1.250 \times 10^{-3}\,gm\,cm^{-3}$

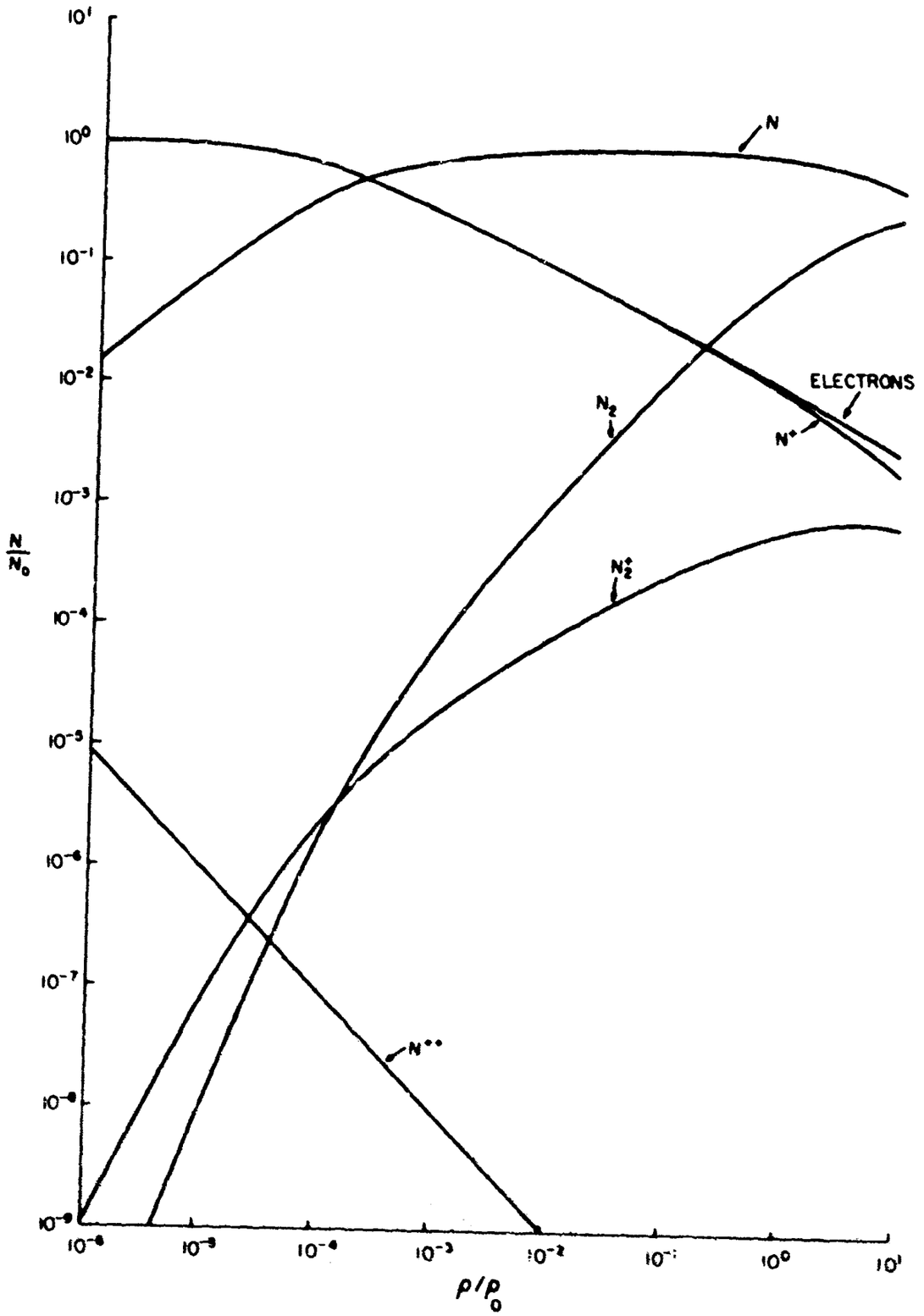

FIG. 5 PARTICLE DENSITIES IN A NITROGEN PLASMA AS A FUNCTION OF DENSITY FOR kT = 1.0 eV (T ≅ 11,605 °K)

$N_0 = 5.374 \times 10^{19} \times \rho/\rho_0 \, cm^{-3}$, $\rho_0 = 1.250 \times 10^{-3} \, gm \, cm^{-3}$

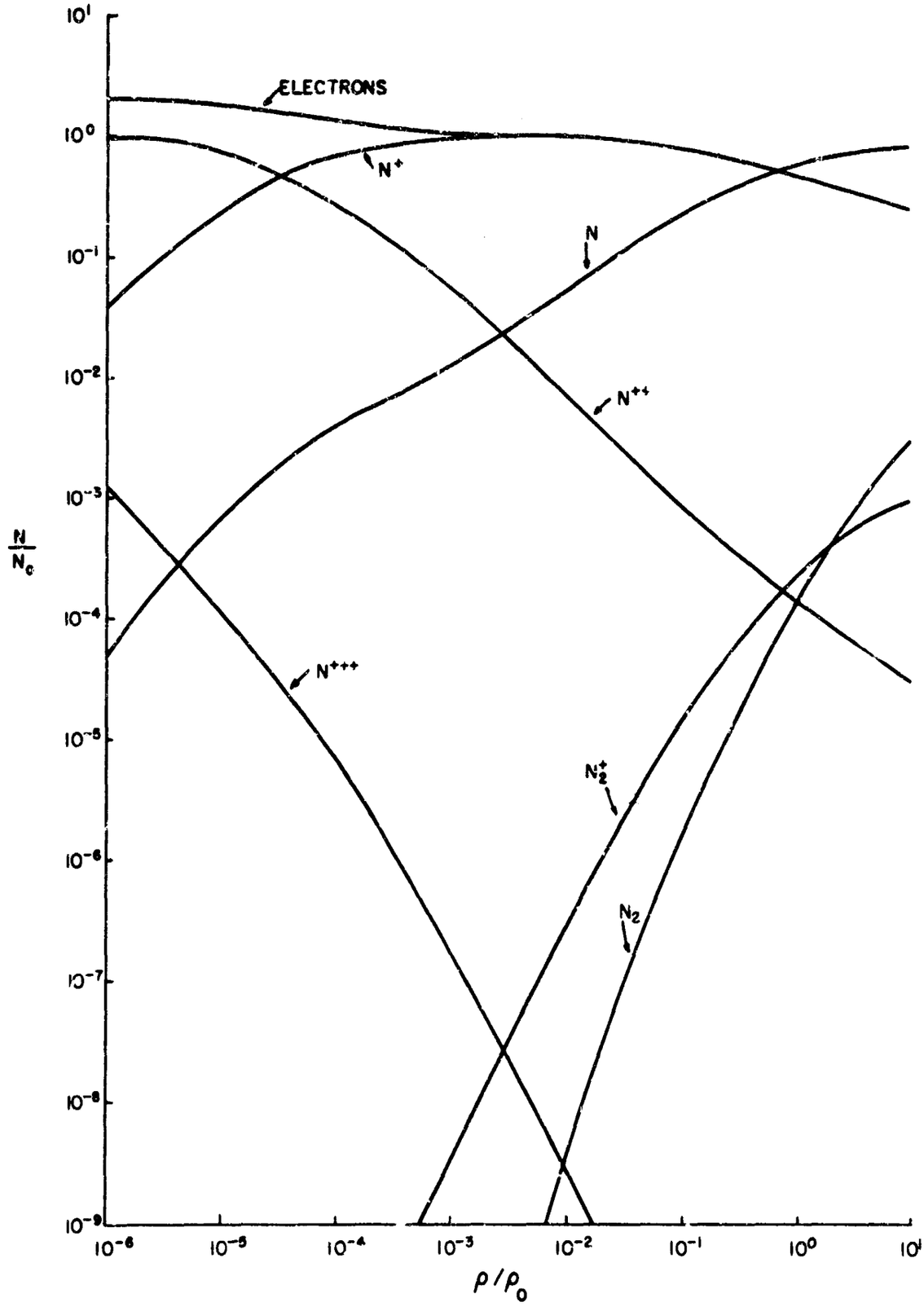

FIG. 6 PARTICLE DENSITIES IN A NITROGEN PLASMA AS A FUNCTION OF DENSITY FOR kT = 2.0 eV (T ≅ 23,211°K)

$N_0 = 5.374 \times 10^{19} \times \rho/\rho_0 \, cm^{-3}, \rho_0 = 1.250 \times 10^{-3} \, gm \, cm^{-3}$

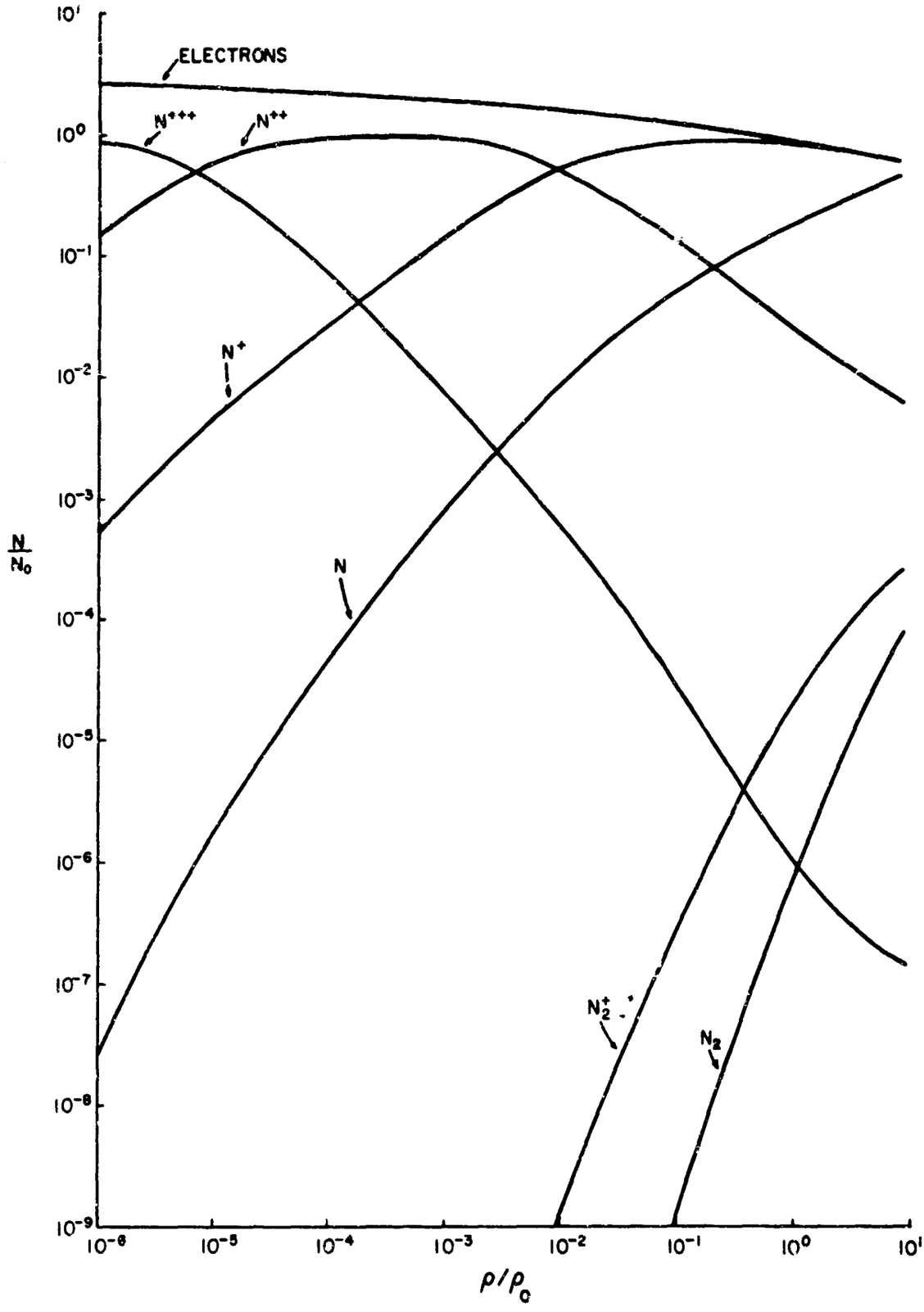

FIG. 7 PARTICLE DENSITIES IN A NITROGEN PLASMA AS A FUNCTION OF DENSITY FOR

$kT = 3.0$ eV ($T \cong 34,816°K$)

$N_0 = 5.374 \times 10^{19} \times \rho/\rho_0 \, cm^{-3}$, $\rho_0 = 1.250 \times 10^{-3} \, gm \, cm^{-3}$

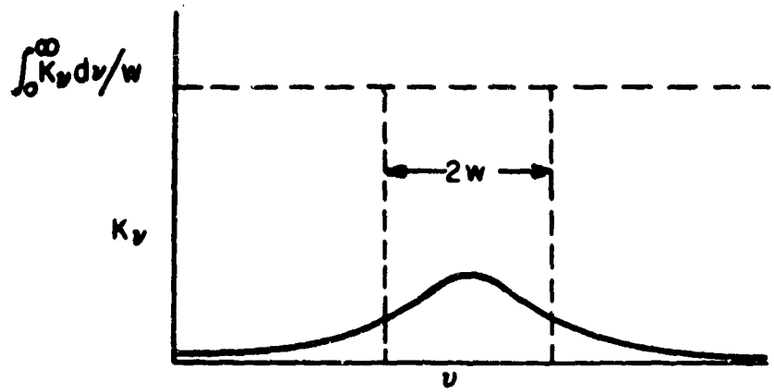

FIG. 8a ABSORPTION COEFFICIENT FOR A LINE WITH A DISPERSION PROFILE.

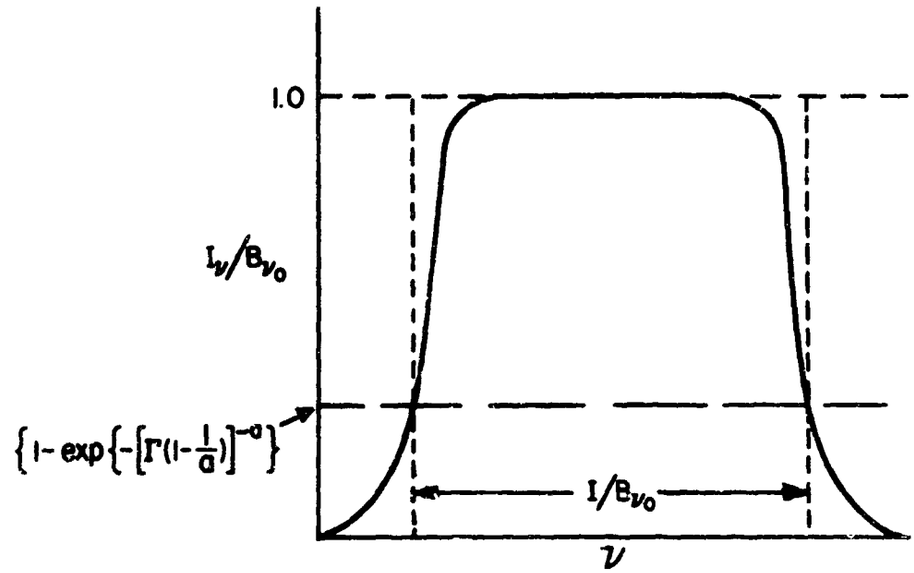

FIG. 8b EQUIVALENT WIDTH AND SPECIFIC INTENSITY AS A FUNCTION OF FREQUENCY FOR A TYPICAL SELF-ABSORBED LINE.

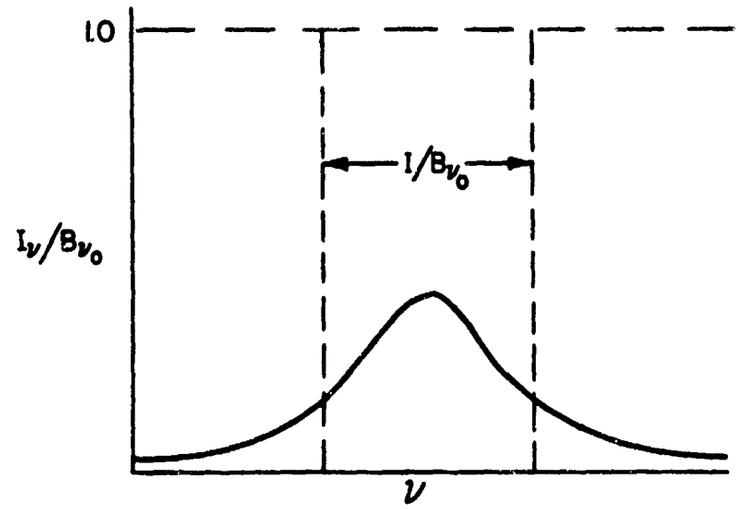

FIG. 8c EQUIVALENT WIDTH AND SPECIFIC INTENSITY AS A FUNCTION OF FREQUENCY FOR A TYPICAL NONABSORBED LINE.

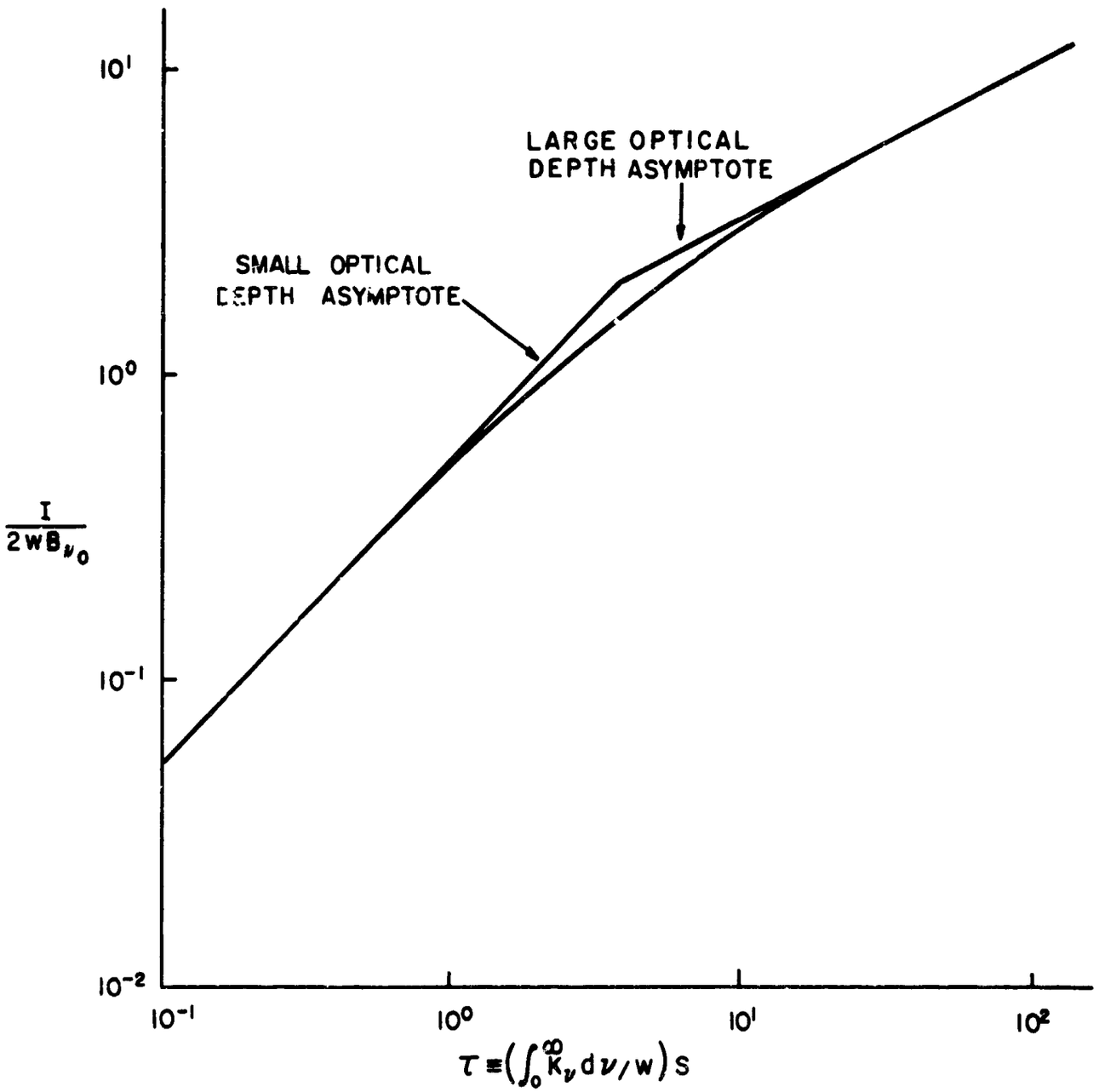

FIG. 9 THE CURVE OF GROWTH OF A PURE DISPERSION LINE PROFILE AND ITS ASYMPTOTIC APPROXIMATIONS

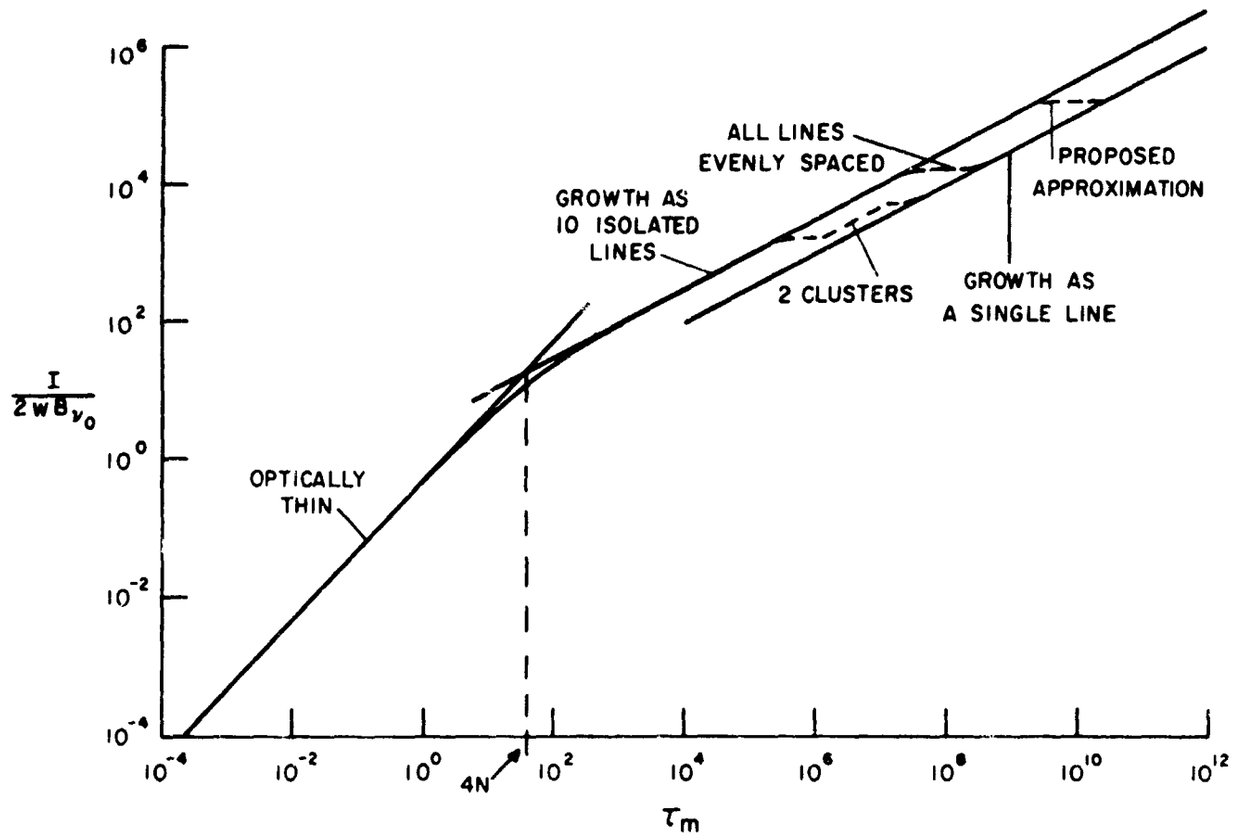

FIG. 10 A SKETCH OF POSSIBLE CURVES OF GROWTH OF A GROUP OF LINES. (THERE IS NO SIGNIFICANCE IN THE RELATIVE POSITIONS OF THE TRANSITION REGIONS ON THE τ_m SCALE)

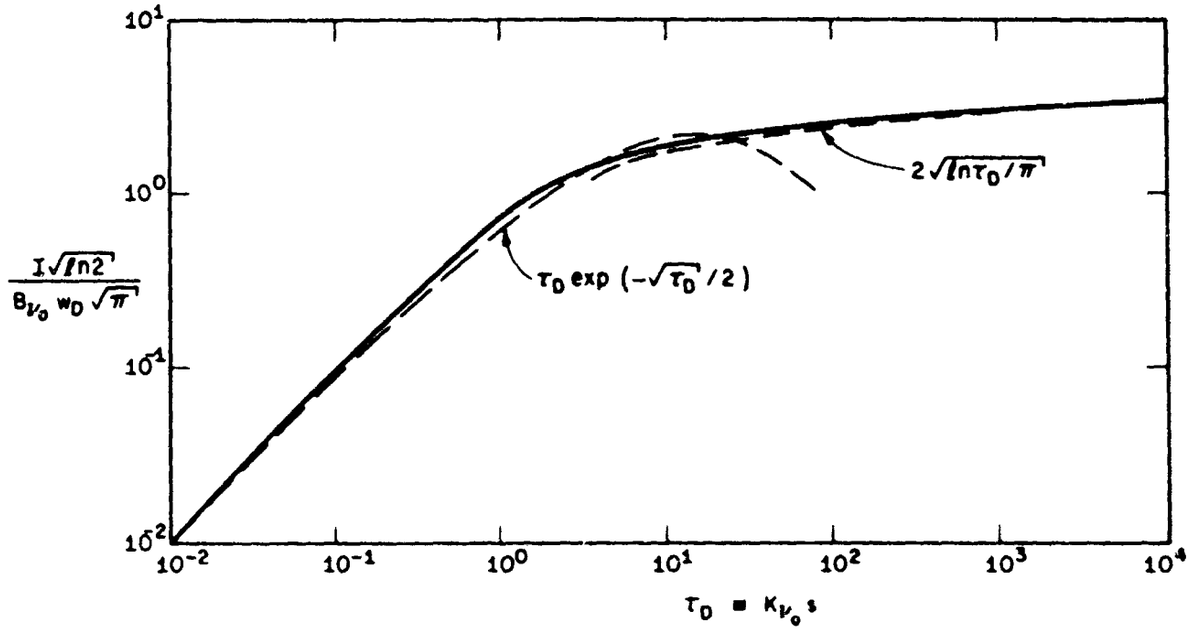

FIG. 11 THE CURVE OF GROWTH OF A PURE DOPPLER LINE PROFILE AND ITS APPROXIMATE REPRESENTATIONS.

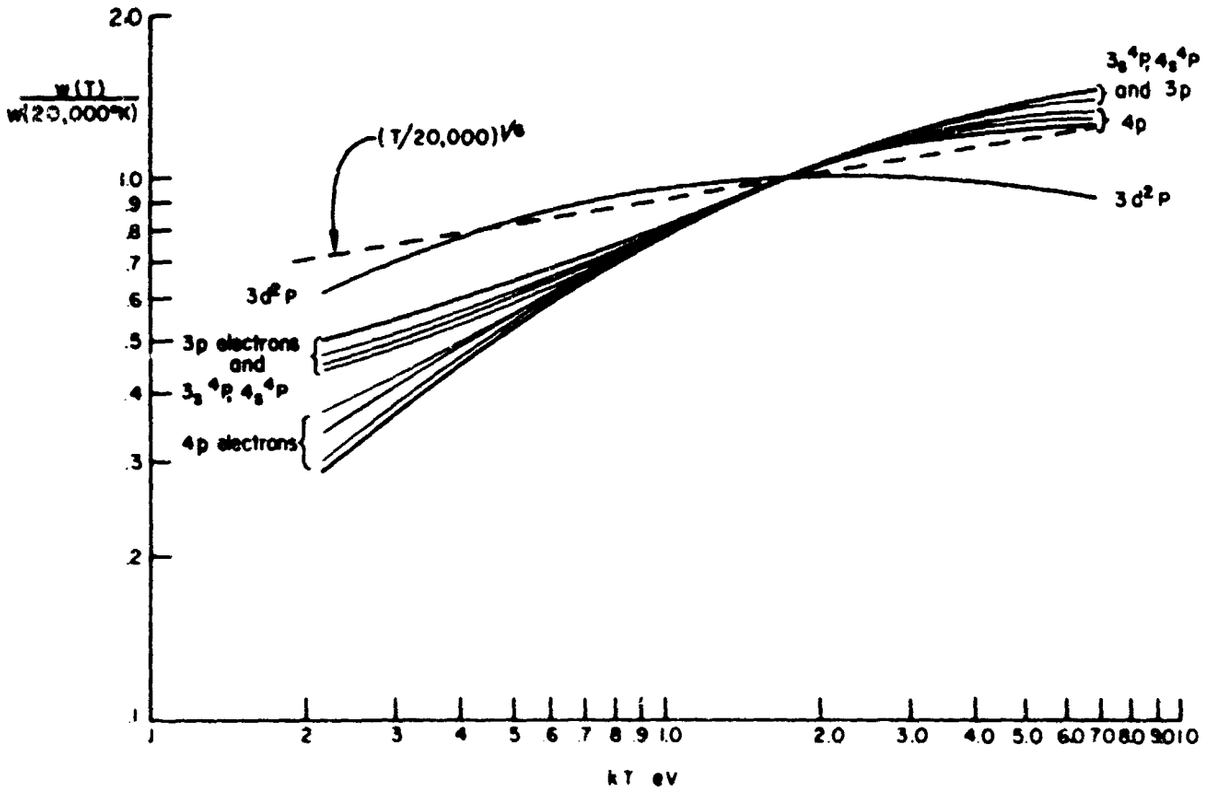

FIG. 12 NORMALISED LINE WIDTHS OF ELECTRON IMPACT BROADENED PROFILES IN THE FIRST SPECTRUM OF NITROGEN. (VALUES TAKEN FROM GRIEM [9])

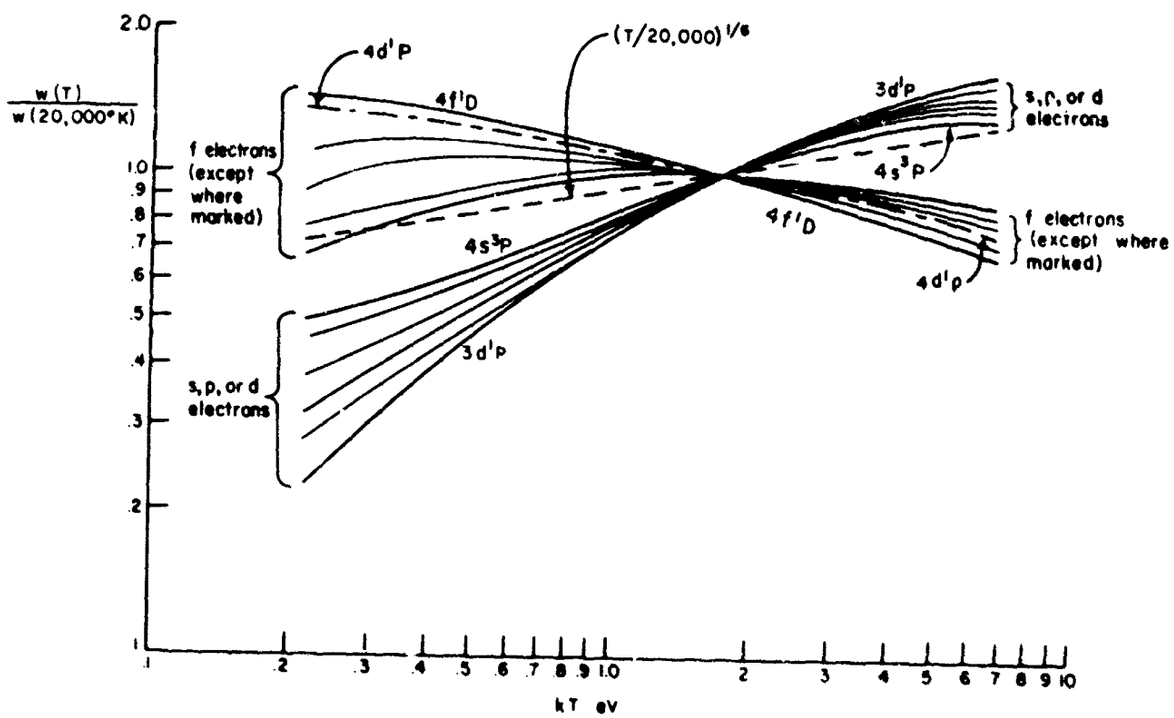

FIG. 13 NORMALISED LINE WIDTHS OF ELECTRON IMPACT BROADENED PROFILES IN THE SECOND SPECTRUM OF NITROGEN. (VALUES) TAKEN FROM GRIEM[9])

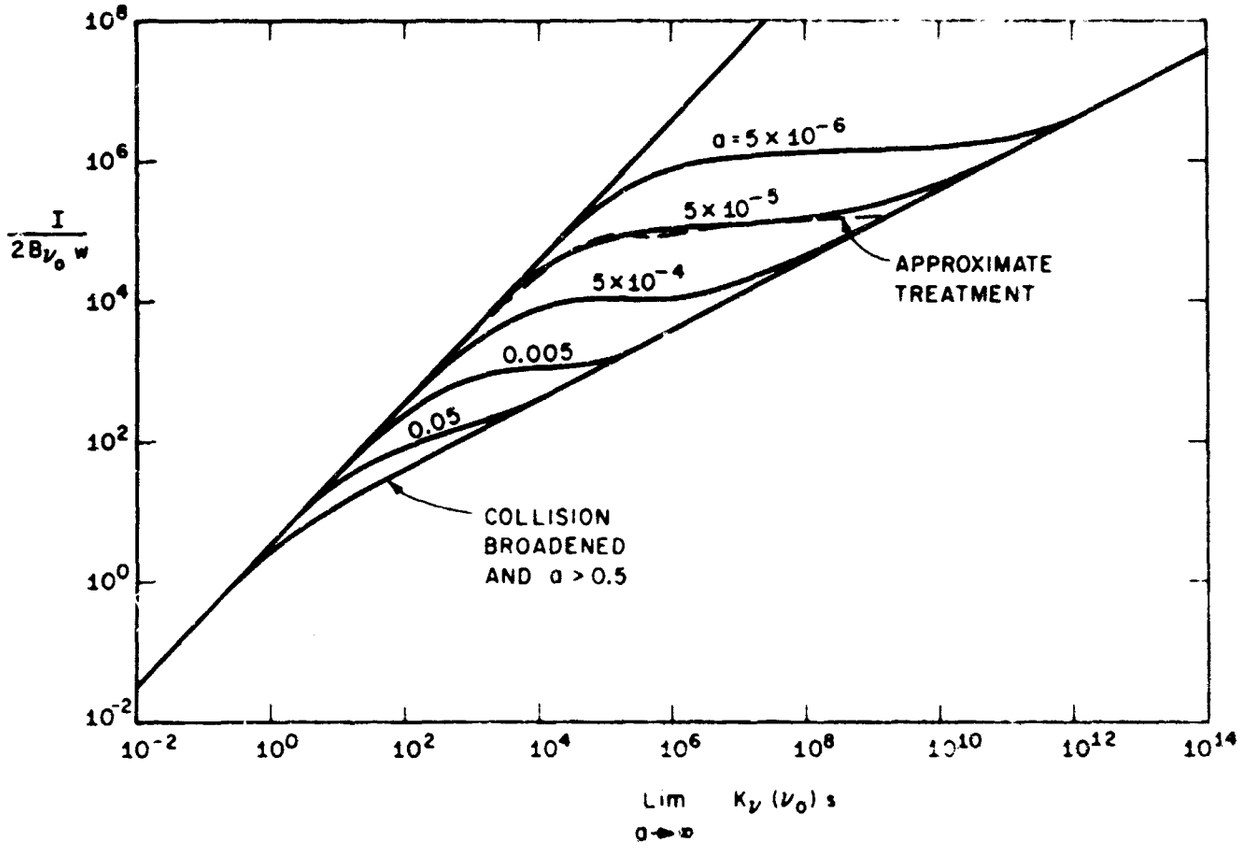

FIG. 14 CURVES OF GROWTH OF COMBINED DOPPLER AND DISPERSION LINE PROFILES BASED UPON THE CORRESPONDING PURE DISPERSION PROFILE PARAMETERS.

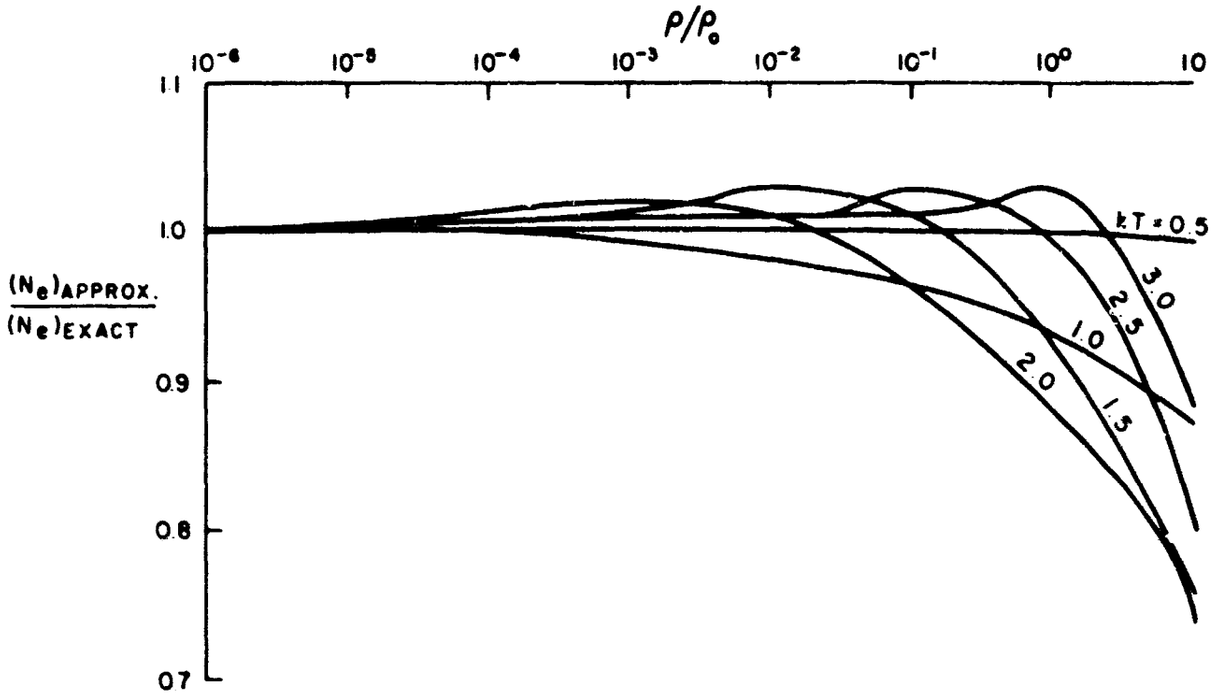

FIG. 15 ERRORS IN ELECTRON DENSITY DUE TO USING VACUUM IONISATION ENERGIES, A 3–TERM PARTITION FUNCTION FOR N AND A 4–TERM PARTITION FUNCTION FOR N^+

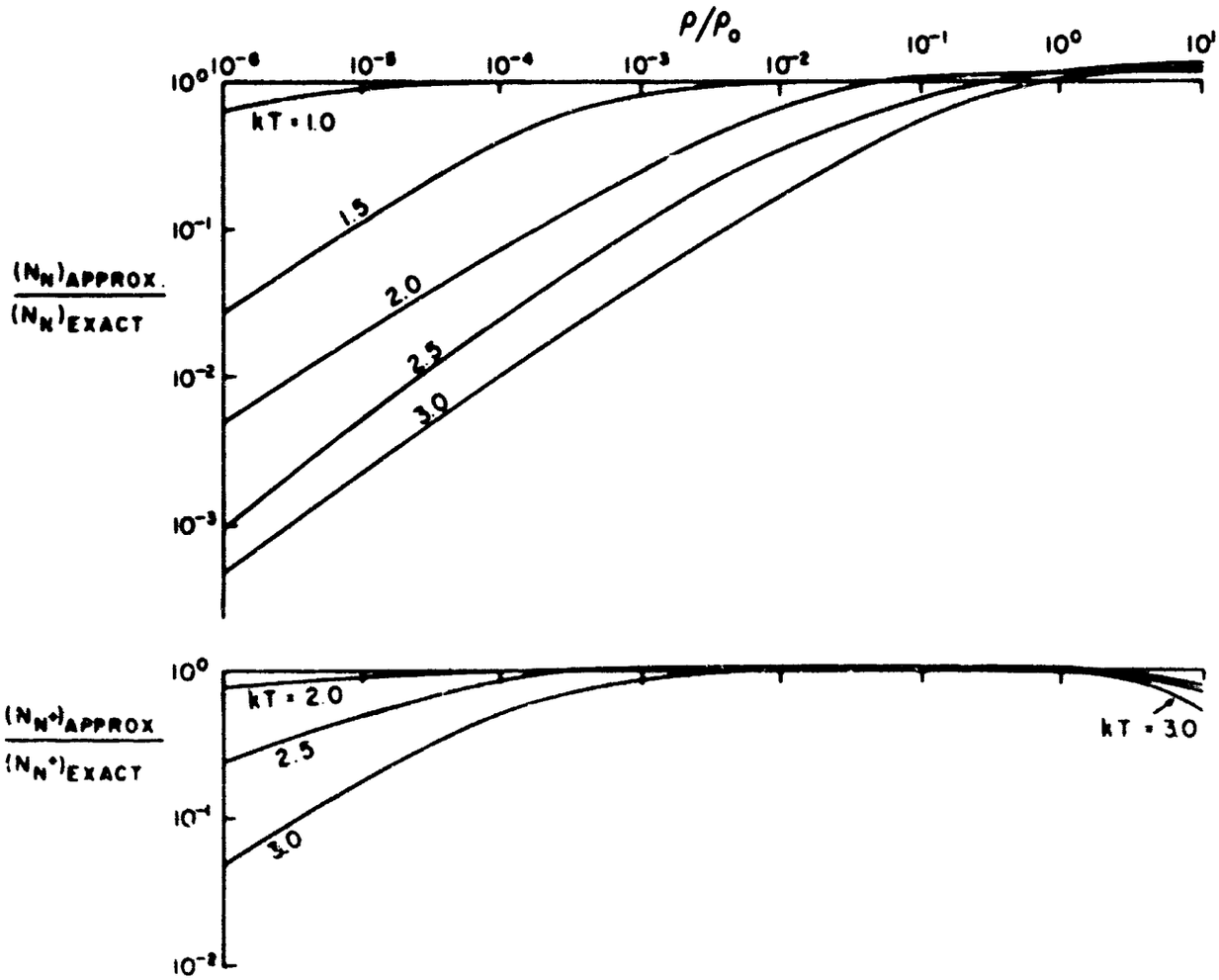

FIGS. 16 and 17 ERRORS IN NUMBER DENSITIES OF N AND N^+ DUE TO USING VACUUM IONISATION ENERGIES, A 3-TERM PARTITION FUNCTION FOR N AND A 4-TERM PARTITION FUNCTION FOR N^+

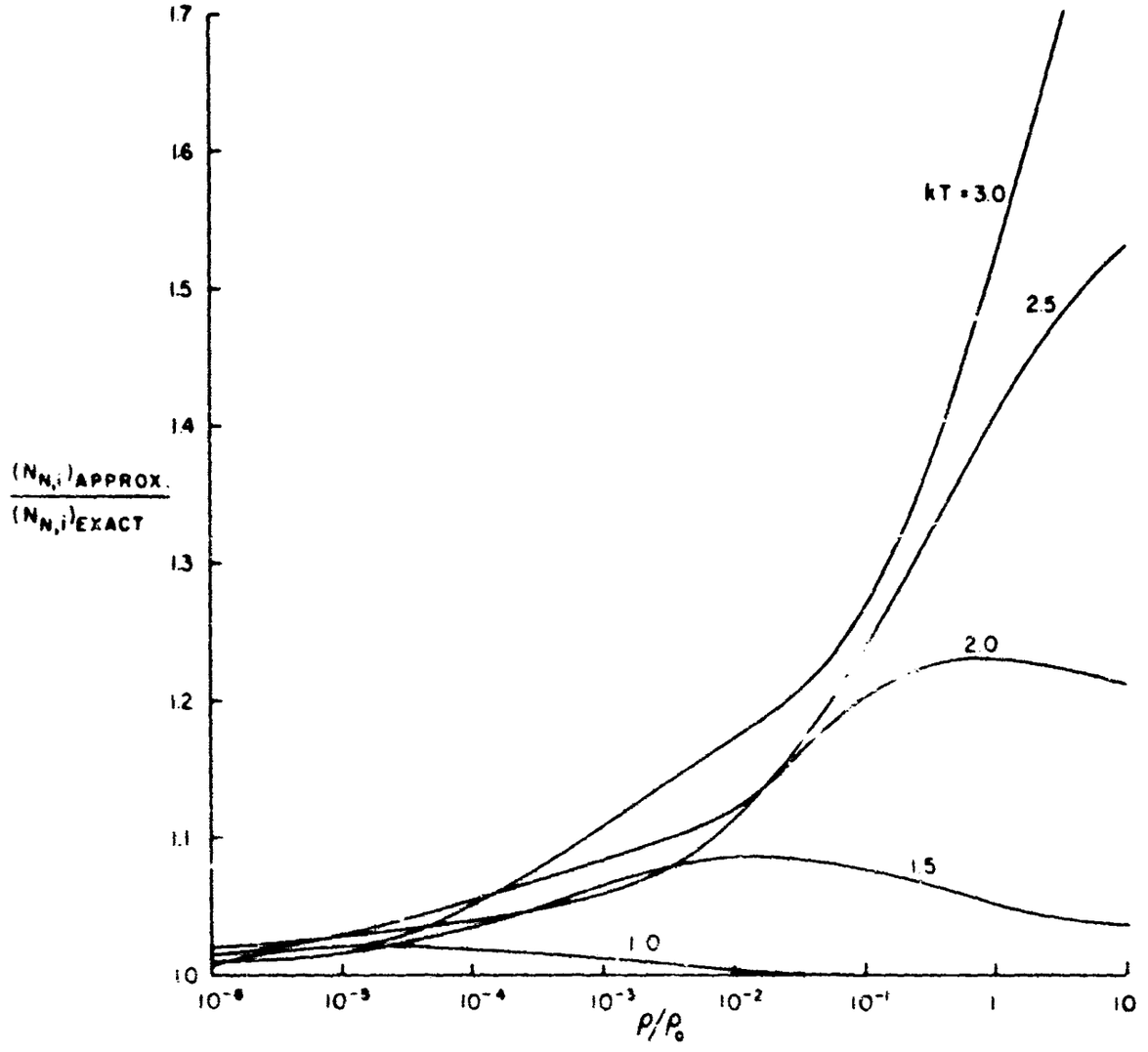

FIG. 18 ERRORS IN THE OCCUPATION NUMBER OF THE iTH ENERGY LEVEL OF N DUE TO USING VACUUM IONISATION ENERGIES, A 3-TERM PARTITION FUNCTION FOR N AND A 4-TERM PARTITION FUNCTION FOR N^+

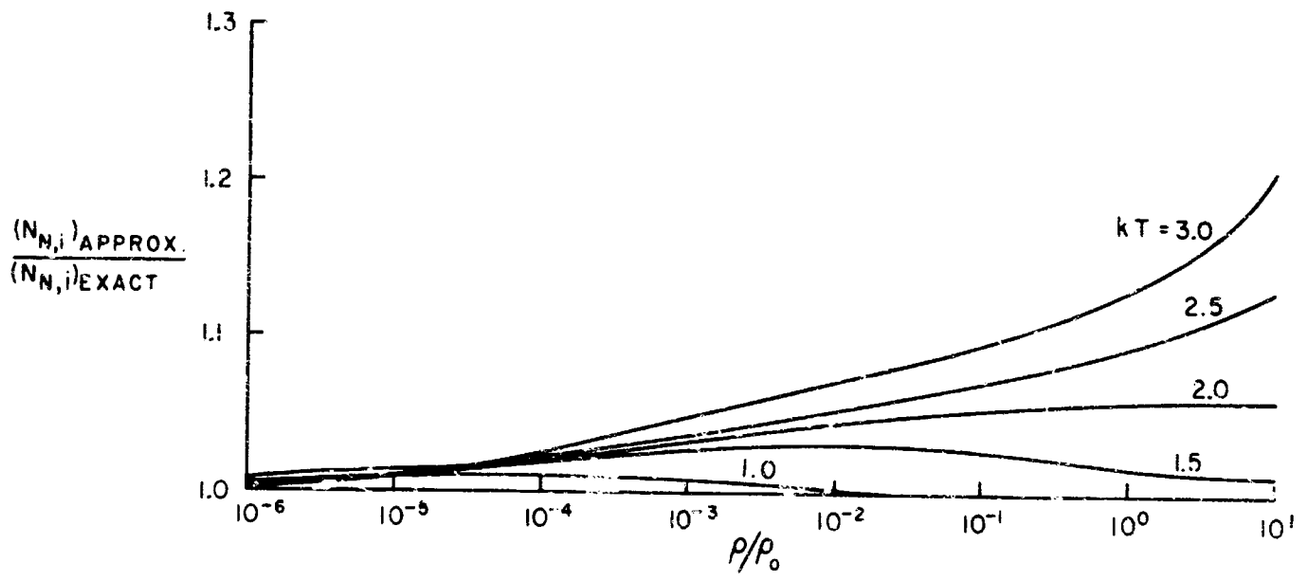

FIG. 15 ERRORS IN THE OCCUPATION NUMBER OF THE ITH ENERGY LEVEL OF N DUE TO USING A 3–TERM PARTITION FUNCTION FOR N AND A 4–TERM PARTITION FUNCTION FOR N^+ (THE IONISATION ENERGIES ARE CORRECTLY DEPRESSED)

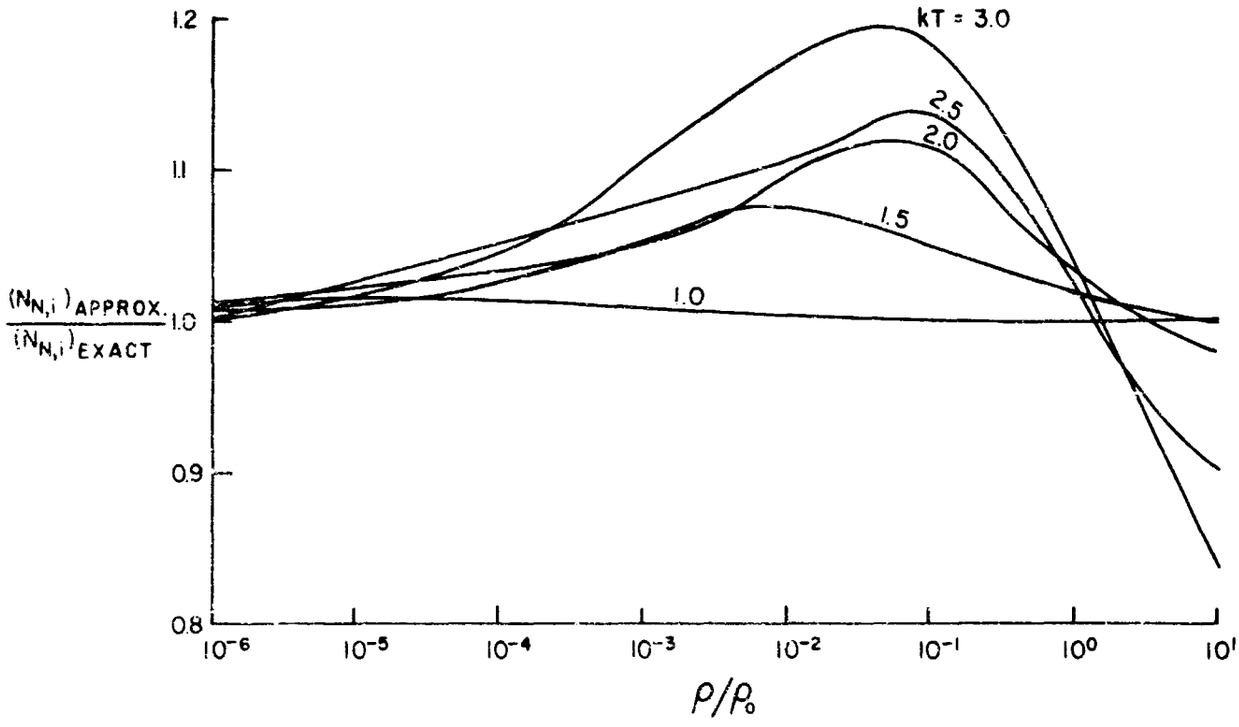

FIG.20 ERRORS IN THE OCCUPATION NUMBER OF THE ITH ENERGY LEVEL OF N DUE TO USING VACUUM IONISATION ENERGIES, A 19-TERM PARTITION FUNCTION FOR N AND A 4-TERM PARTITION FUNCTION FOR N^+

Unclassified
Security Classification

DOCUMENT CONTROL DATA - R&D

(Security classification of title, body of abstract and indexing annotation must be entered when the overall report is classified)

1. ORIGINATING ACTIVITY (Corporate author)	2a. REPORT SECURITY CLASSIFICATION
Brown University, Providence, R. I. 02912	Unclassified
	2b. GROUP

3. REPORT TITLE

RADIATIVE TRANSFER IN A GAS OF UNIFORM PROPERTIES IN LOCAL THERMODYNAMIC EQUILIBRIUM.
PART 1: ABSORPTION COEFFICIENTS IN NONHYDROGENIC GASES

4. DESCRIPTIVE NOTES *(Type of report and inclusive dates)*

5. AUTHOR(S) *(Last name, first name, initial)*

Hunt, Brian L. and Sibulkin, Merwin

6. REPORT DATE	7a. TOTAL NO. OF PAGES	7b. NO. OF REFS
December, 1966	105	62

8a. CONTRACT OR GRANT NO.	9a. ORIGINATOR'S REPORT NUMBER(S)
Nonr 562(35)	Nonr 562(35)/16
b. PROJECT NO. Task NR 061-132	
c.	9b. OTHER REPORT NO(S) *(Any other numbers that may be assigned this report)*
d. ARPA Project Code Number 2740	

10. AVAILABILITY/LIMITATION NOTICES

11. SUPPLEMENTARY NOTES	12. SPONSORING MILITARY ACTIVITY
	Advanced Research Projects Agency and Office of Naval Research

13. ABSTRACT

This report discusses the data needed to perform radiative transfer calculations in nonhydrogenic gases in local thermodynamic equilibrium and presents some approximate methods for computing the radiative energy transferred by spectral lines where the properties of the gas are uniform.

The methods currently available for calculating the cross sections of radiative processes are described and compared. An accurate method for calculating the species composition of nitrogen is described and the results of such a calculation are presented. The important line broadening mechanisms are discussed and the potentially accurate, modern theories of line broadening are outlined. The results of these theories are used to justify approximate line profiles which are simple enough for use in radiative transfer calculations.

Simple approximations to the exact curves of growth of intensity are described for lines with Doppler profiles and for lines with profiles of a class which includes the dispersion and quasi-static forms. The concept of the effective width of a line intensity profile is introduced and techniques are developed for dealing with the overlapping of the intensity profiles of small groups of closely spaced lines (as, for example, in a multiplet).

DD FORM 1 JAN 64 1473

Unclassified
Security Classification

14. KEY WORDS	LINK A		LINK B		LINK C	
	ROLE	WT	ROLE	WT	ROLE	WT
Absorption coefficient						
Radiative transfer						
Species composition						
Spectral lines						

INSTRUCTIONS

1. ORIGINATING ACTIVITY: Enter the name and address of the contractor, subcontractor, grantee, Department of Defense activity or other organization *(corporate author)* issuing the report.

2a. REPORT SECURITY CLASSIFICATION: Enter the overall security classification of the report. Indicate whether "Restricted Data" is included. Marking is to be in accordance with appropriate security regulations.

2b. GROUP: Automatic downgrading is specified in DoD Directive 5200.10 and Armed Forces Industrial Manual. Enter the group number. Also, when applicable, show that optional markings have been used for Group 3 and Group 4 as authorized.

3. REPORT TITLE: Enter the complete report title in all capital letters. Titles in all cases should be unclassified. If a meaningful title cannot be selected without classification, show title classification in all capitals in parenthesis immediately following the title.

4. DESCRIPTIVE NOTES: If appropriate, enter the type of report, e.g., interim, progress, summary, annual, or final. Give the inclusive dates when a specific reporting period is covered.

5. AUTHOR(S): Enter the name(s) of author(s) as shown on or in the report. Enter last name, first name, middle initial. If military, show rank and branch of service. The name of the principal author is an absolute minimum requirement.

6. REPORT DATE: Enter the date of the report as day, month, year; or month, year. If more than one date appears on the report, use date of publication.

7a. TOTAL NUMBER OF PAGES: The total page count should follow normal pagination procedures, i.e., enter the number of pages containing information.

7b. NUMBER OF REFERENCES: Enter the total number of references cited in the report.

8a. CONTRACT OR GRANT NUMBER: If appropriate, enter the applicable number of the contract or grant under which the report was written.

8b, 8c, & 8d. PROJECT NUMBER: Enter the appropriate military department identification, such as project number, subproject number, system numbers, task number, etc.

9a. ORIGINATOR'S REPORT NUMBER(S): Enter the official report number by which the document will be identified and controlled by the originating activity. This number must be unique to this report.

9b. OTHER REPORT NUMBER(S): If the report has been assigned any other report numbers *(either by the originator or by the sponsor)*, also enter this number(s).

10. AVAILABILITY/LIMITATION NOTICES: Enter any limitations on further dissemination of the report, other than those imposed by security classification, using standard statements such as:

(1) "Qualified requesters may obtain copies of this report from DDC."

(2) "Foreign announcement and dissemination of this report by DDC is not authorized."

(3) "U. S. Government agencies may obtain copies of this report directly from DDC. Other qualified DDC users shall request through _____."

(4) "U. S. military agencies may obtain copies of this report directly from DDC. Other qualified users shall request through _____."

(5) "All distribution of this report is controlled. Qualified DDC users shall request through _____."

If the report has been furnished to the Office of Technical Services, Department of Commerce, for sale to the public, indicate this fact and enter the price, if known.

11. SUPPLEMENTARY NOTES: Use for additional explanatory notes.

12. SPONSORING MILITARY ACTIVITY: Enter the name of the departmental project office or laboratory sponsoring *(paying for)* the research and development. Include address.

13. ABSTRACT: Enter an abstract giving a brief and factual summary of the document indicative of the report, even though it may also appear elsewhere in the body of the technical report. If additional space is required, a continuation sheet shall be attached.

It is highly desirable that the abstract of classified reports be unclassified. Each paragraph of the abstract shall end with an indication of the military security classification of the information in the paragraph, represented as *(TS), (S), (C), or (U)*

There is no limitation on the length of the abstract. However, the suggested length is from 150 to 225 words.

14. KEY WORDS: Key words are technically meaningful terms or short phrases that characterize a report and may be used as index entries for cataloging the report. Key words must be selected so that no security classification is required. Identifiers, such as equipment model designation, trade name, military project code name, geographic location, may be used as key words but will be followed by an indication of technical context. The assignment of links, rules, and weights is optional.